INFLUENCE OF TEMPERATURE ON THE METAL DUSTING OF ALLOY 800

A research Report submitted to the Faculty of Engineering and the Built Environment, University of the Witwatersrand, in fulfilment of the requirements for the degree of Master of Science in Engineering (50/50).

Kholo Veronica Morudu

UNIVERSITY OF THE
WITWATERSRAND,
JOHANNESBURG

University of the Witwatersrand

Johannesburg, September 2018

Declaration

I, Kholo Veronica Morudu, declare that this is my own, unaided work. It is being submitted for Master of Science in Engineering (50/50): Metallurgical Engineering at the University of the Witwatersrand, Johannesburg. This is not a reproduced copy nor has it been previously submitted previously at this, or any other university for any degree or examination. I further declare that all sources cited or quoted are indicated and acknowledged by means of a comprehensive list of references.

_____ _____

Signature Date

ABSTRACT

Metal dusting (MD) is a severe form of corrosion in which iron, steels, and nickel (Ni) and cobalt (Co) based alloys disintegrate into a metal or carbide powder with a coke deposit when exposed to strongly carburising gases (carbon activity, a_C>1) at elevated temperatures (400-800°C). Temperature affects both the driving force and rate of the reaction, represented by gas phase supersaturation with carbon, and the rates of the various processes involved in converting that energy difference into the dusting process. Therefore, process streams such as reformer gas can be benign when hot, but becomes aggressive below critical temperatures. There are different views in literature about the effect of temperature on metal dusting of different materials and alloys.

Alloy 800 experiences metal dusting (MD) at 525°C, which is the temperature of the tube sheet of reformers in petrochemical industry. This alloy is specifically used for tube ferrules in the reformers. The reformer trains can reach a critical (highest) internal temperature of 650°C. Therefore, these two temperatures were compared. The effect of temperature and exposure time on the metal dusting of Alloy 800 were investigated in terms of the form of attack and the degradation mechanism. From the results obtained, it was observed that the longer exposure periods result in more carbon deposition and the carbon filaments in the coke become finer as compared to the nanotubes obtained after shorter exposure periods. The alloy suffered metal dusting attack after a relatively short exposure period of three days (72 hours) at both temperatures of 525°C and 650°C, with very little coking.

ACKNOWLEDGEMENTS

I would like to express my appreciation and gratitude to the following people and organisations for their assistance and support and making this research report possible.

- The All Mighty GOD for his unconditional love, protection, wisdom, strength, mercy and most importantly, without whom I would not be in existence.
- The South African Department of Science and Technology (DST) and the Advanced Metals Initiative (AMI) and the Ferrous Metals Development Network (FMDN) are gratefully acknowledged for providing support and funding.
- Mintek, for their support in terms of facilities, financial assistance and permission to publish these results
- Dr Josias van der Merwe, my supervisor at Wits, for believing in me by accepting me as his student, for his guidance, support, advice and immeasurable contribution to this work and investing knowledge and time in me.
- Mr.Marandela Mulaudzi, my supervisor at Mintek, for all his continuous guidance and support, scientific knowledge and sharing of technical information about this subject. He was never too busy to listen and give advice to all my questions and confusions.
- To the Advanced Materials Division at Mintek, especially Dr Jones Papo and Mr Joseph Moema for encouragement to study further in order to gain more knowledge and growth. Ms Mosima Maja, for assisting with most of the technical laboratory work where extra hands were needed, Mr. Richard Couperthwaite, for his assistance with SEM and XRD techniques at Mintek and Dr Philemon Matabola for his assistance with raman spectroscopy techniques at Mintek.
- Mr. Siyasanga Mpelane for their assistance with TEM techniques at the University of Johannesburg.
- Finally, and most importantly, I would like to thank my wonderful family. You have always been my greatest strength and support throughout this journey, you have given me your full support and above all, you have always put your trust in me. Kealeboga!

Ø Dedication

This work is dedicated to my special mother, Ngwakwana Regina Morudu, my son, Phetola Reratilwe Morudu, my sisters, Dikgang Priscilla Morudu and Mmaselaelo Dorcus Ramabu, my brother, Mahlodi Samson Morudu and my two later brothers, Nhlangoe Jacob Morudu and Mothibi Elias Morudu.

Scientific activity arising from this work

List of presentations/publications

1. Morudu K.V., Mulaudzi F.M.L, van der Merwe J., Maja M., and Moema J.S. (19-21 October 2016), Influence of Temperature on the Metal Dusting of Alloy 800, Paper orally presentation at the Ferrous and Base Metals Development Network Conference, Durban, KwaZulu-Natal.

2. Morudu K.V., Mulaudzi F.M.L, van der Merwe J., Maja M., and Moema J.S. (18-20 July 2018), Influence of Temperature and Exposure Time on the Metal Dusting of Alloy 800, Oral presentation at the AfriCORR 2018 Congress, Johannesburg, Gauteng

Table of Contents

LIST OF FIGURES

LIST OF TABLES

CHAPTER 1: INTRODUCTION

1.1 General background

Metal dusting (MD) is a severe form of corrosion in which iron, steels, and Ni- and Co-based alloys disintegrate into metal or carbide particles in a coke deposit when exposed to strongly carburizing gases (carbon activity ac>1) at elevated temperatures (400-800°C) (Zhang, Schneider and Inden, 2003). Temperature affects both the driving force and rates for reaction, represented by gas phase supersaturation with carbon, and the rates of the various processes involved in converting that energy difference into the dusting process. Dusting occurs only when ac>1. Therefore, process streams such as reformer gas can be benign when hot, but becomes aggressive below critical temperatures. There is considerable confusion in literature as to the effect of temperature on metal dusting (Young, Zhang, Geers and Schütze, 2011).

Alloy 800 is an iron-nickel-chromium alloy that has moderate strength and good resistance to oxidation and carburization at elevated temperatures. It is useful for high-temperature equipment in the petrochemical industry, as the alloy does not form the embrittling sigma phase after long time exposure at 649°C. Excellent resistance to chloride stress-corrosion cracking is another important feature of alloy 800 (www.specialmetals.com, 2004). The alloy has the following typical applications: heat exchangers and process piping; carburizing fixtures and retorts; furnace components; electric range heating-element sheathing; extruded tubing for ethylene and steam methane reforming furnaces; and ammonia effluent coolers (www.hightempmetals.com, 08-06-2017).

The limiting chemical composition of alloy 800 is shown in Table 1. The chromium in the alloy imparts both aqueous and heat resistance. Iron provides resistance to internal oxidation. The nickel content maintains a ductile, austenitic structure. Thus, alloy 800 is readily formed, welded, and machined (www.specialmetals.com, 2004).

Table 1: Chemical Composition of Alloy 800 (www.specialmetals.com, 2004)

Elements	Specification	Alloy 800, As-received
	Weight %	
Carbon	0.10 max	0.07
Manganese	1.50 max	0.76
Chromium	19-23	19.82
Nickel	30-35	31.39
Iron	39.5 min	46.43
Silicon	1.0 max	0.17
Sulphur	0.015 max	0.002
Copper	0.75 max	0.30
Aluminum	0.15-0.60	0.20
Titanium	0.15-0.60	0.27

Alloy 800 experiences metal dusting (MD) at 525°C, which is the temperature at the tube sheet in reformers. The alloy is also used for tube ferrules of the reformers in the petrochemical industry. The temperature inside a reformer train can reach a critical (highest) temperature of 650°C. Therefore, it was the aim of the present work to perform a detailed study of the influence of temperature with time under metal dusting conditions for Alloy 800, with particular emphasis on the tube sheet temperature of 525°C. Special focus is directed towards the microstructural features and the influence of temperature.

Figure 1 shows a schematic diagram of a secondary reformer train at South African Refinery showing areas where metal dusting is prevalent.

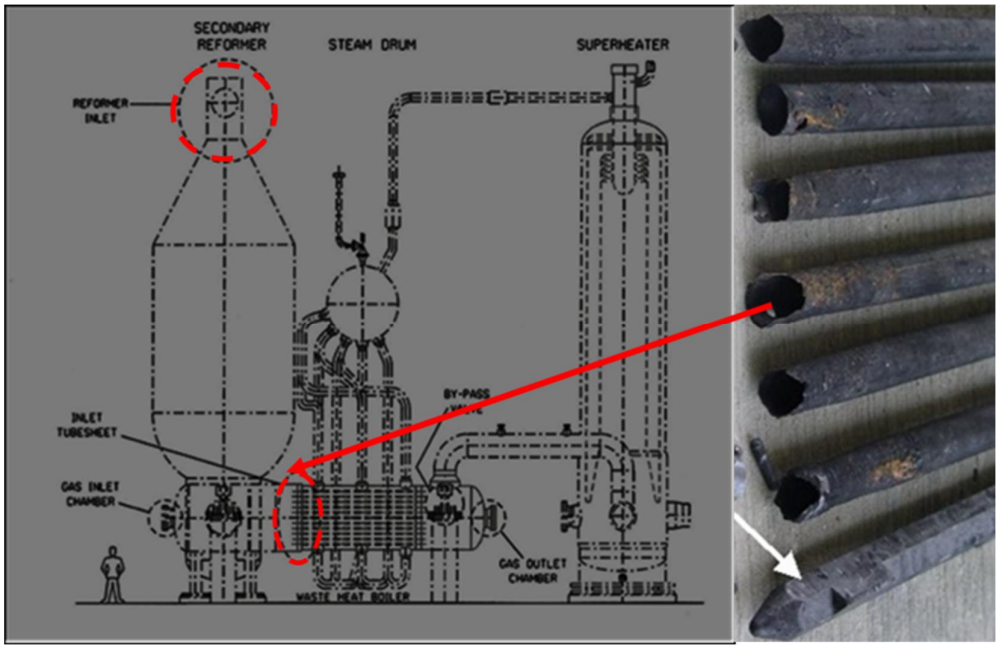

Figure 1. Schematic outline of the secondary reformer train at South African Refinery showing areas where metal dusting mostly occurs (Holland and de Bruyn, 1996).

CHAPTER 2: LITERATURE REVIEW

2.1 Examples of metal dusting

Metal dusting (MD) or catastrophic carburisation is the disintegration of metals and alloys into a dust of metal particles, oxides and graphite with the formation of hemispherical pits or general attack. This occurs at high temperatures in carburising atmospheres or, more commonly, in carburising and selectively oxidising atmospheres (Rohnert, Phillip, Reuther, Weber, Wessel and Shutze, 2007). Chromium-containing alloys can form a protective chromia (Cr_2O_3) scale to resist MD (Rohnert *et al.,* 2007). However, extensive chromium carbide (Cr_3C_2, $Cr_{23}C_6$) precipitation results in the depletion of chromium to such an extent that the protective chromia scale is not maintained, and therefore, MD occurs (Zhang *et al,* 2003). The phenomenon is complex and the corrosion resistance depends on many factors such as the type of material, the stability of the oxide scale with respect to gas composition, temperature, pressure and time, i.e. both environmental and metallurgical factors (Albertsen, 2007).

In many industries, metallic alloys are used as structural components at elevated temperatures in environments of high-carbon activity. For example, in hydrogen and syngas plants, methane and other hydrocarbons are reformed or partially oxidized to produce hydrogen and carbon monoxide. When the carbon-bearing gases are catalysed at elevated temperature, carbon is deposited on the surfaces of vessels, gas-transfer pipes, and other process equipment. The deposited carbon is transferred into the alloy and eventually leads to disintegration into fine particles that are carried away by the flowing gas steam. In the metal-wastage process, pits develop on the surface of alloys and accumulate on the surface forming a mixture of fine powder of carbide or pure metal and carbon dust. This metal-wastage process, called ‘metal dusting’’, is a much more severe problem than carburisation, because equipment or pipes will be totally destroyed after the alloys are pulverised (Zeng and Natesan, 2006). Figure 2 shows an example of MD attack on ferrules in a waste heat boiler in a petrochemical plant (Agüero, et al. 2011).

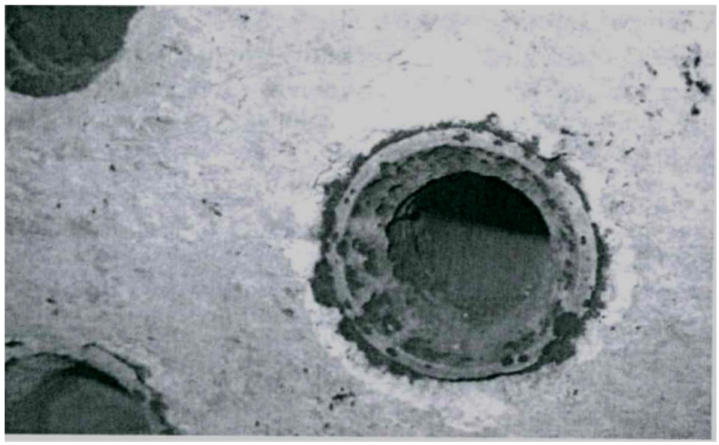

Figure 2.An example of metal dusting attack on ferrules in a waste heat boiler in a petrochemical plant (Agüero, et al. 2011).

Petroleum refineries also operate in a high-carbon-activity environment and experience metal-wastage problems in processes that involve hydrodealkylation and catalyst regeneration. Metal wastage also occurs in direct iron-ore-reduction plants wherein the synthesis gas, comprising of CO and H_2, is dried and reheated to enhance ore-reduction efficiency. The ammonia synthesis process has experienced metal dusting in the heat-recovery section of the reformed-gas system and in the reformer itself. Gases used in the heat-treating systems mix with oil residue on the work-piece and form gases that are chemically favorable for metal dusting (Zeng and Natesan, 2006).

Gas mixtures used for carburising can also cause metal wastage, if the gas chemistry and thereby, the carbon activity, is not controlled. Other scenarios wherein metal wastage occurs are processes that employ carbon dioxide for cooling, recycle-gas loop equipment of coal-gasification units, iron-making blast furnaces in steel plants, and fuel cells that use hydrocarbons (Zeng ***et al.***, 2006). An example of a severe metal dusting attack on a steel sheet from a direct reduction furnace is shown in Figure 3 and Figure 4 shows metal dusting attack in a heater tube of a direct reduction plant at about 600°C.

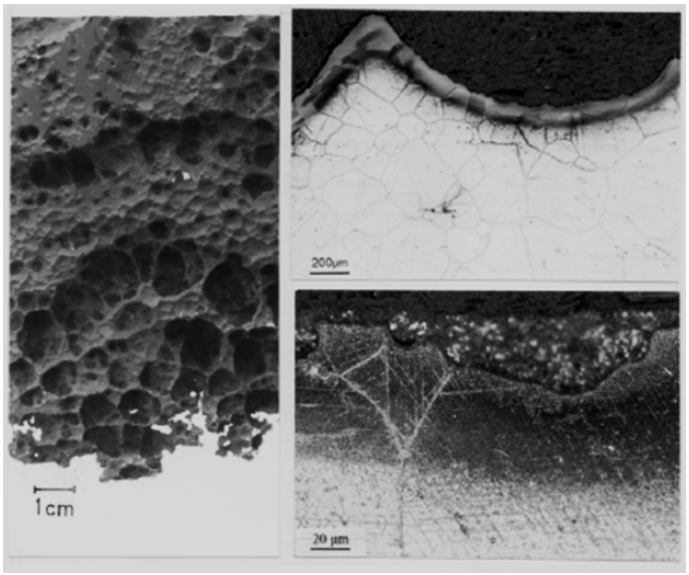

Figure 3. Severe metal dusting attack on a steel sheet (Alloy 800) from a direct reduction furnace; a) piece of the steel sheet with vast erratic pitting, b) and c) metallographic cross sections, showing pits with carburized zone and coke (Grabke and Spiegel, 2003).

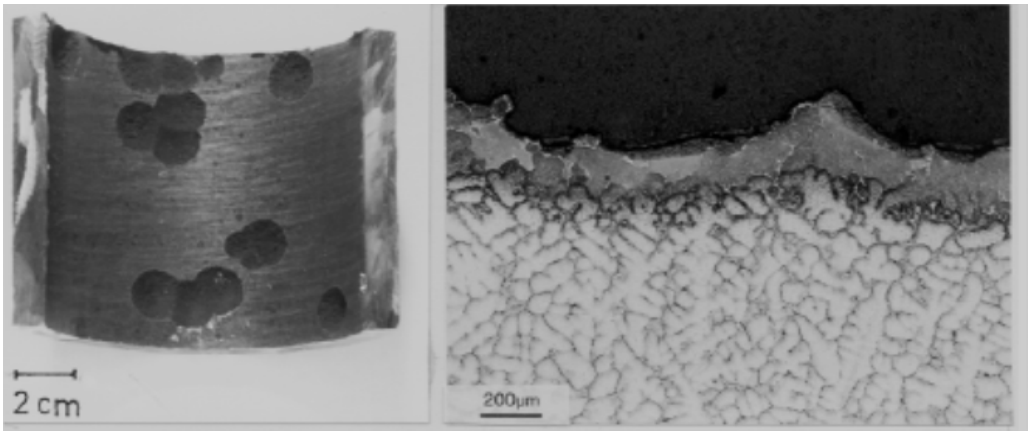

Figure 4. Images of metal dusting attack in a heater tube of a direct reduction plant at about 600°C; a) tube section of HK40with deep pits, b) metallographic cross section, showing pits and carburised zone (Grabke et al., 2003).

2.2 Thermodynamics and kinetics of gas-metal reactions

The precursor for MD is carbon formation from the carbon sources, which are often CO and CH_4. The main reactions for carbon formation from CO are (Agüero*et al.*, 2011):

(i) The Boudouard reaction:

$2CO = C + CO_2 \quad \Delta H_1 = -172.4$ …….....(1)

(ii) The reduction reaction:

$CO + H_2 = C + H_2O \quad \Delta H_2 = -131.3$ kJ ……(2)

The main reaction for C formation from CH_4 is:

$CH_4 = C + 2H_2$ $\Delta H_3 = 74.6$ kJ ….……..……..……..(3)

The thermodynamic potential for the above reactions to proceed to the right, i.e., forming C, is represented by the carbon activity, a_c, which is calculated for these three reactions as:

$$a_{C1} = K_{p1}\frac{P_{CO}^2}{P_{CO_2}} \quad \text{……(4)}$$

$$a_{C2} = K_{p2}\frac{P_{CO}P_{H_2}}{P_{H_2}O} \text{……(5)}$$

$$a_{C3} = K_{p3}\frac{P_{CH_4}}{P_{H_2}^2} \text{……..…….....…..(6)}$$

Where K*pi* is the equilibrium constant of the corresponding reaction and P*i* is the partial pressure of the corresponding gas. When a_c is greater than unity, carbon has the potential to form via the corresponding reaction, although the extent of carbon formation may be limited by the kinetics of the process. When a_c is smaller than unity, thermodynamics state that graphite should not form. It is noted from the above equations that a_c is a function of the temperature and the partial pressures of the gases involved (Agüero *et al.*, 2011).

2.3 Protection by oxide scaling

Surface oxide scales play an important role in the long-term performance of alloys under dusting conditions. Using radioactive carbon, it has been shown that the solubility of carbon in Cr_2O_3 and Al_2O_3 at 1000°C is below the detection limit of 0.01 ppm (Wolf and Grabke, 1985). Scales of these oxides are therefore expected to provide effective diffusion barriers to carbon. Furthermore, most observations suggest that these oxides provide no significant catalytic effect for carbon deposition from the gas (Nishiyama *et al.*, 2005). For such an oxide to continue as a diffusion barrier, it must retain its mechanical integrity as well as chemical stability.

The oxides of iron, cobalt and nickel are unstable at low oxygen potentials of typical dusting atmospheres attack (Young, Zhang, Geers and Schütze, 2011). However, Cr_2O_3, Al_2O_3, SiO_2 and $FeCr_2O_4$ are all stable, and the heat resisting alloys commonly used should therefore be expected to resist metal dusting. However, most of these alloys do fail. One reason is the

relative low temperatures involved and the consequently low alloy diffusion rate. A second reason is that most heat resisting alloys are designed to form external, rather than internal oxides. However, in gases such as synthesis gas, the competing processes are external oxide scaling and carbon attack (Young *et al.*, 2011). Selective oxidation of chromium produces a Cr_2O_3 scale and a chromium-depleted subsurface alloy layer, until local scale damage allows gas access to the metal.

Oxide scales at high temperatures are evolving systems, in which accumulated intrinsic growth stresses interact with stress relief mechanisms, as shown by acoustic emission and microstructural investigations for purely oxidising conditions (Khanna and Jha, 1987 andShutze, 1987). The results of Raman investigations (Rohnert *et al.,* 2007) revealed a chromia peak shift, indicating a high level of compressive stresses in the scale was developed under metal dusting conditions. The present understanding of the stress relief mechanisms in the oxide under these conditions assumes temporary microcracking and subsequent microcrack healing due to the on-going oxidation, resulting in a nano- or microcavity network filled with molecular species from the gas (Shutze, 1987 and Atkinson and Smart, 1987).

The outcome of carbon penetration of the scale will depend on the carbon activity, as well as the other conditions at the scale-alloy interface. A schematic diagram of the mechanisms leading to pitting as a consequence of oxide scale failure is given in Figure 5 (Young *et al.,* 2011).

Figure 5.1 shows the intact oxide scale, or a scale interspersed with fine graphite precipitates. In Figure 5.2 the scale formed cracks through intrinsic oxide growth stresses or by graphite precipitation and growth. The scale cracks wider and further by graphite growth at scale cracks/delaminatios as shown in Figure 5.3. Lastly, a MD pit forms, shown in Figure 5.4, as a consequence of the local scale cracking processes, followed by graphite formation. “Repassivation” can take place in the case of sufficient resupply of protective oxide scale forming alloying elements from the alloy interior.

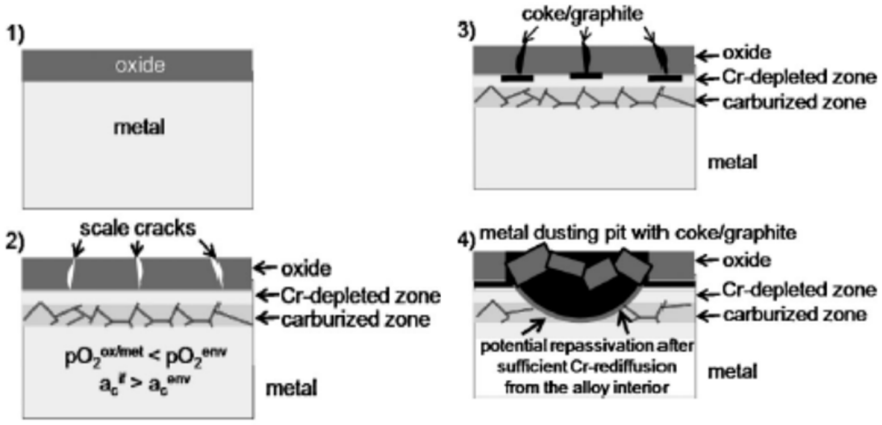

Figure 5.Processes occurring on high alloy materials during local oxide scale failure leading to a growing metal dusting pit (Young et al., 2011).

2.4 metal dusting Mechanisms

The phenomenon of metal dusting has been studied for decades. However, the mechanism of this complex process is still not well understood, although several models have been proposed (Young *et al.*, 2011).

2.4.1 Mechanisms proposed for metal dusting

The phenomenon of metal dusting (MD) may be divided into three main mechanisms denoted Type I, Type II and Type III. Type I, first described by Hochman et al. (1996) and further detailed by Grabke (1995) involves decomposition of metastable cementite. Type II, may be described as disintegration of a carbon supersaturated phase by internal graphitization and was first described by Hultgren and Hillert (1953). Type III, which operates on high alloyed steels and Ni-base alloys, proposed by Szakálos *et al.* (2002) involves selective oxidation of alloyed carbides, i.e. not pure Fe-carbides. A secondary mechanism may be added, carbon nanotube formation, Type IV and may be described as a continued fragmentation of the corrosion products and involves carbon nanotube formation (Szakálos *et al;* 2004). There is seldom only one MD-mechanism operating on a steel or a Ni-base alloy. For example, Types II and III mechanisms operate in conjunction on austenitic stainless steels and Ni-base alloys (Szakálos, 2002). Basic mechanism involves the deposition of carbon, which leads to disintegration of substrate followed by:

- Type I: decomposition of metastable cementite
- Type II: disintegration of carbide by graphitisation
- Type III: selective oxidation alloyed carbides

- Type IV: continued fragmentation of corrosion products by carbon nanotube formation (Hochman and Burson, 1996, Hultgren and Hillert, 1953, Szakálos *et al.,* 2002 and Szakálos, 2004).

2.4.2 Mechanism of Ni-based Alloys

The mechanism of MD depends strongly on the type of alloy involved (Alvarez *et al.,* 2008). The mechanism of MD for iron-base alloys begins with saturation of the alloy matrix with carbon/carbide, usually in a localised manner, and subsequent formation of metastable cementite (Fe_3C). Decomposition of the Fe_3C as the carbon activity approaches unity produces iron particles and powdery carbon. The metal particles then strongly catalyze further carbon deposition. A different mechanism is proposed for nickel-based alloys, which does not involve the formation of intermediate metastable carbide. Such a mechanism begins in the same way as for iron-base alloys, with saturation of the alloy matrix with carbon/carbides. However, in the case of nickel-base alloys, the saturated matrix decomposes directly into metal particles and graphite (Baker and Smith, 2016).

The MD mechanism of Ni alloys differs from that of ferritic material in that cementite is not formed, and the corresponding nickel carbide is unstable. MD of high alloyed steels and CrFeNi-alloys are described with a schematic representation, as shown in Figure 6. The proposed mechanism includes several principal steps (Grakbe and Schütze, 2007) viz: carbon diffuses into the structure, primarily at breaks in the chromium oxide layer, followed by carburization and formation of very fine Cr-rich M_7C_3-carbides (grey zone) and $M_{23}C_6$ carbides in the grain boundaries. Then formation of possibly metastable $(Fe,Ni)_3C$ cementite in the Cr-depleted matrix, followed by cementite decomposition (Type I) and direct fragmentation by graphitisation (Type II). The corrosion products would thus be cementite or Fe/Ni particles, graphite and Cr-rich carbide particles. Lastly, oxidation of the corrosion products in the coke, i.e. oxidation of the very fine Cr-rich carbides, which subsequently would give very fine spinel/chromia particles in the coke.

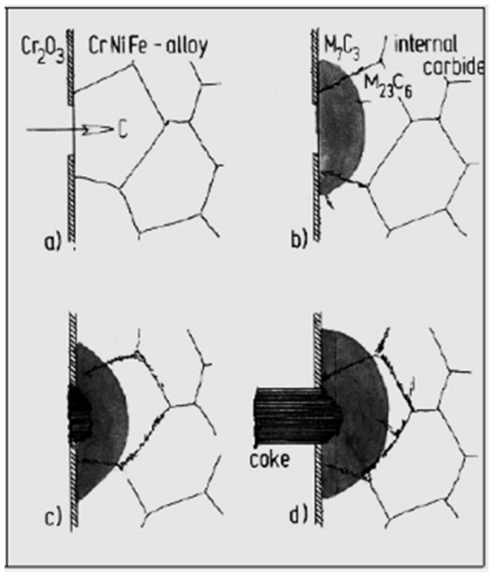

Figure 6.Schematic illustration of the metal dusting mechanism on high alloyed steels and CrFeNi-alloys (Grakbe and Schütze, 2007).

CHAPTER 3. EXPERIMENTAL PROCEDURE

3.1 Introduction

Metal dusting is of great significance to the petrochemical industry because of the potential for costly plant replacement and down-time (Mulaudzi *et al.,* 2012). Prevention of this phenomenon would represent substantial savings in several industrial sectors including: chemical, petrochemical, materials processing (direct reduction and heat treating), power generation among others, where loses due to metal dusting have a significant impact. Futhermore, prevention of metal dusting may also be beneficial in the development of alternative energy resources (Alvarez *et al.,* 2008).

Safe and secure operation of critical plant items requires a recognition and an understanding of the processes that affect component integrity and life. Carburization is common in many fired heater tubes in hydrocarbon service; certain components in fluidized catalytic cracking units (FCCUs) can be affected and the issue is also known in steam methane reformers (SMRs).Carburization in refinery fired heaters tends to be specific to certain types of service – crude and vacuum heaters, coker heaters and visbreakers are often affected and share a trend in progressively increasing feedstock density, (Franks et al., 2017).

3.2 Research objectives:

The aim of this work was to determine the mechanism of MD for Alloy 800 at two different temperatures of 525°C and 650°C. In order to do this the following objectives apply:

- To evaluate the effect of temperature and time on the MD of Alloy 800; two temperatures at five different exposure times, under a controlled metal dusting environment of $25CO - 70H_2 - 5H_20$.
- To investigate the effects of metal dusting on the grain boundary of Alloy 800.

3.3 Test samples and parameters

Duplicate coupons of Alloy 800 of 20x20 mm with a 5 mm hole (in the centre) size were used for the experiments. The research approach of the project was to expose Alloy 800 to two different temperatures of 525°C and 650°C, under a controlled metal dusting environment of $25CO–70H_2–5H_20$, to determine the deterioration with exposure time. The samples were

suspended in the furnace, as shown in Figure 7. Table 2 gives a summary of the test parameters that were used during exposure of the samples.

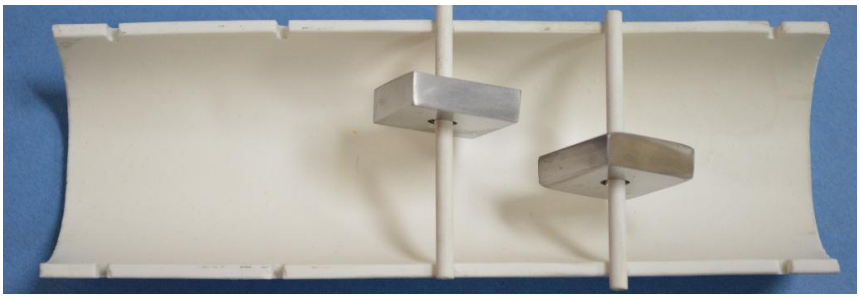

Figure 7. A photograph of the samples illustrating how they were suspended inside the ceramic boat.

Table 2. Test parameters used during exposure of the samples

Exposure time (h)	**Temperature (°C)**	
	525	**650**
24	2	2
72	2	2
168	2	2
336	2	2

3.4 Sample preparation

The surface condition affects the metal dusting resistance, since ground surfaces are more resistant due to greater mobility of chromium to repair surface protective scales. Therefore, samples were tested in the ground condition with a 320-grit silicon carbide finish. This was done to closely simulate the condition of material surfaces encountered in practice and to obtain a direct comparison between the different experimental results and plant life.

The dimensions of the samples were measured with a digital calliper to the nearest 0.1mm and the samples were stored in plastic bags. Immediately prior to testing, the samples were degreased with acetone and weighed to the nearest 0.1 mg.

3.5 Test procedures

The tests were performed in a test rig, shown in Figure 8, which was purpose built to control the gas compositions at elevated temperatures in the MD regime. For this, a horizontal ceramic

tube furnace (Vectstar furnaces) was used with 316 stainless steel gas tubing capable of supplying a constant mixture of CO and H_2.

Figure 8.A photograph of the Metal Dusting Test Rig at Mintek

Nitrogen was also used as a purging gas before the tests were started. Mass flow controllers were used to regulate the gas flow rates to obtain the desired mixing ratios. Water vapour was supplied with a HPLC pump. All the gas and water vapour tubes were wrapped with heating tape and the temperature was maintained at 120°C. Firstly, nitrogen was passed through the furnace once the samples were loaded to flush out any oxygen in the system and to reduce the oxygen partial pressure. The system was flushed with nitrogen for a minimum of one hour before the temperature was increased to the test temperature. Once the furnace reached the set temperature, the CO and H_2 flow rates were adjusted using mass flow controllers that regulates the gas mixtures. The gas was mixed together with the water vapour, and passed through the furnace. The gas flow rate and temperature was maintained constant throughout the different exposure periods used (i.e. isothermal testing).

3.6 Sample characteristics

Before exposure the samples were visually examined and photographs were taken with a digital camera in the as-ground condition. This was to ensure that a record was kept of the samples before exposure. The weight change of the samples was determined to assess coking and metal wastage. The samples were also weighed before and after exposure. After exposure the samples were sectioned and copper plated using a solution of cupric sulphate (Cu_2SO_4), to retain products on the surface and for edge retention during polishing. Metallography was performed using an optical microscope (Olympus DSX – CB, Model DSX-HRSU) to do microstructural analysis of the samples in the as-polished and etched conditions. Scanning electron microscopy

(SEM) (FEI, NOVASEM 200, Model - D8107) equipped with energy-dispersive X-ray spectroscopy (EDX) was used for the surface and cross-sectional analysis. X-ray diffraction (XRD) (Bruker AXS, Model - Diffractometer D8) was also used for phase identification and crystal structure of the metal samples and coke product. Raman spectroscopy (Perkin Elmer Precisely, Model - RamanStation 200) and Transmission Electron Microscope (TEM) (JEOL, Model – JEM – 2100F) were used to characterise the coke product that formed.

CHAPTER 4: RESULTS

This section will cover all the results obtained from the tests and analyses performed on the Alloy 800 samples. The alloy was exposed at two different temperatures of 525°C and 650°C, for one day (24 hours), three days (72 hours), seven days (168 hours) and fourteen days (336 hours) continuously in a tube furnace. In all the tests, duplicate coupon samples were exposed and inserted simultaneously into the furnace, to a gas mixture of 25CO–70H_2 5H_2O. Following the exposure in the furnace, all the samples were analysed visually, by photographic record, weight / mass change, metallography, Scanning Electron Microscopy (SEM), X-ray diffraction (XRD), Raman spectrometry and Transmission Electron Microscopy (TEM).

4.1 24 h exposure

Samples 10 and 12 were exposed to the gas mixture at 525°C and samples 1 and 2 at 650°C.

4.1.1 Visual examination

Figure 9(a) and 10(a) show the photographs of the samples after exposure for 24 h at 525°C and 650°C, also demonstrating how the samples were suspended in a ceramic boat with ceramic rods. After exposure the samples had a brownish/purplish colour on the surface, as shown on Figure 9(b) and 10(b).

Figure 9. Photographs of the samples after 24 h exposure at a temperature of 525°C, a) from the furnace and b) removed from the boat.

Very little coking or attack initiation was observed on sample1 tested at 650°C, see Figure 10(a). All the samples showed minor discolouration and no appreciable weight changes. This suggest that no significant corrosive attack took place.

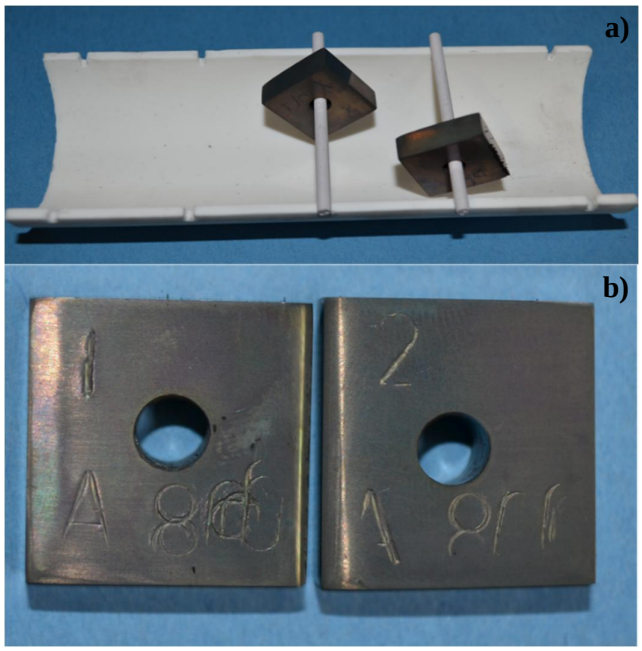

Figure 10. Photographs of the samples after 24 h exposure at a temperature of 650°C, a) from the furnace and b) removed from the boat.

4.1.2 Weight Change

Table 3 gives a summary of the weight changes data observed on the samples tested. No significant weight changes were observed on the samples exposed for 24 has removed from the furnace. However, Samples 1, 2 & 12 have gained little weight, while sample 10 lost a bit of weight.

Table 3. Weight / mass change data after all the tests

Expo. Time (Hrs)	Temp. (°C)		Sample ID	Weight Loss / Gain (g)	Corrosion Rate, mm/yr	Average Corrosion Rate, mm/yr
	525	650				
24	√		10	0.0010	0.0379	-0.0249
	√		12	-0.0023	-0.0877	
		√	1	-0.0003	-0.0113	-0.0208
		√	2	-0.0008	-0.0302	
72	√		20	0.0009	0.0114	0.0191
	√		21	0.0021	0.0267	
		√	3	0.0006	0.0076	0.0178
		√	4	0.0022	0.0279	
168	√		7	0.0019	0.0103	0.00708
	√		8	0.0007	0.0038	
		√	18	0.0068	0.0370	0.04624
		√	19	0.0102	0.0555	
336	√		5	0.0075	0.0203	0.0103
	√		6	0.0001	0.0003	
		√	1*	0.0068	0.0183	0.0249
		√	2*	0.0117	0.0315	

4.1.3 Metallography

Cross-sections of the samples exposed for 24 h at 525°C and 650°C were investigated. The samples were analysed in the as-polished condition and no attack was evident, as shown in Figure 11 and 13. The samples were then etched and still did not show any attack, see Figures 12 and 14.

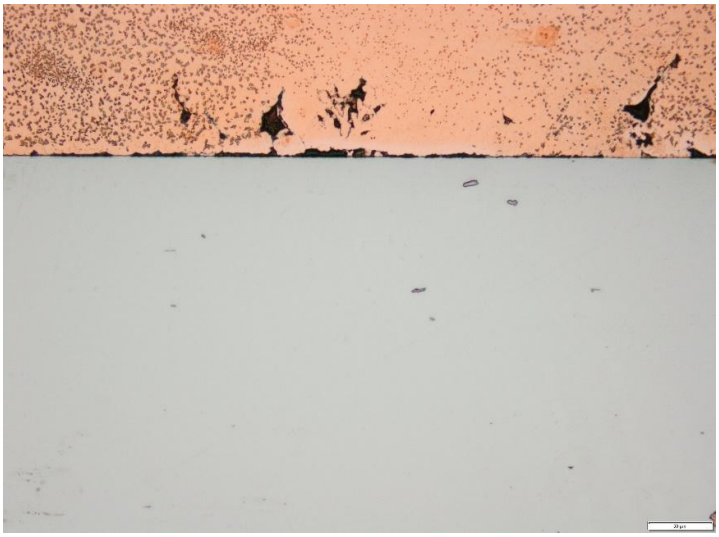

Figure 11. Micrograph of a cross-section through 24 h exposure, 525°C sample (copper plated) showing no significant metal wastage.

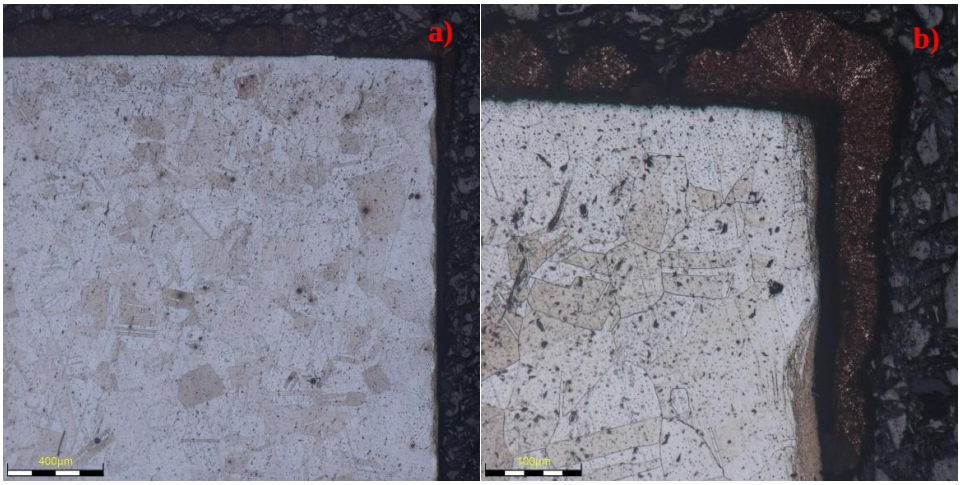

Figure 12. Micrographs of the samples after 24 h exposure at 525°C, after etching, a) low magnification and b) high magnification.

Figure 13. Micrograph of the sample after 24 h exposure at 650°C.

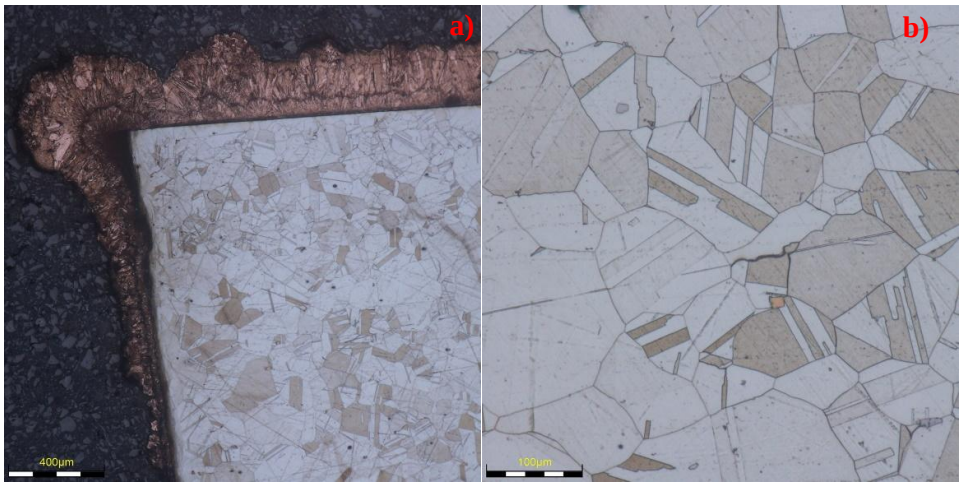

Figure 14. Micrographs of the samples after 24 h exposure at 650°C after etching, a) low magnification and b) high magnification.

4.1.4 Scanning Electron Microscopy (SEM)

The samples did not show any significant surface features under the SEM after 24 h exposure at 525°C. There was no also significant coking observed on these samples. Figure 15 is a SEM image of the sample tested at 525°C showing small platelets as well as black and grey deposits, on the surface. At 650°C, the sample surface had more platelets as compared to the sample exposed at 525°C, as shown in Figure 16. At both temperatures of 525°C and 650°C, the samples formed a more uniform oxide layer, although at 650°C the layer was thicker, as shown in Figures 17 and 18.

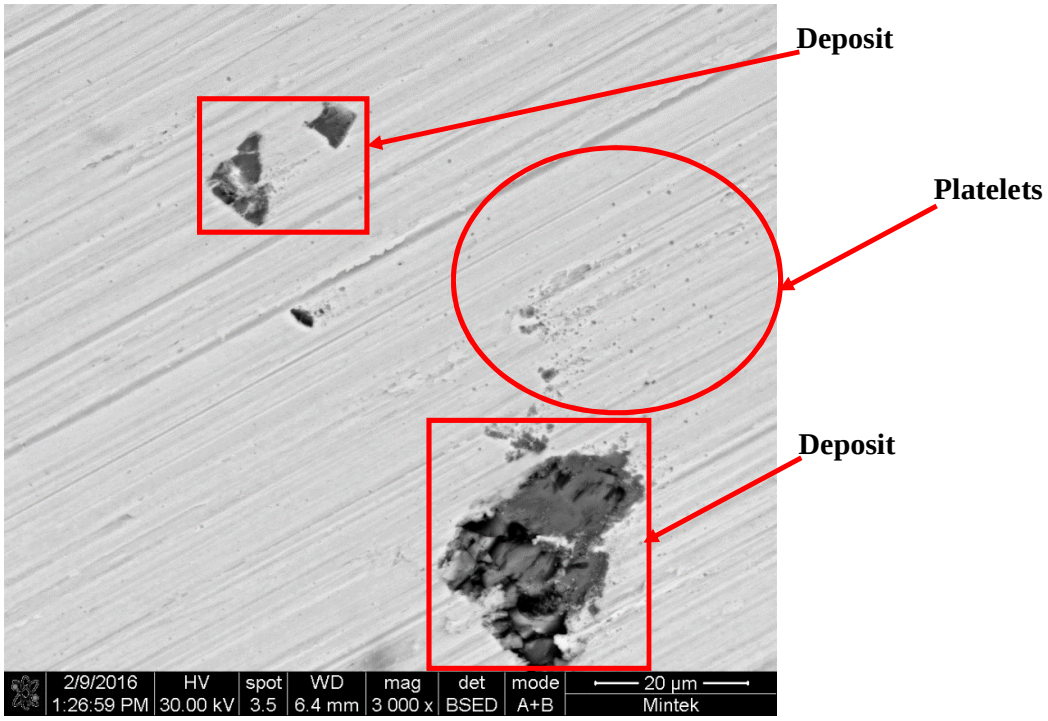

Figure 15. SEM image of the sample surface after 24 h exposure at 525°C, showing small platelets and deposits.

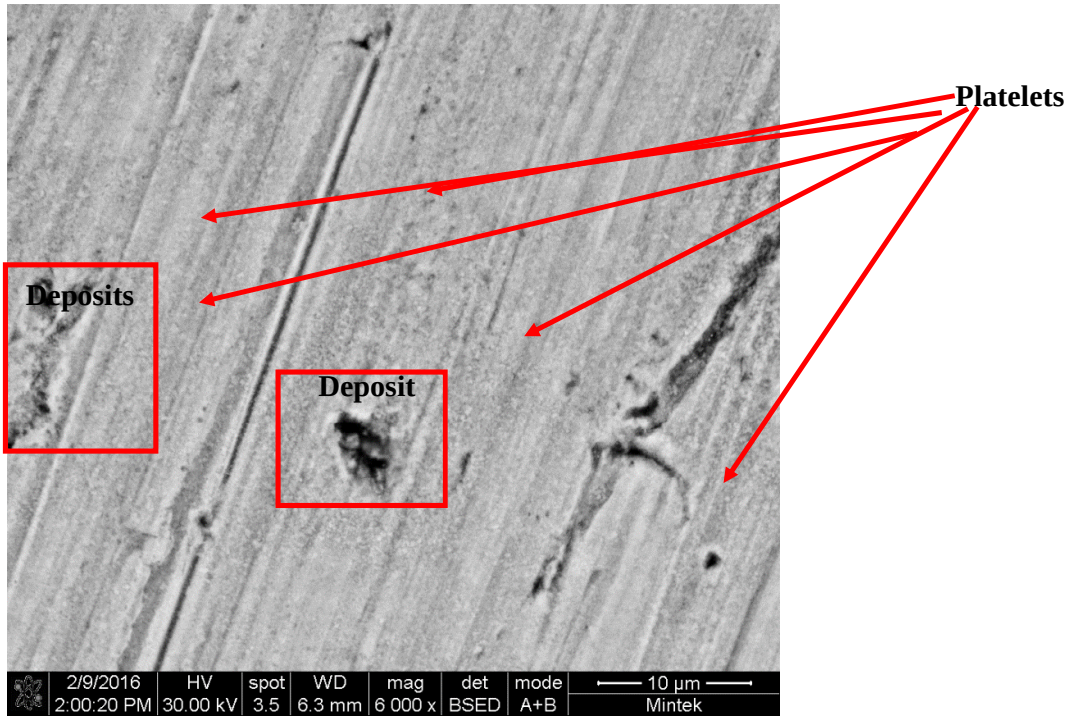

Figure 16. SEM image of the sample surface after 24 h exposure at 650°C, showing more platelets on the surface.

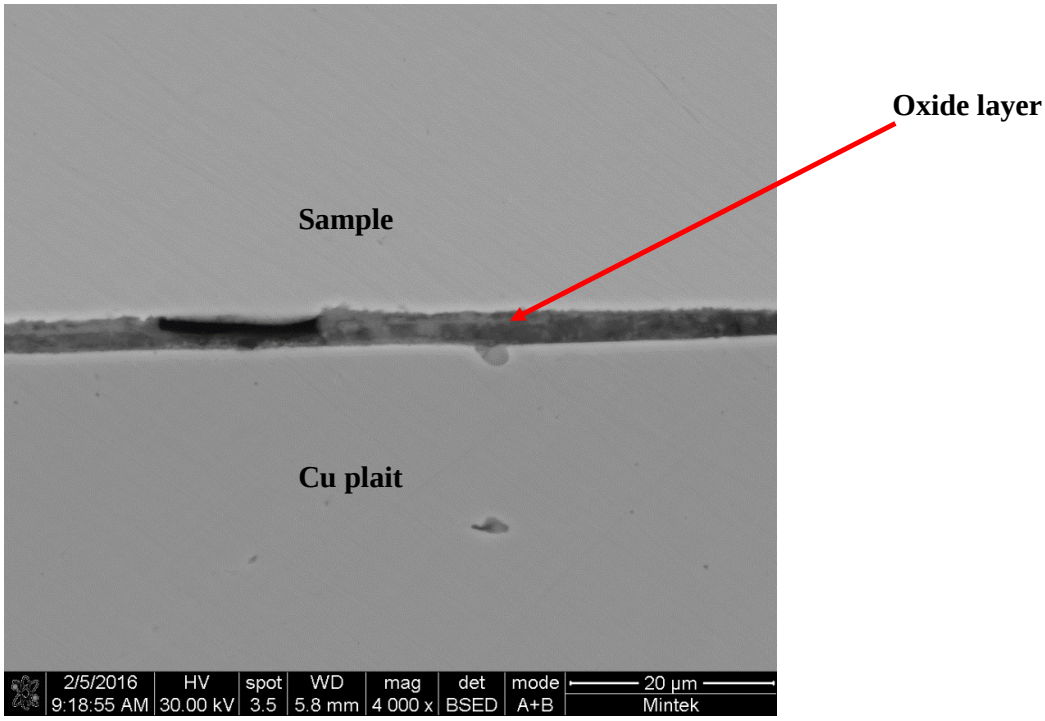

Figure 17. A SEM image of the sample surface after 24 h exposure at 525°C, showing a uniform oxide layer.

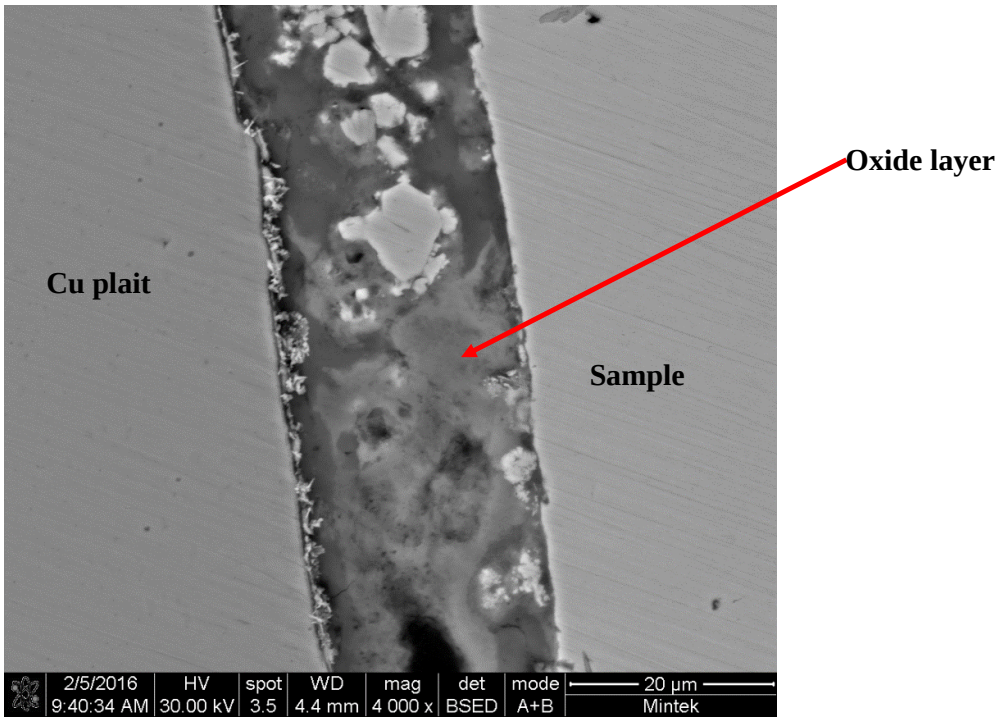

Figure 18. A SEM image of the sample surface after 24 h exposure at 650°C, showing a thicker and uniform oxide layer.

Figure 19 is an EDX spectrum of the oxide layer/deposit on the mounted sample exposed at 525°C which consisted predominantly of iron, nickel and chromium with manganese, titanium, oxygen, chloride and molybdenum; the copper was from the copper plating used to protect the surface of the samples. Figure 20 is an EDX spectrum of the oxide layer/deposit on the mounted sample exposed at 650°C illustrating that it primarily consists of iron and chromium, with oxygen, chloride and sulphur; the copper was from the copper plating used to protect the surface of the samples after exposure.

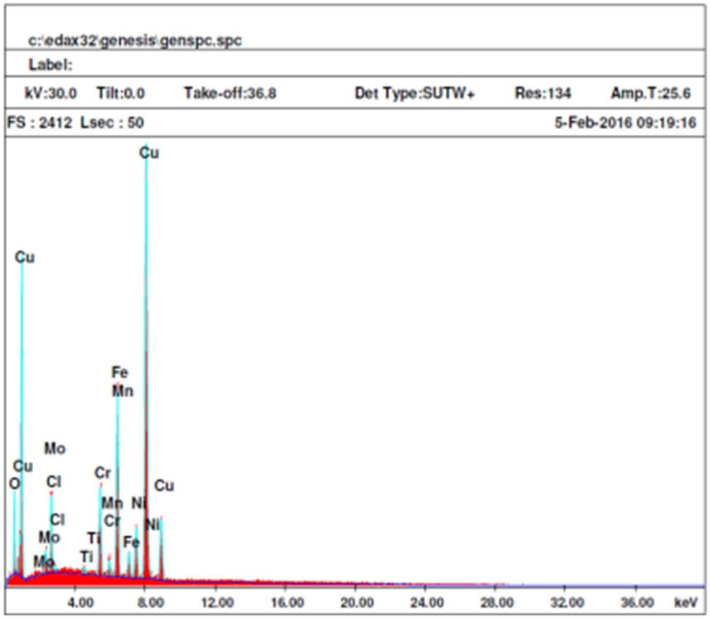

Figure 19. EDX spectrum of the sample exposed for 24 hours at 525°C and the oxide layer (including matrix) consisting predominantly of iron, nickel and chromium with manganese, titanium, oxygen, chloride and molybdenum; the copper is from the copper plating.

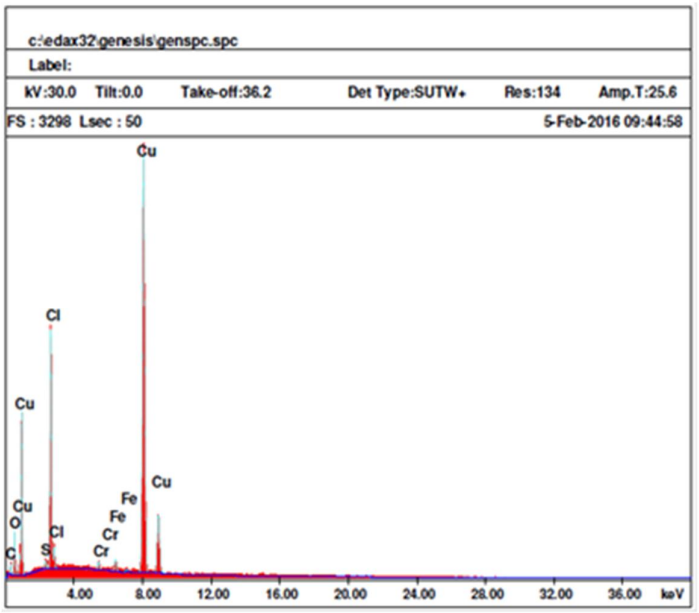

Figure 20. EDX spectrum of the sample exposed for 24 hours at 650°C and oxide layer (including matrix) consisting predominantly of iron and chromium, with oxygen, chloride and sulphur; the copper is from the copper plating.

4.1.5 X-ray diffraction (XRD)

Figures 21 and 22 show the X-ray spectrum of the surface of the metal samples exposed for 24 h at 525°C and 650°C. The structure predominantly consists of ferrite (Fe) and chromium-carbide, as expected.

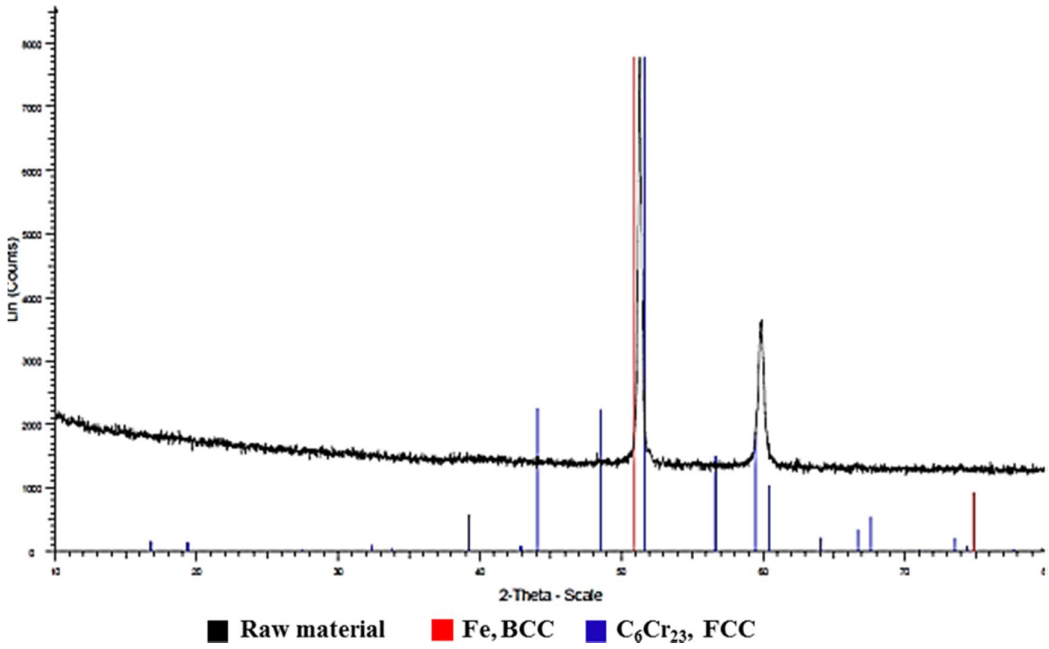

Figure 21. X-ray spectrum of the sample exposed for 24 h at 525° showing the Fe and C_6Cr_{23} peaks.

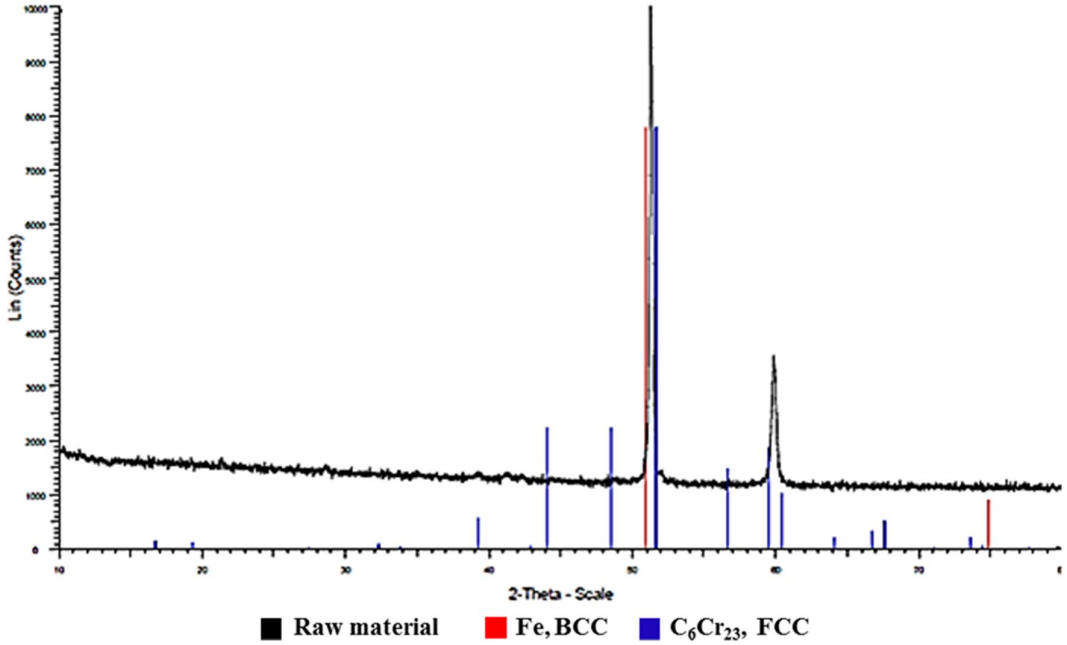

Figure 22. X-ray spectrum of the sample exposed for 24 h at 650°C showing the Fe and C_6Cr_{23} peaks.

4.2 72 h exposure period

The alloy suffered metal dusting attack after a relatively short period of exposure time of 72 hours at both 525°C and 650°C. The samples tested here were labelled as 3, 4, 20 and 21.

4.2.1 Visual examination

Photographs of the samples as-removed from the furnace are shown in Figure 23 and 24. Minor coking was observed with minor pitting at 650°C. These samples appeared slightly more tarnished than the samples that were exposed for 24 h, see Figure 23(b) and 24(b) for close-up images of the samples. Isolated pits were observed on sample 3 and 4 tested at 650°C. No pitting was observed on sample 20 and 21 tested at 525°C.

Figure 23. The samples after 72 h exposure at a temperature of 525°C, a) from the furnace and b) removed from the boat.

Figure 24. The samples after 72 h exposure at a temperature of 650°C, a) from the furnace and b) removed from the boat.

4.2.2 Weight change

Samples 3 and 20 showed minor weight loss as compared to samples 4 and 21, which showed slightly more weight loss and a significant corrosion rate. More coking was observed on both of these samples, as seen in Figure 24(a). Table 3 gives a summary of these weight changes.

4.2.3 Metallography

These samples were also sectioned and analysed in the as-polished as well as etched condition. Figure 25 shows a micrograph of the sample exposed for 72 h at 525℃, in the as-polished condition showing no attack. The sample did not show any attack even after etching, as seen in Figure 26.

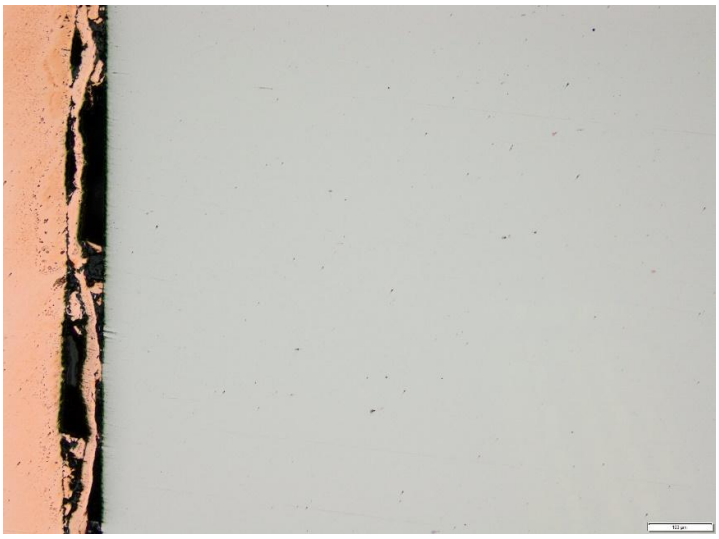

Figure 25. Micrograph of the sample after 72 hr exposure at 525°C.

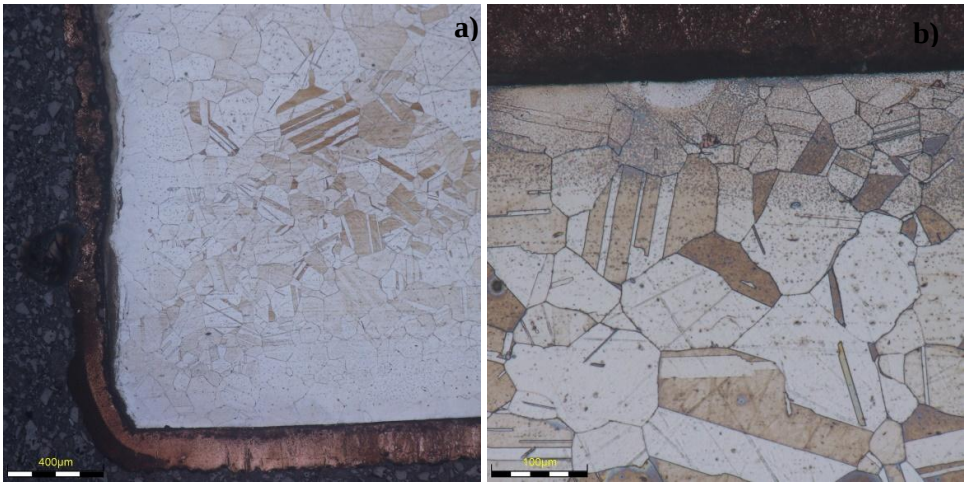

Figure 26. Micrograph of the sample after 72 hr exposure at 525°C, after etching, (a) low magnification and (b) high magnification.

After exposure at a temperature of 650℃ for 72 h, the samples showed some selective attack associated with the titanium carbo-nitride precipitates, as seen Figure 27. Figure 28 shows the micrographs after etching.

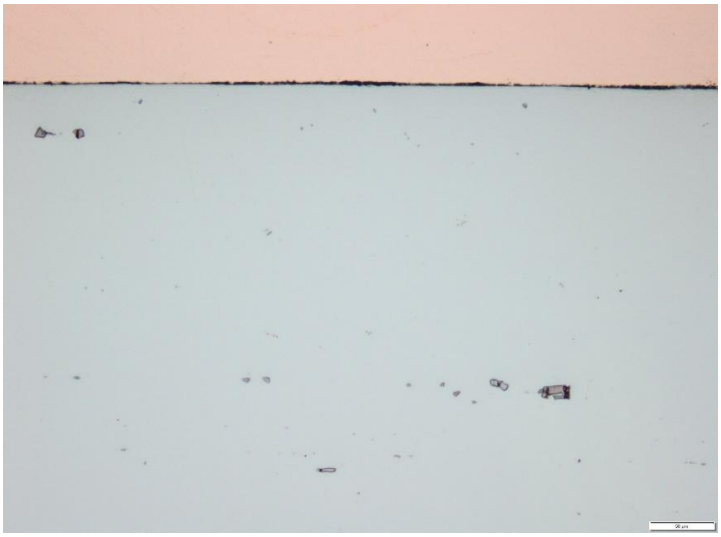

Figure 27. Micrograph of the sample after 72 h exposure at 650°C, showing the titanium carbo-nitride precipitates.

Figure 28. Micrograph of the sample after 72 h exposure at 650°C, after etching showing attack on the edges in a form of a pit, (a) low magnification and (b) high magnification.

4.2.4 Scanning Electron Microscopy (SEM)

4.2.4.1 SEM of metal samples

After the 72 h exposure at 525°C, a uniform oxide layer was evident as shown in Figure 30, than the one observed after 24 h exposure at 525°C. Figure 29 is a SEM image of the sample surface tested at 525°C for 72 h showing more platelets and black deposit on the surface. Intergranular attack was also evident on the sample, under SEM, as seen in Figure 31 and 32. The EDX spectrum of the substrate after the 72 h at 525°C test consisted of iron, nickel and chromium with titanium and vanadium, see Figure 32. Figure 33 shows the EDX spectrum of the black deposit on the surface of the sample (as shown in Figure 29). The EDX spectrum of

the matrix on the surface is shown in Figure 34 and consists of iron, nickel and chromium with chloride, silicon and sulphur; the copper is from the copper plating.

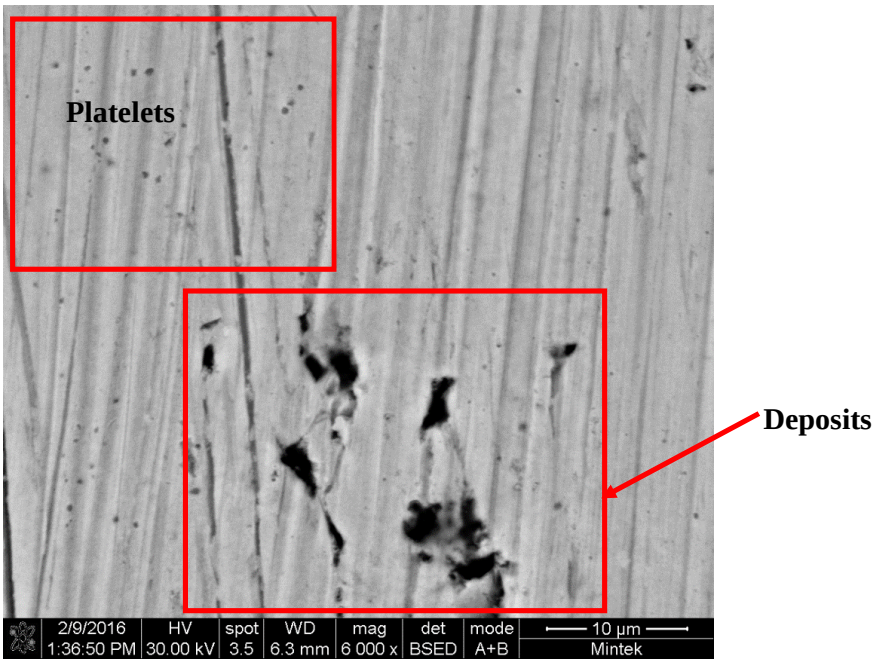

Figure 29. SEM image of the sample surface after 72 h exposure at 525°C, showing platelets and deposits (black).

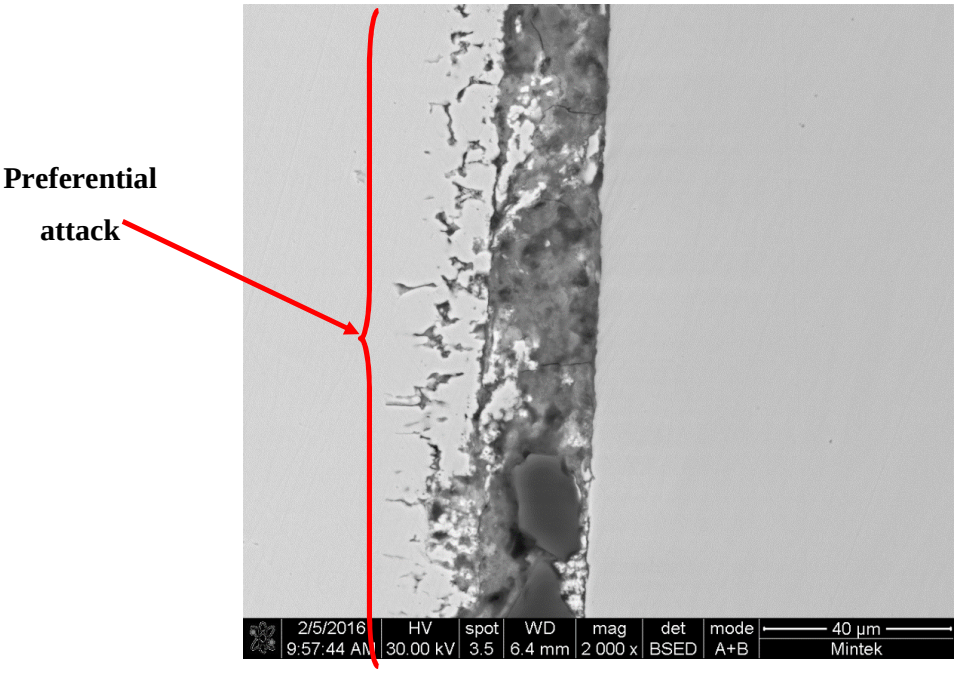

Figure 30. SEM image of the sample surface after 72 h exposure at 525°C, showing a uniform thick layer and preferential attack.

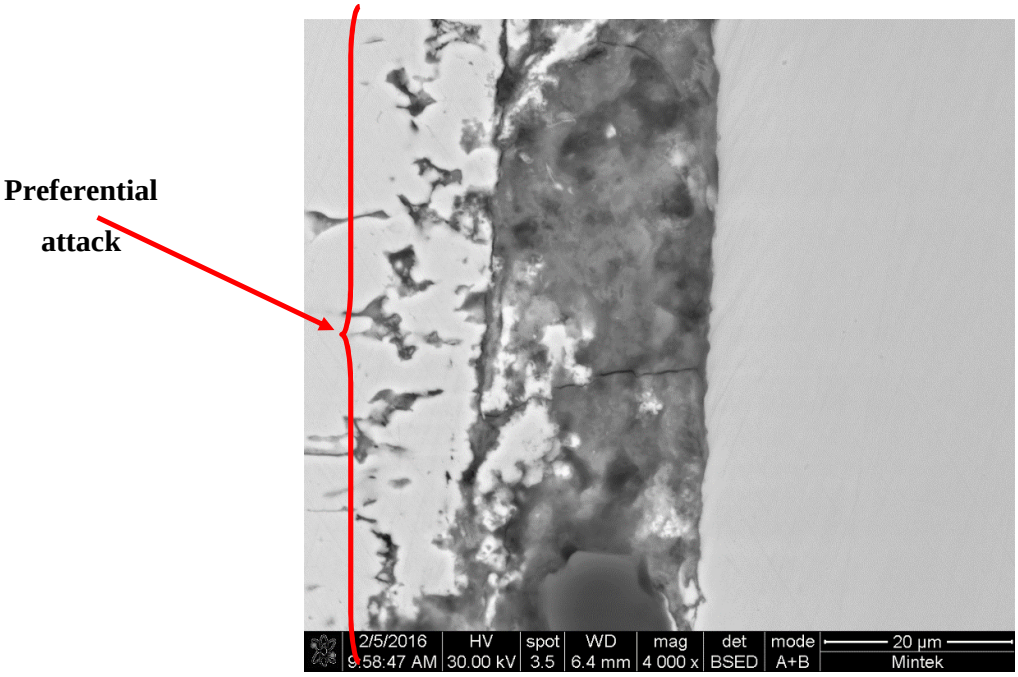

Figure 31. A higher magnification of SEM image of the sample surface after 72 h exposure at 525°C, showing a uniform thick layer and preferential attack.

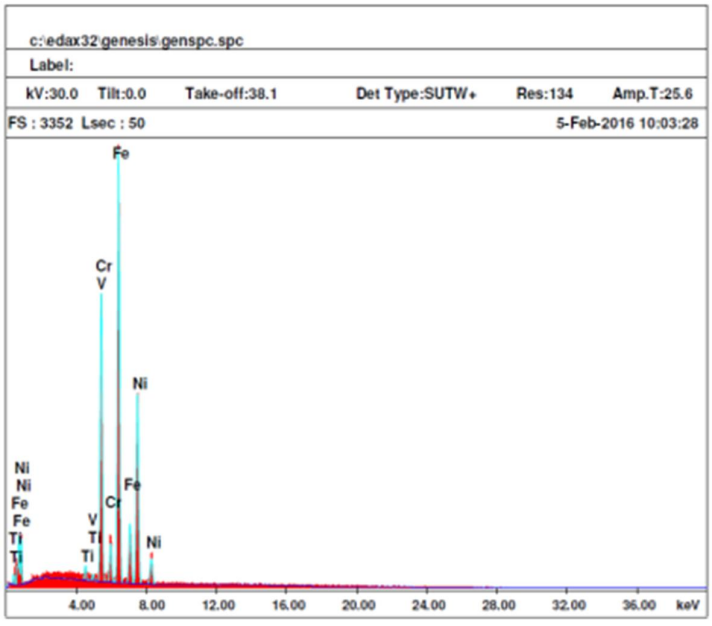

Figure 32. EDX spectrum of the sample exposed for 72 h at 525°C substrate consisting predominantly of iron, nickel, chromium and vanadium, with titanium.

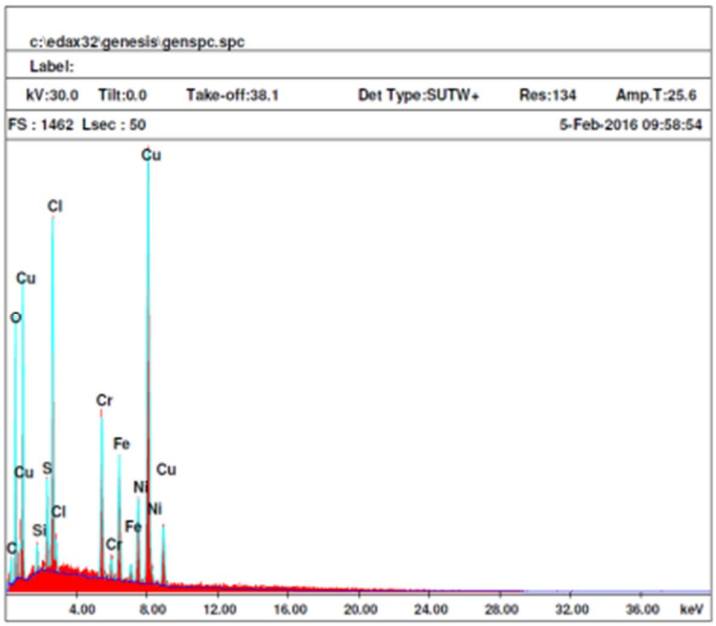

Figure 33. EDX spectrum of the matrix/surface after 72 h at 525°C exposure which consisted of iron, nickel and chromium with chloride, silicon and sulphur; the copper is from the copper plating.

More platelets were observed on the sample exposed at 650°C as compared to the sample at 525°C, as seen Figure 34. A more uniform oxide layer was also observed under the SEM on the samples exposed for 72 h at 650°C, although there was no attack evident on the surface, as shown in Figure 35. The EDX spectrum of the substrate after the 72 h at 650°C exposure sample consists of iron, nickel and chromium with titanium and vanadium, as shown in Figure 36.

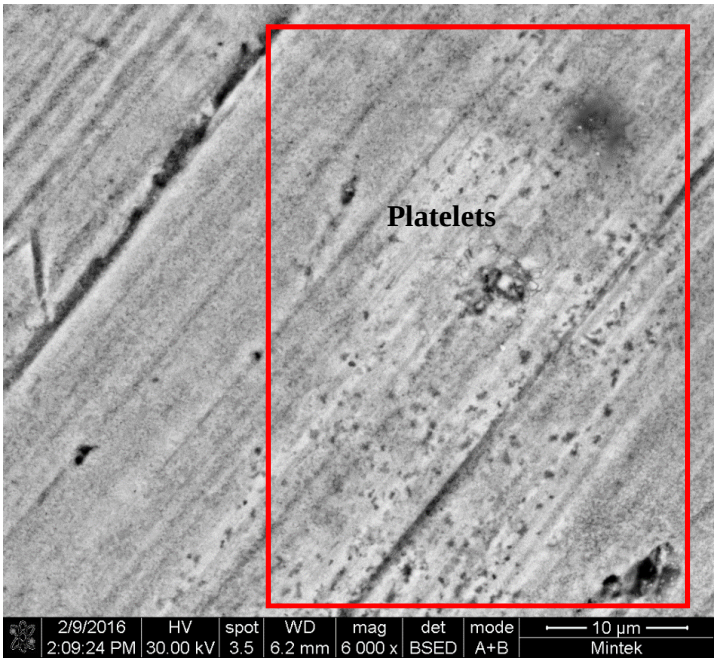

Figure 34. A SEM image of the sample surface after 72 h exposure at 650°C, showing more platelets.

Figure 37 is an EDX spectrum of the oxide layer / deposit on the mounted sample exposed at 650°C illustrating that it primarily consists of iron and chromium with oxygen, sulphur, cobalt, chloride and manganese; the copper is from the copper plating used to protect the surface of the samples after exposure.

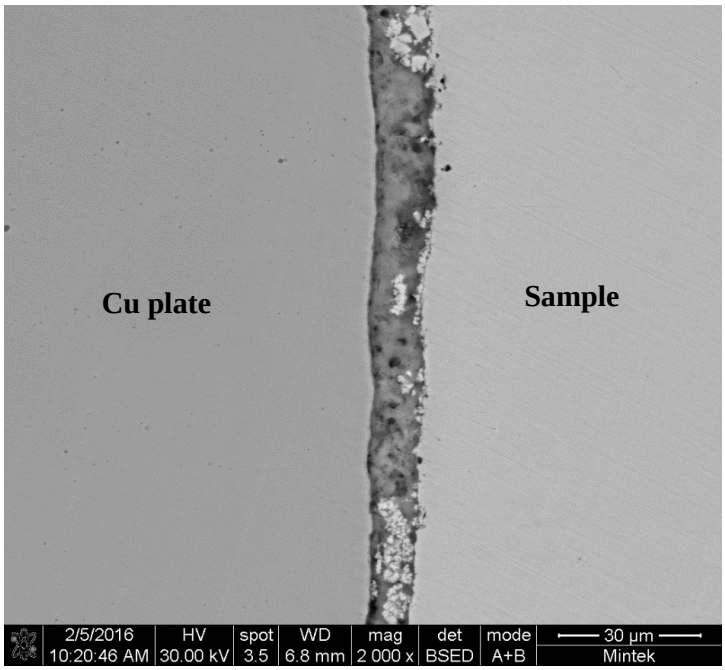

Figure 35. SEM image of the sample surface after 72 h exposure at 650°C, showing a uniform layer.

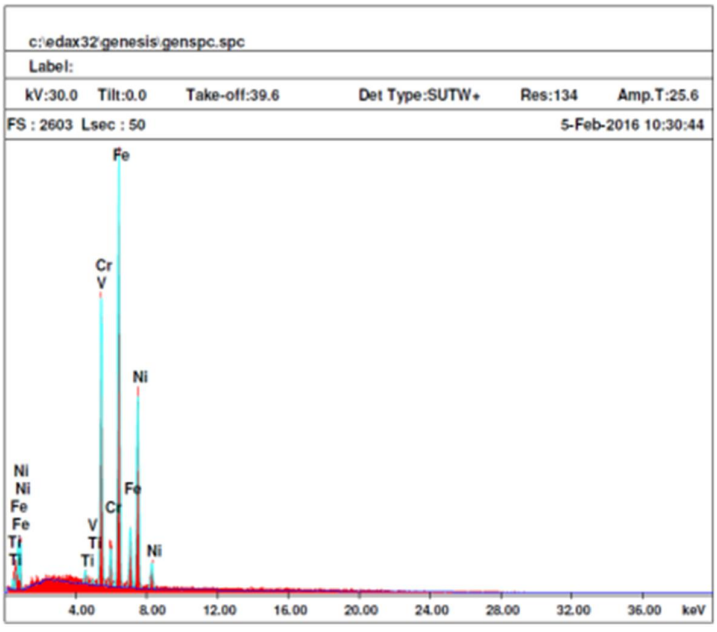

Figure 36. EDX spectrum of the matrix of the sample exposed for 72 h at 650°C, which consisted predominantly of iron, nickel, chromium and vanadium, with titanium.

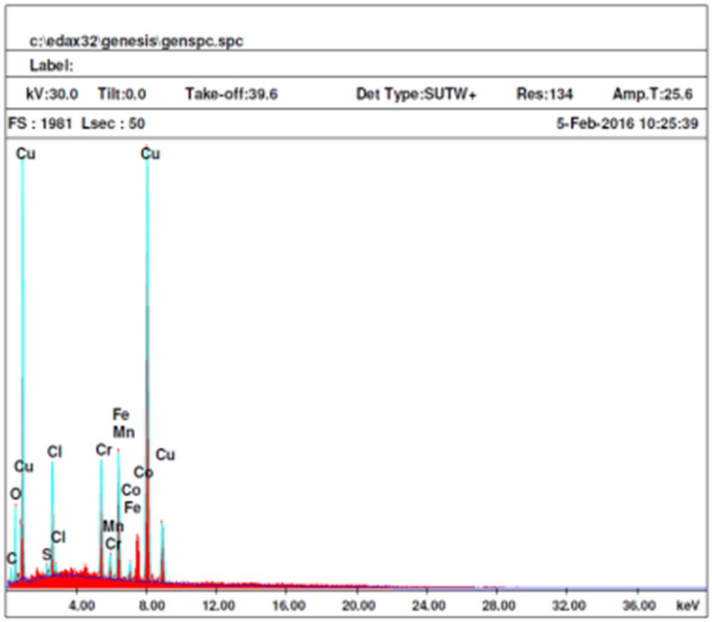

Figure 37. EDX spectrum of the mounted sample (72 hours - 650°C) surface deposit consisting of iron and chromium with oxygen, sulphur, cobalt, chloride and manganese; the copper is from the copper plating.

4.2.4.2 SEM of coke products (72 h at 525°C and 650°C)

Figure 38 and 40 are SEM images of the coke products from the samples exposed for 72 h at 525°C and 650°C. The images show the coke filaments with carbides (metal dust at the tips, found in the coke product as expected. Figure 39 and 41 is an EDX spectrum of the coke product after 72 h exposure at 525°C and 650°C, which consisted of carbon, iron, chromium, nickel and oxygen.

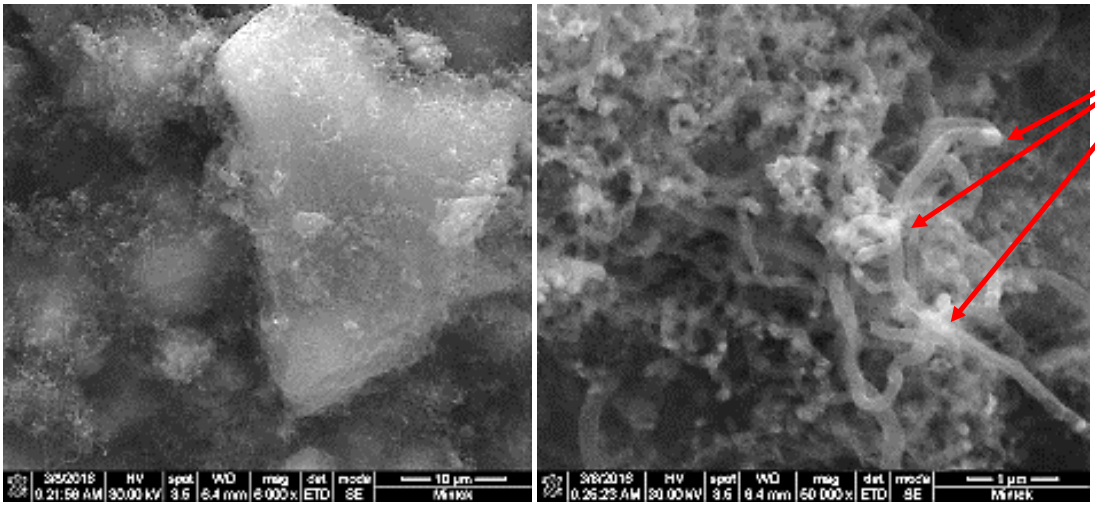

Figure 38. SEM images of carbon filaments of the coke product after 72 h exposure at 525°C with carbides (metal dust) at the tips, left – low magnification and right – high magnification.

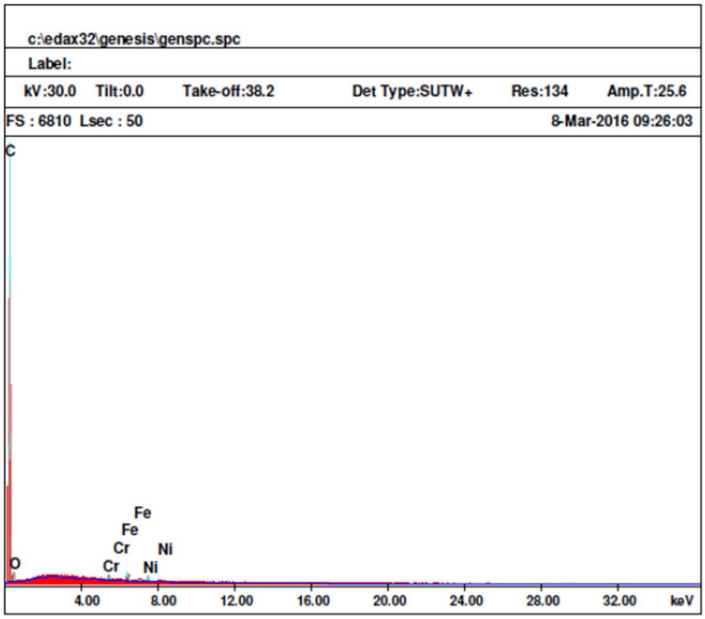

Figure 39. EDX spectrum of the coke product of the sample after 72 hours at 525°C which consisted of carbon, iron, chromium, nickel and oxygen.

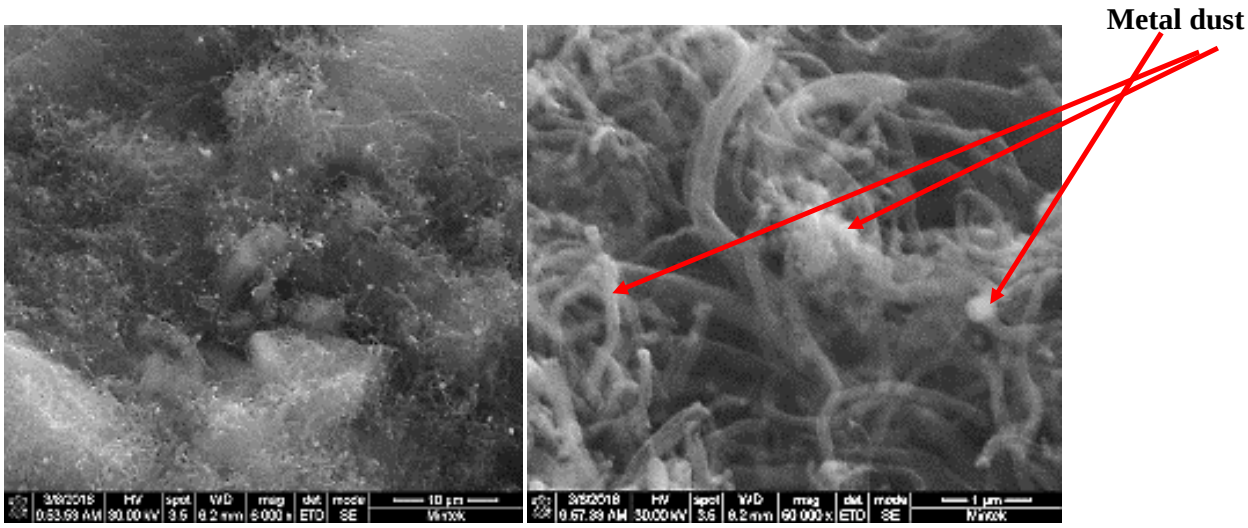

Figure 40. SEM images of carbon filaments of the coke product after 72 hr exposure at 650°C with carbides (metal dust) at the tips, left – low magnification and right – high magnification.

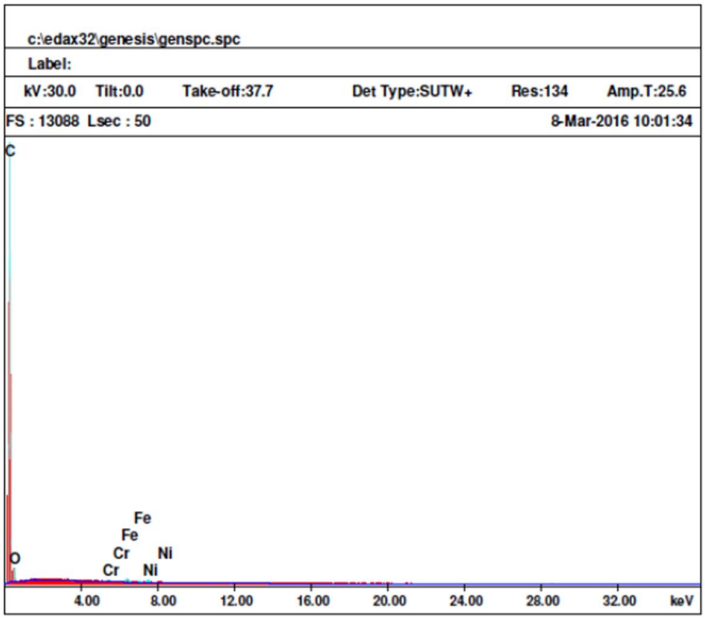

Figure 41. EDX spectrum of the coke product of the sample after 72 hours at 650°C which consisted of carbon, iron, chromium, nickel and oxygen.

4.2.5 X-ray diffraction (XRD)

4.2.5.1 XRD of metal samples

Figure 42 and 43 show the XRD spectrums of the metal/matrix of the samples after exposure for 72 h at 525°C and 650°C, which consisted of iron (Fe) and chromium carbide (C_6Cr_{23}), as expected.

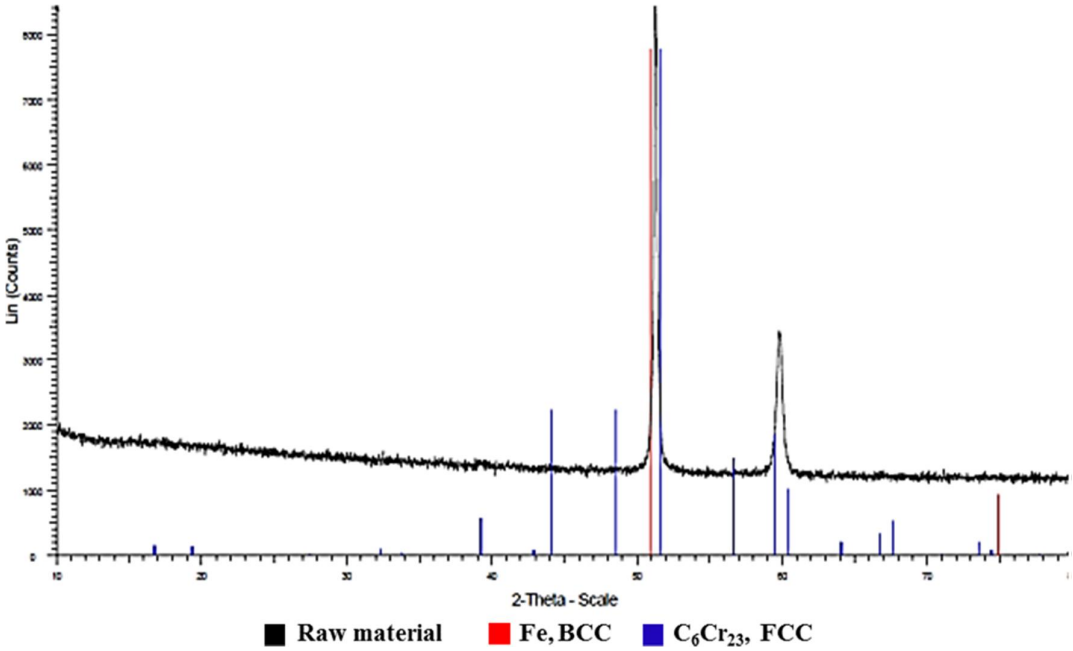

Figure 42. X-ray spectrum of the sample exposed for 72 hours at 525°C showing the Fe and C_6Cr_{23} peaks.

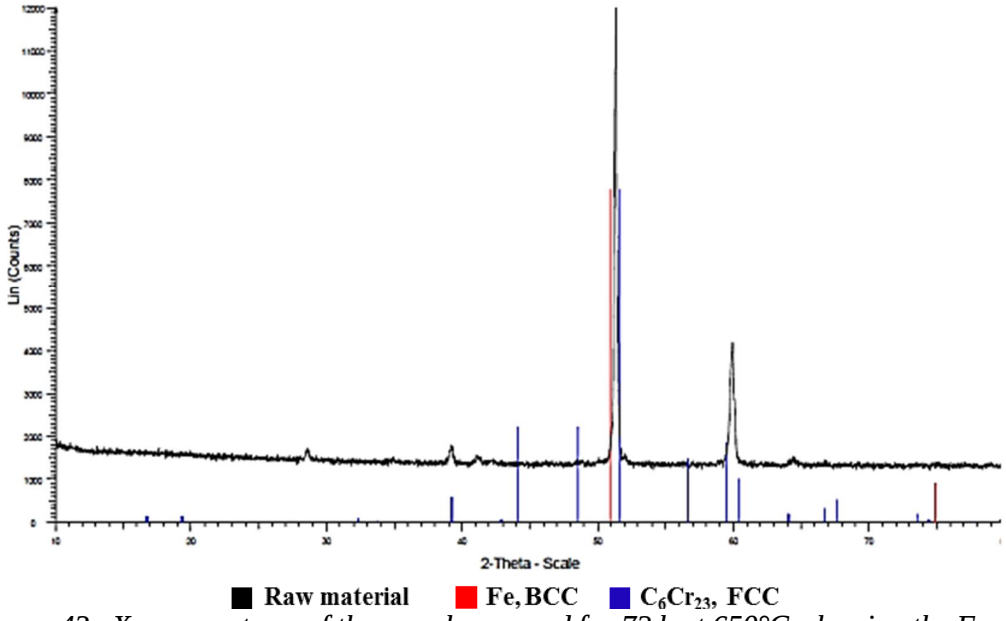

Figure 43. X-ray spectrum of the sample exposed for 72 h at 650°C, showing the Fe and C_6Cr_{23} peaks.

4.2.5.2 XRD of coke products

Figure 44 and 45 show the XRD spectrums of the coke product of the samples after exposure for 72 h at 525℃ and 650℃, which consisted of iron (Fe) and chromium carbide (C_6Cr_{23}), as expected.

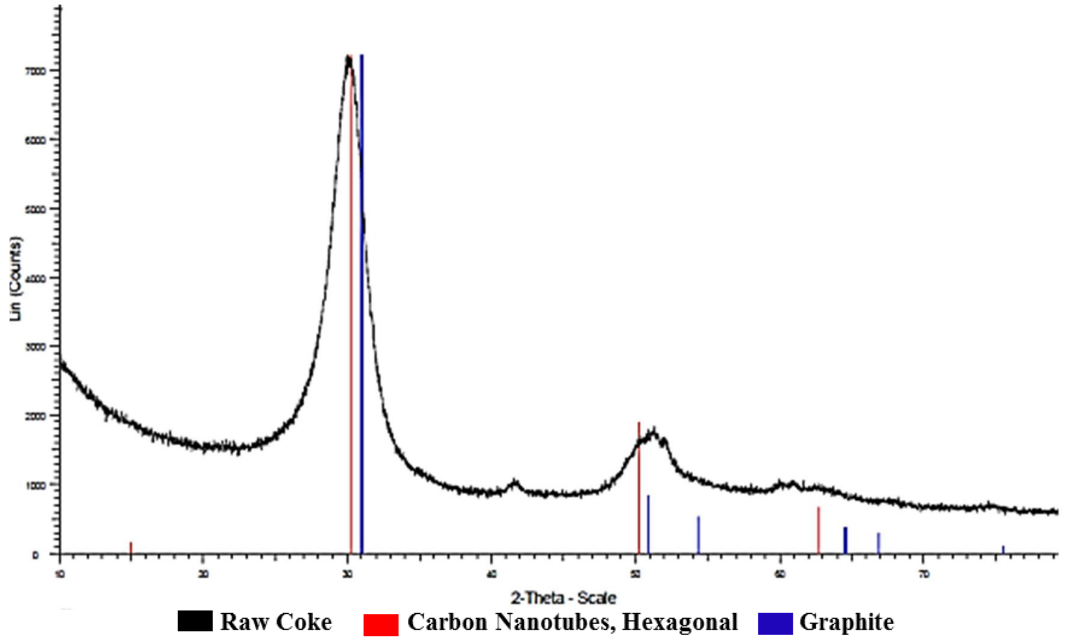

Figure 44. X-ray spectrum of the coke products from samples exposed for 72 h at 525°C, which consists of carbon nanotubes and graphite.

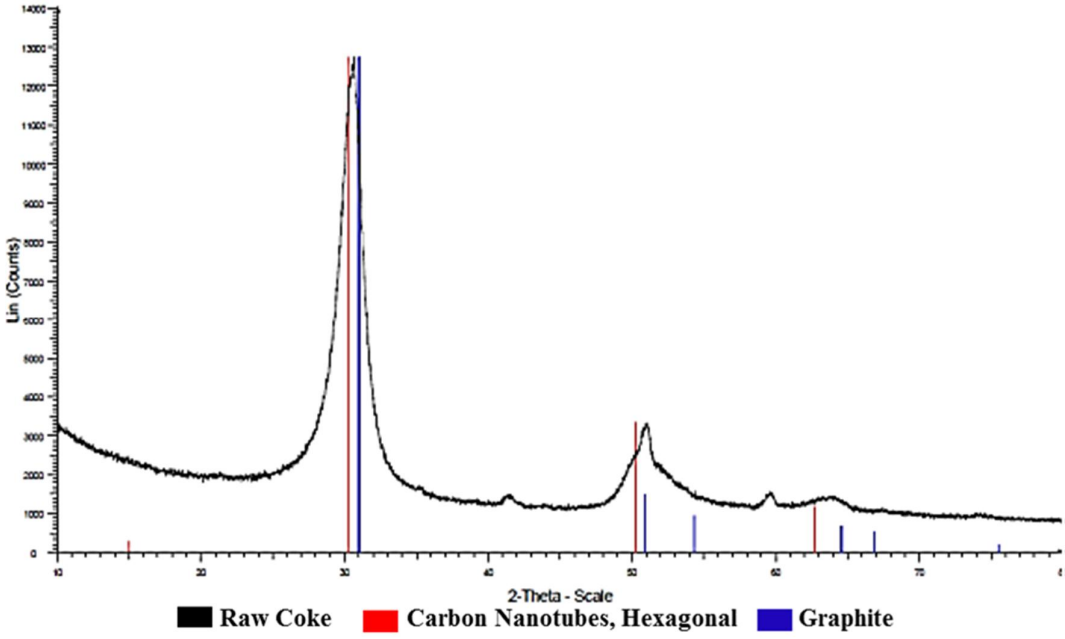

Figure 45. X-ray spectrum of the coke products from samples exposed for 72 h at 650°C, which consists of carbon nanotubes and graphite.

4.2.6 Raman spectrometry of all the coke products (72, 168 and 336 h exposure at 525°C and 650°C)

Figure 46 is the Raman spectrograph of all of the coke products confirming that they consist of carbon nanotubes and graphite. The D and G peaks are clearly depicted on these graphical

representations. It can also be seen from the graph that the G peaks for 650°C temperature tests are sharper as compared to the ones tested at a temperature of 525°C.

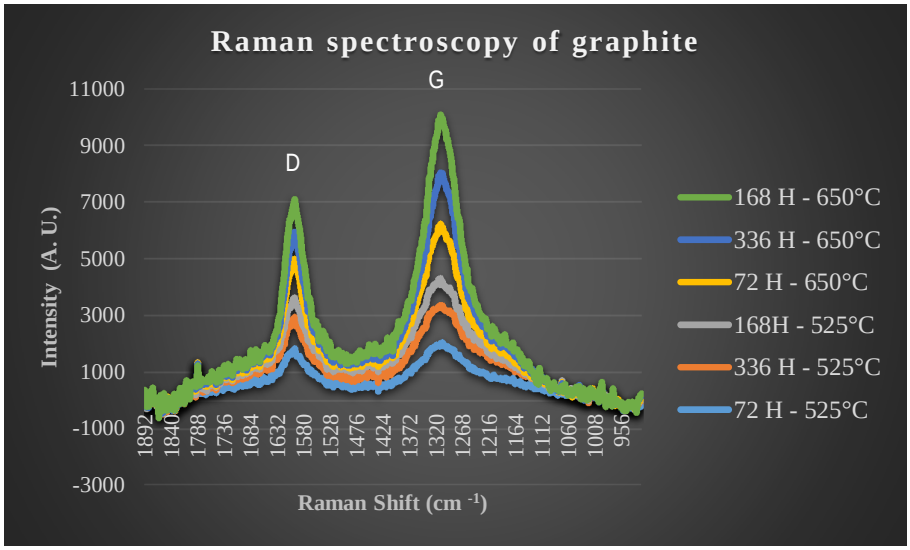

Figure 46. Raman spectrum of graphite that was observed on the alloy at different exposure periods and temperatures, showing the D and G peaks / modes.

4.2.7 Transmission Electron Microscopy (TEM) of coke products

The coke products were also analysed under the TEM, see Figure 47 and 48, illustrating that the coke products consists of carbon nanotubes and carbide (dark area), for the samples tested for 3 72 h at 525°C. These images illustrate that the filaments are hollow tubes, as shown in Figure 48.

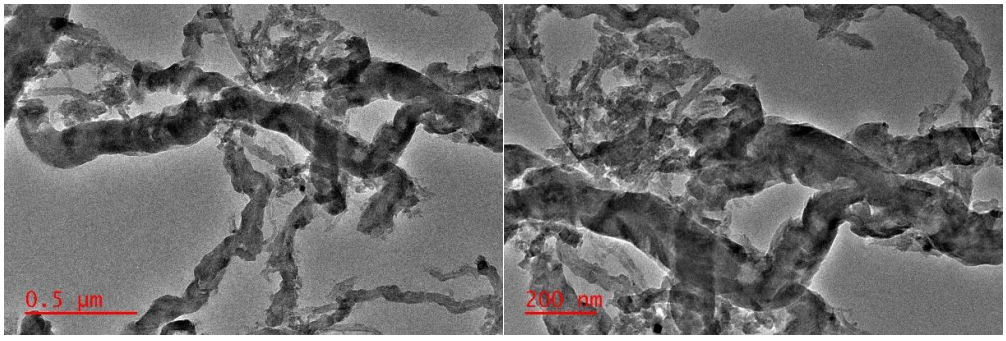

Figure 47. TEM images of carbon nanotubes and carbides (dark area) for the samples exposed for 72 h at 525°C, left – low magnification and right – high magnification.

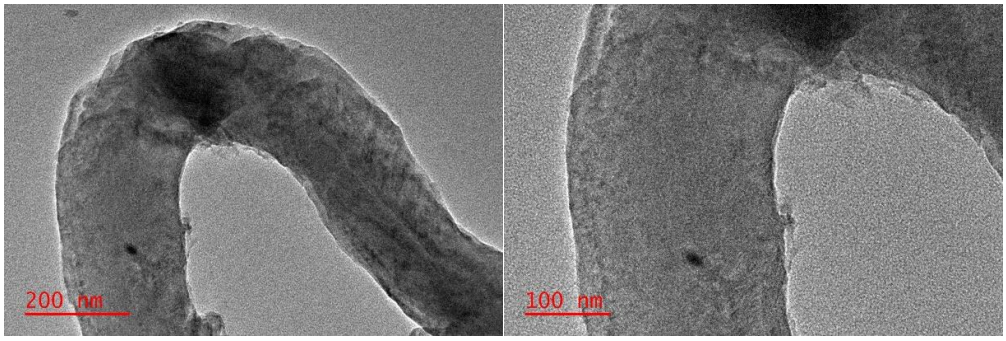

Figure 48. TEM images of carbon nanotubes and carbides (dark area) for the samples exposed for 72 h at 525°C, left – low magnification and right – high magnification.

At a temperature of 650°C the TEM images show a rather different shape of the filaments which are finer and flatter, as compared to the ones for 525°C, see Figure 49.

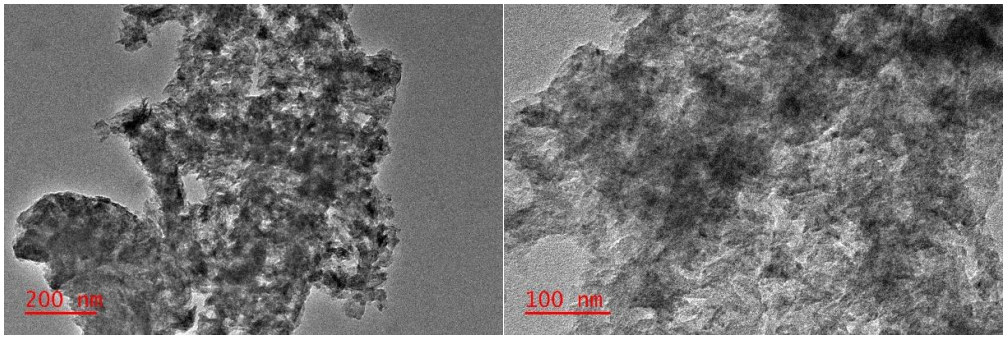

Figure 49. TEM images of carbon nanotubes and carbides (dark area) for the samples exposed at 72 h at 650°C, left – low magnification and right – high magnification.

Figure 50 is a TEM spectrum of the samples exposed for 72 h at 525°C, which consisted of iron, nickel and chromium with oxygen. The copper is from the thin film used to put the coke particles for TEM analysis. The TEM spectrum of the samples exposed 72 h at 650°C, consists of carbon and chromium with oxygen, as shown in Figure 51.

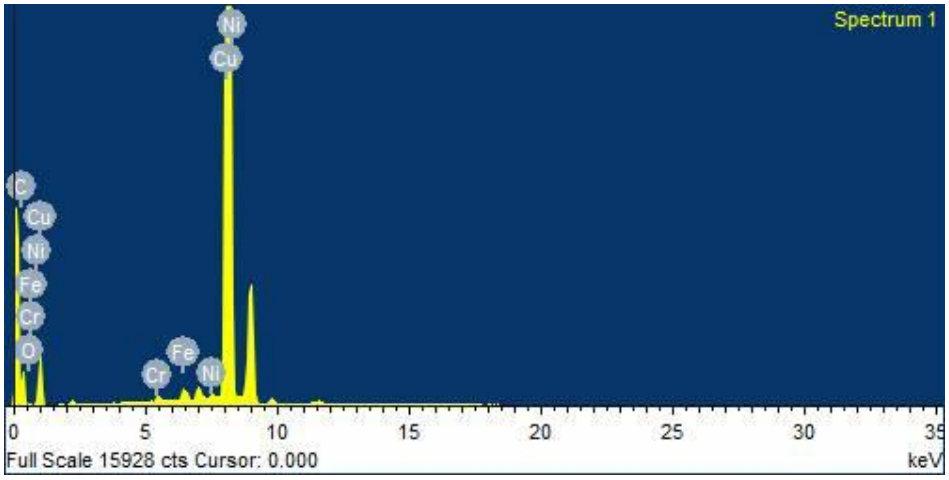

Figure 50. TEM spectrum of samples exposed for the samples exposed for 72 h at 525°C showing iron, nickel and chromium with oxygen. The copper is from the thin film used to put the coke particles for TEM analysis.

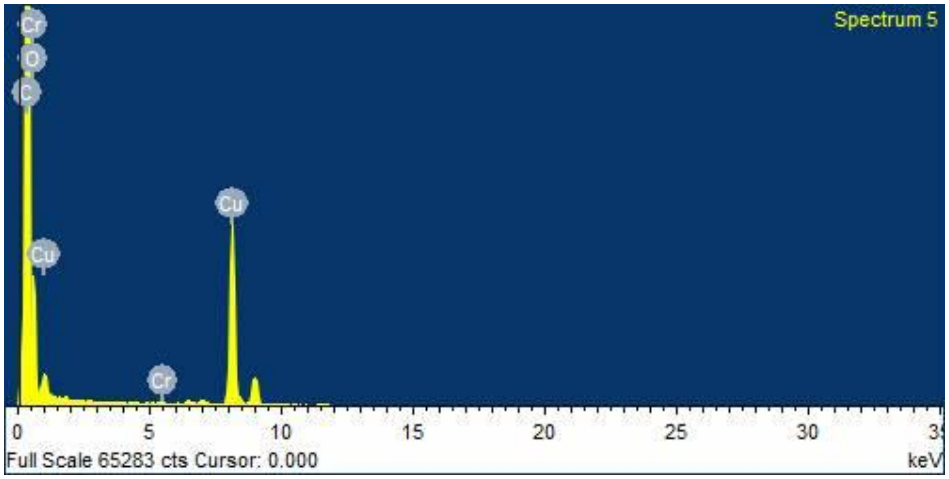

Figure 51. TEM spectrum of the samples exposed for 72 hours at 650°C, which consists of carbon and chromium with oxygen. The copper is from the thin film used to put the coke particles for TEM analysis.

4.3 168 h exposure

4.3.1 Visual examination

The alloy was also exposed for 168 h at both the temperature of 525°C and 650°C. The samples tested here were labelled as 7, 8, 18 and 19. There was slightly more attack and coking on these samples as expected, see Figure 52 and 53. These photographs also illustrate how the samples were suspended in a ceramic boat with ceramic rods. More coking was observed after exposure of these samples, with isolated pits on sample 19 that was exposed at 650°C.

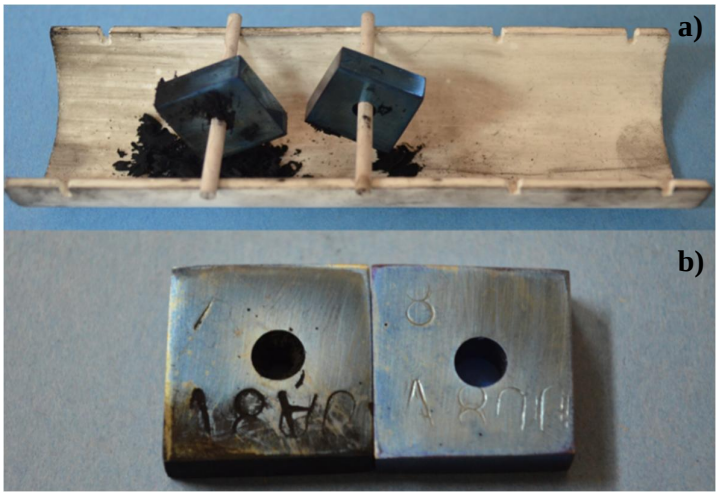

Figure 52. Photographs of the samples after 168 h exposure at a temperature of 525°C, showing coking (a) and after coke removal (b).

Figure 53. Photographs of the samples after 168 h exposure at a temperature of 650°C, (a) coking and (b) after coke removal (b)..

4.3.2 Weight change

These samples showed significant weight loss, see Table 1. This is due to the fact that significant amount of coking occurred on the samples.

4.3.3 Metallography

These samples were also sectioned and analysed in the as-polished as well as etched condition. Figure 54 and 55 show micrographs of the samples after 72 h in the as-polished condition showing some attack in the form of nitride precipitation on the microstructure. This attack was more pronounced on the etched images of the micrograph, on and along the grain boundaries, as seen on Figure 56 and 57.

Figure 54. Micrograph of the samples exposed for 168 h at 525°C in the as-polished condition, showing the carbo-nitrite particles.

Figure 55. Micrograph of the samples exposed for 168 h at 650°C in the as-polished condition, showing the carbo-nitrite particles.

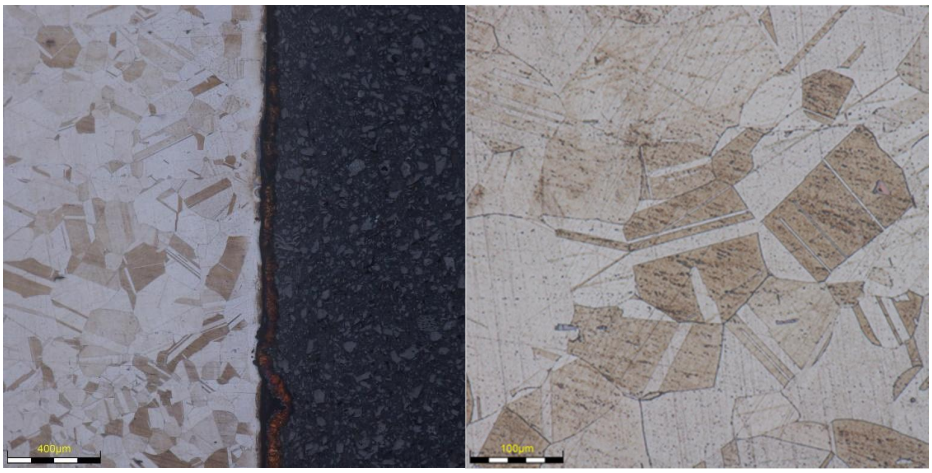

Figure 56. Micrographs of the samples tested for 168 h at 525°C in the etched condition, showing the carbo-nitrite particles on the grain boundaries.

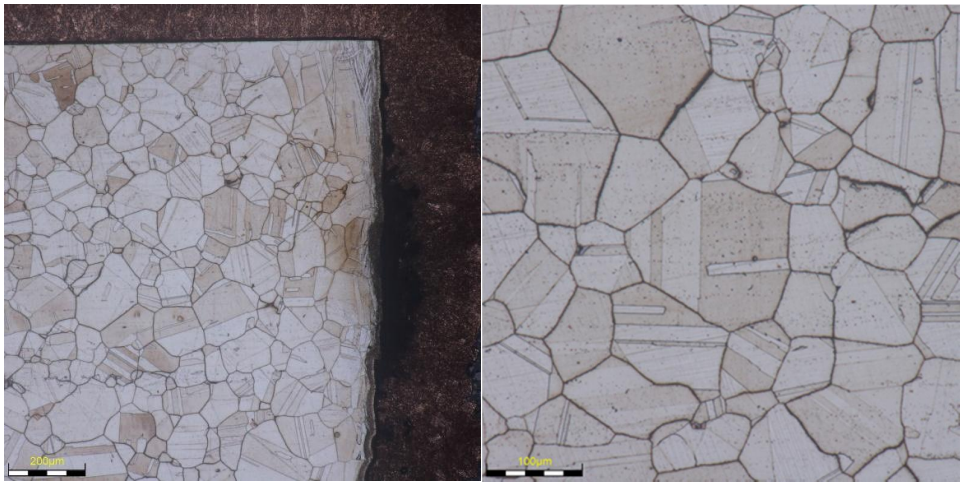

Figure 57. Micrographs of the samples exposed for 168 h at 650°C in the etched condition, showing the carbo-nitrite particles along the grain boundaries.

4.3.4 Scanning Electron Microscopy (SEM)

4.3.4.1 SEM analysis of metal samples

Figure 58 is a SEM image of the sample surface after exposure at 525°C for 72 h showing some platelets and attack (black deposit) on the surface. After exposure for 168 h at 525°C, the oxide layer observed was not uniform, as seen in Figure 59. Preferential attack was also evident on the sample, under SEM, also seen in Figure 59. More platelets were observed on the surface of the samples exposed to 650°C, as seen in Figure 60 and Figure 61 is an oxide layer observed after 168 h exposure at 650°C, which is also not uniform and is accompanied by preferential attack.

The EDX spectrum of the substrate after the 168 h exposure at 525°C, which consisted of iron, nickel and chromium with titanium and vanadium, as shown in Figure 62 and Figure 63, shows the EDX spectrum of the black deposit on the surface of the sample. The EDX spectrum of the surface of the samples exposed for 168 h at 650°C is shown in Figure 64 and consists of iron, nickel, chromium and vanadium, with titanium and that of the deposit layer is shown in Figure 65, which consisted of iron, nickel, and chromium with carbon, oxygen, sulphur, titanium and chloride; the copper is from the copper plating.

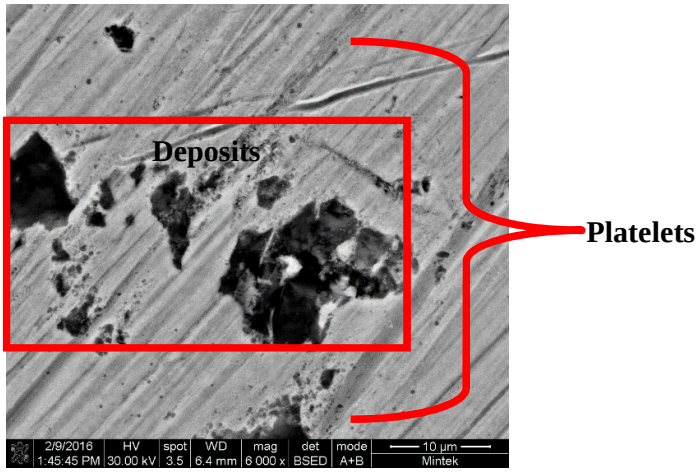

Figure 58. SEM image of the sample surface after 168 h exposure at 525°C, showing platelets and black deposits.

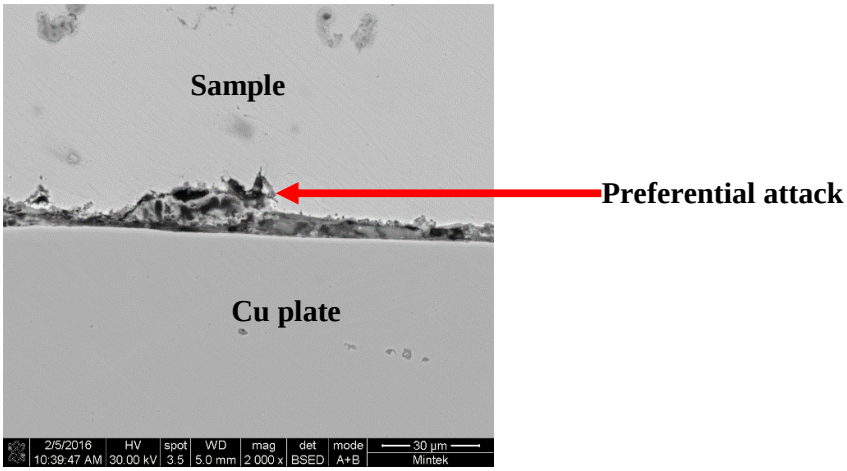

Figure 59. SEM image of the sample surface after 168 h exposure at 525°C, showing a deposit layer.

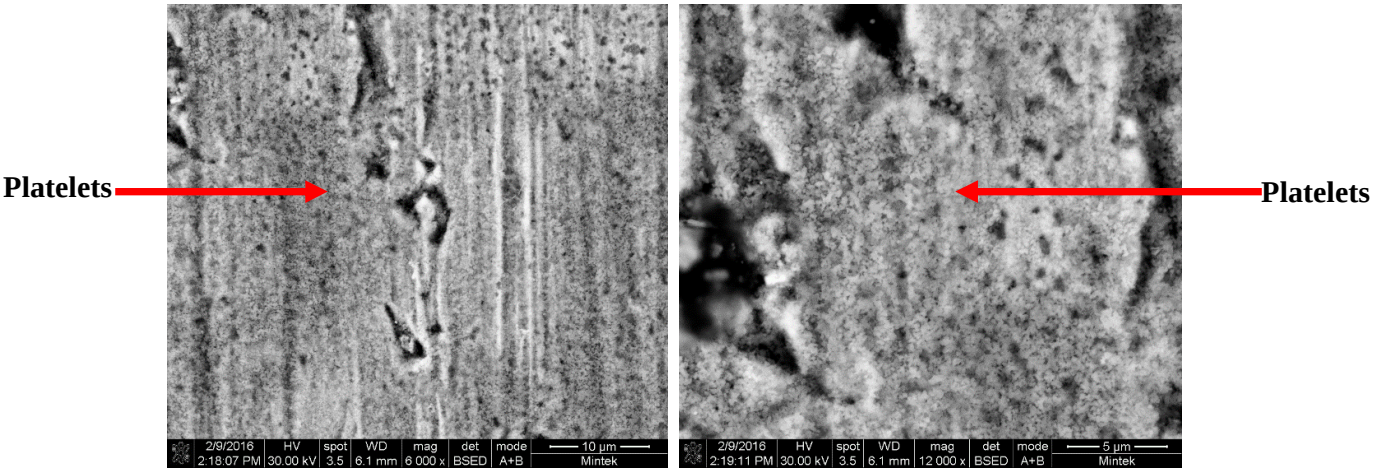

Figure 60. SEM images of the sample surface after 168 h exposure at 650°C, showing more platelets and black deposits, left – low magnification and right – high magnification.

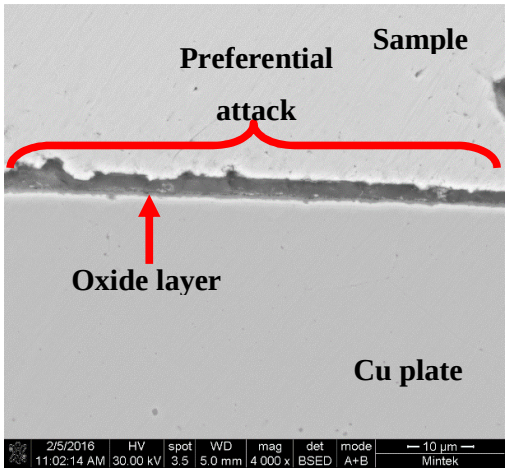

Figure 61. SEM image of the sample surface after 168 h exposure at 650°C, showing an oxide layer and preferential attack.

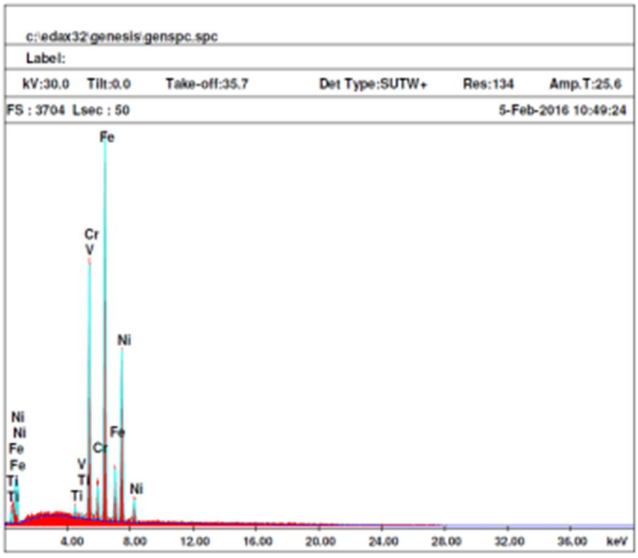

Figure 62. EDX spectrum of sample substrate exposed for 168 h at 525°C consisting predominantly of iron, nickel, chromium and vanadium, with titanium.

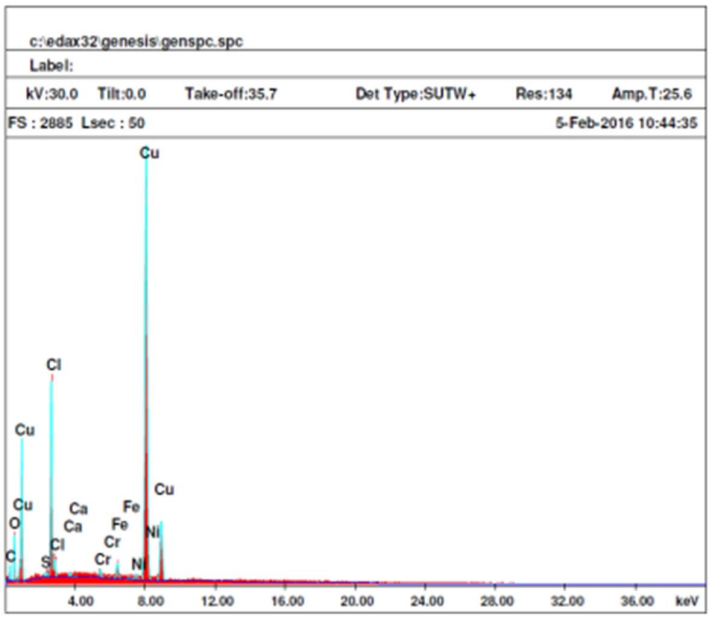

Figure 63. EDX spectrum of the samples exposed for 168 h at 525°C on the oxide/deposit layer which consisting of iron, nickel, and chromium with carbon, oxygen, sulphur, calcium and chloride; the copper is from the copper plating.

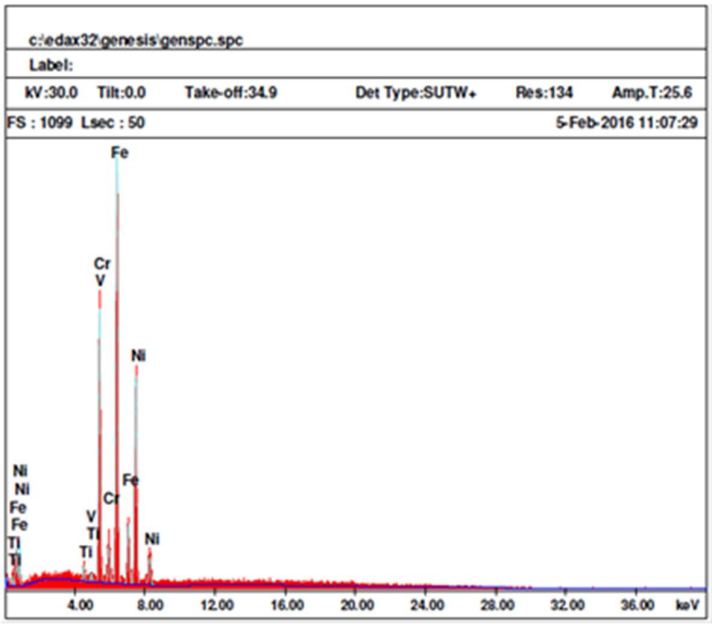

Figure 64. EDX spectrum of the sample substrate exposed for 168 h at 650°C, which consisted predominantly of iron, nickel, chromium and vanadium, with titanium.

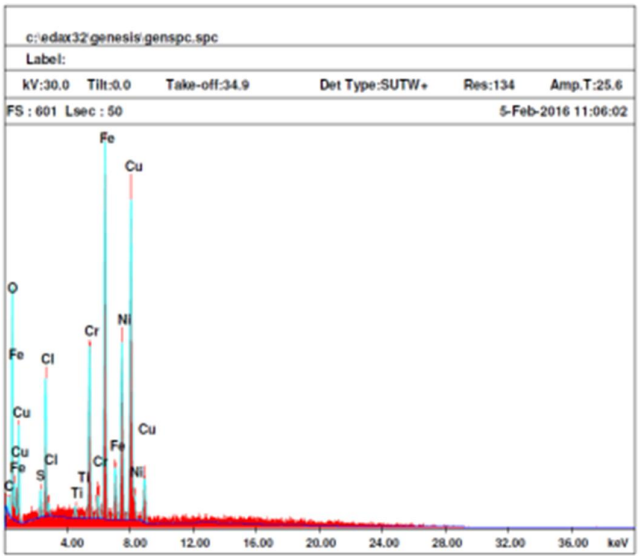

Figure 65. EDX spectrum of the sample exposed for 168 h at 650°C (deposit layer) which consisted of iron, nickel, and chromium with carbon, oxygen, sulphur, titanium and chloride; the copper is from the copper plating.

4.3.4.2 SEM analysis of coke product for samples exposed for 168 h at 525 °C and 650°C

The coke products were also analysed under the SEM and as expected, the images show the coke filaments with carbides (metal dust at the tips, found in the coke product) as shown in Figure 66 and 68. The coke product for both the temperatures consisted of carbon, iron, chromium, nickel and oxygen, as seen in Figures 67 and 69.

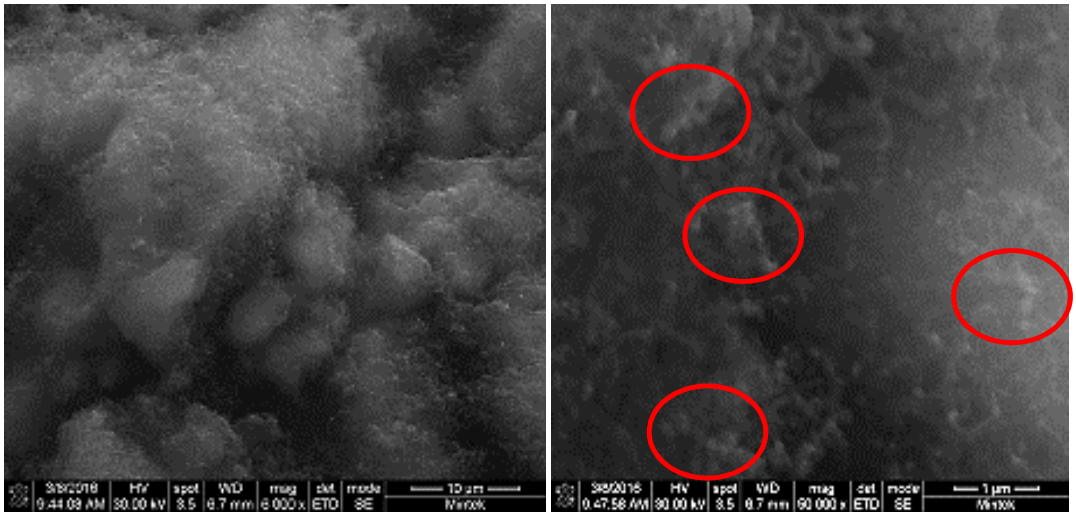

Figure 66. SEM images of carbon filaments of the coke after 168 h exposure at 525°C with carbides (metal dust) at the tips, circled, left – low magnification and right – high magnification.

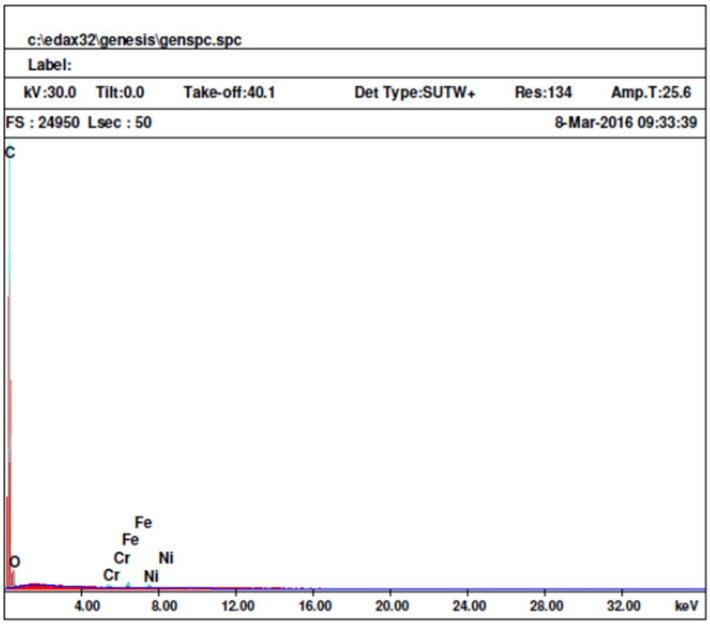

Figure 67. EDX spectrum of the coke product from the samples that were exposed for 168 h at 525°C which consisted of carbon, iron, nickel, and chromium with oxygen.

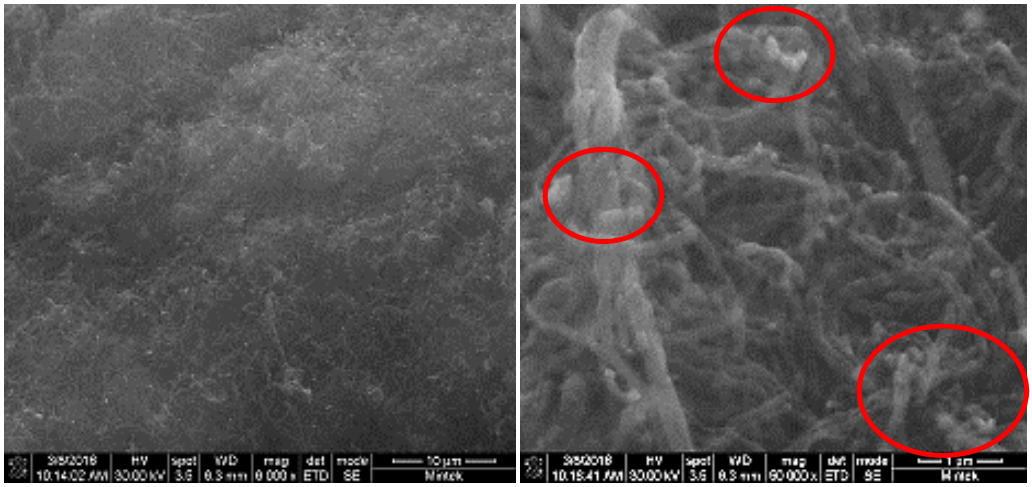

Figure 68. SEM images of carbon filaments of the coke after 168 h exposure at 650°C with carbides (metal dust) at the tips, circled, left – low magnification and right – high magnification.

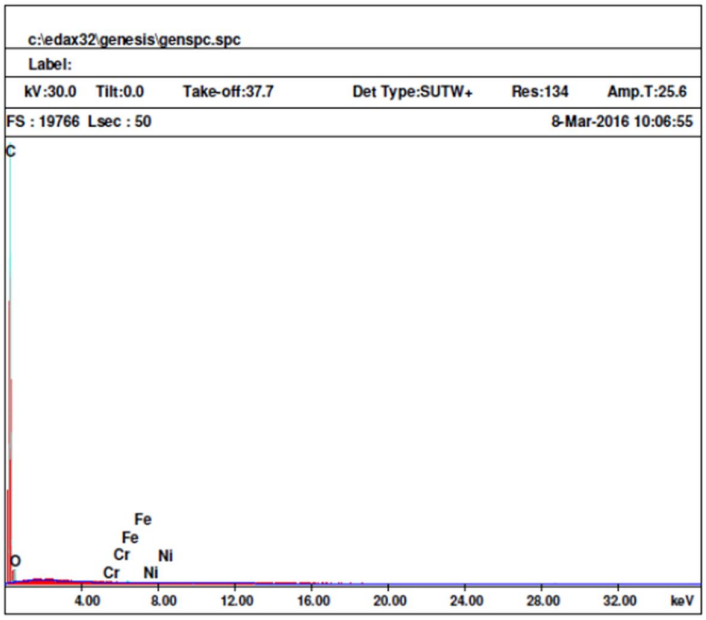

Figure 69. EDX spectrum of the coke product from the samples that were exposed for 168 h at 525°C which consisted of carbon, iron, nickel, and chromium with oxygen.

4.3.4.3 X-ray diffraction for samples exposed for 168 h at 525 °C and 650°C

These samples were also analysed under the XRD and the metal seemed to be Ferrite (Fe) and Cr-carbide (C_6Cr_{23}). The coke was a mixture of carbon nanotubes and graphite, as expected. The XRD spectrums can be seen in Figures 70 to 61.

4.3.4.4 XRD of metal samples

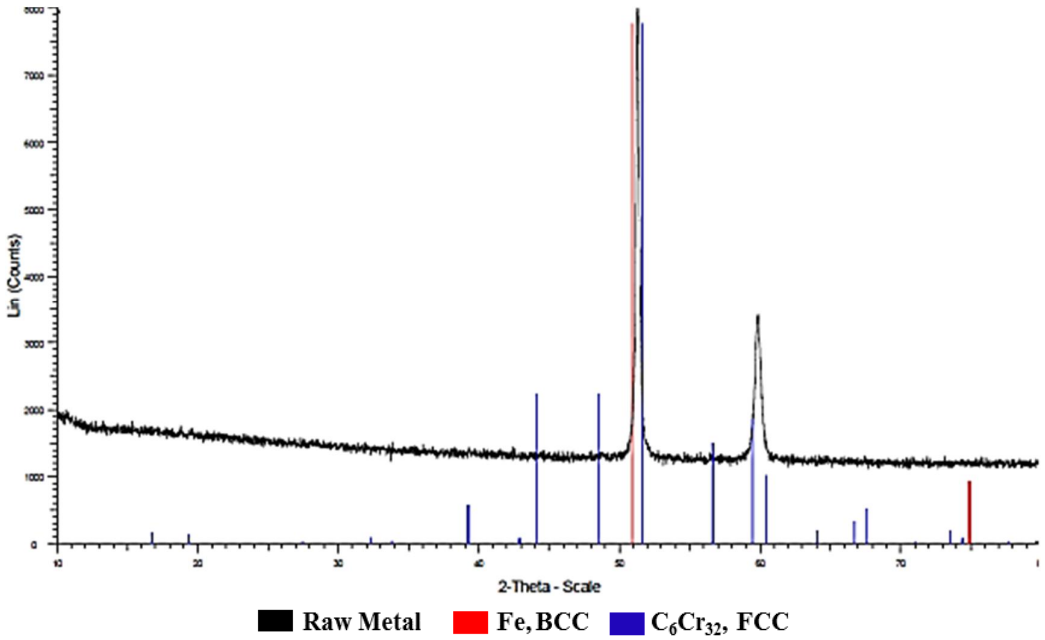

Figure 70. X-ray spectrum of the sample exposed for 168 h at 525°C, showing the Fe and C_6Cr_{23} peaks.

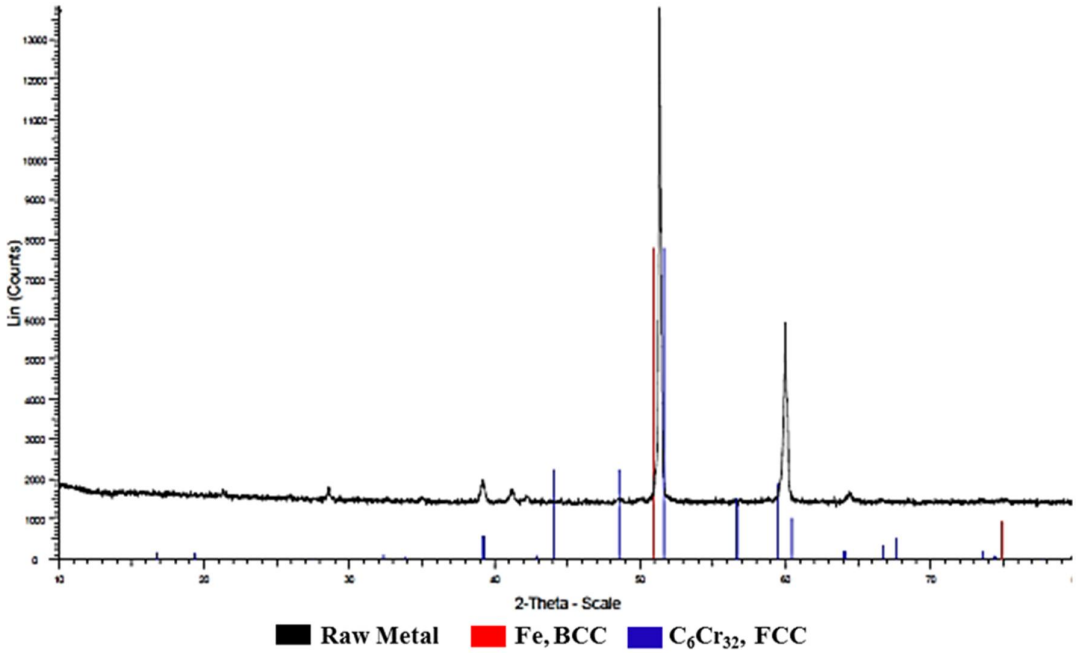

Figure 71. X-ray spectrum of the sample exposed for 168 h at 650°C, showing the Fe and C_6Cr_{23} peaks.

4.3.4.5 XRD of coke products

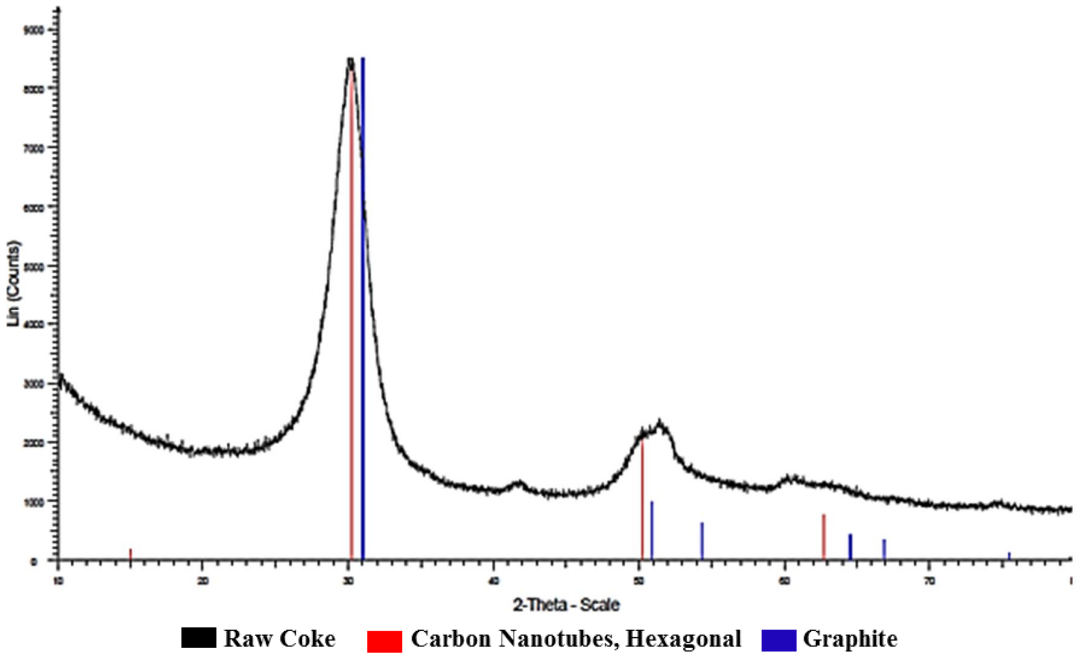

Figure 72. X-ray spectrum of the coke product after 168 h at 525°C, which consisted of carbon nanotubes and graphite.

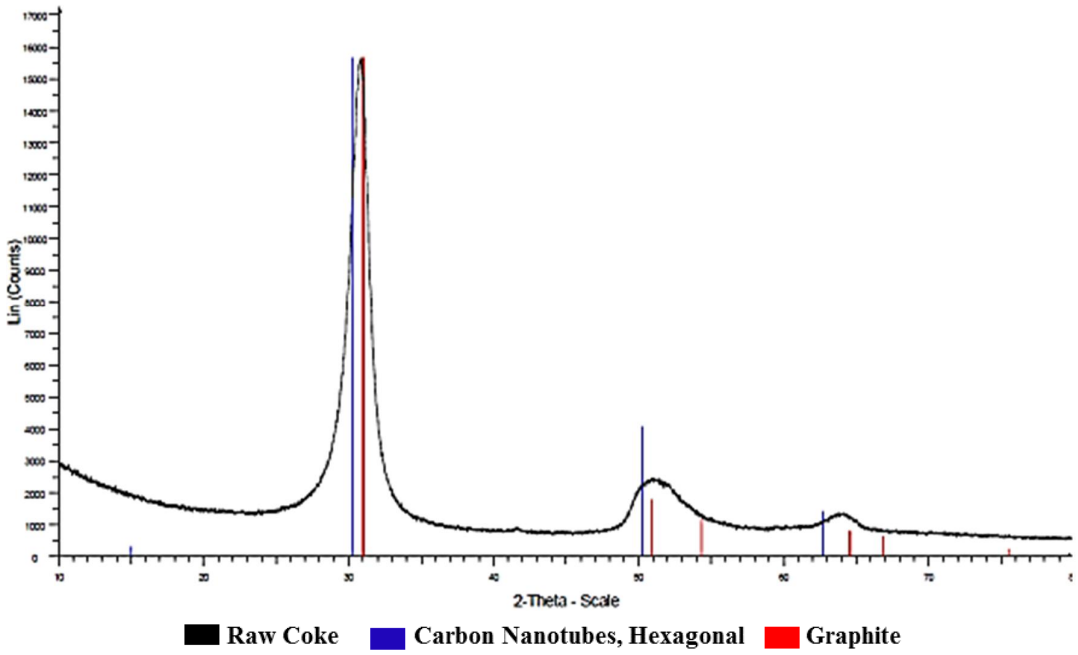

Figure 73. X-ray spectrum of the coke product after 168 h at 650°C, which consisted of carbon nanotubes and graphite.

4.3.5 Transmission Electron Microscopy (TEM) of coke products

The coke products of these samples were also analysed under the TEM, see Figure 74 to 79, illustrating that the coke products consisted of carbon nanotubes and carbide (dark area).

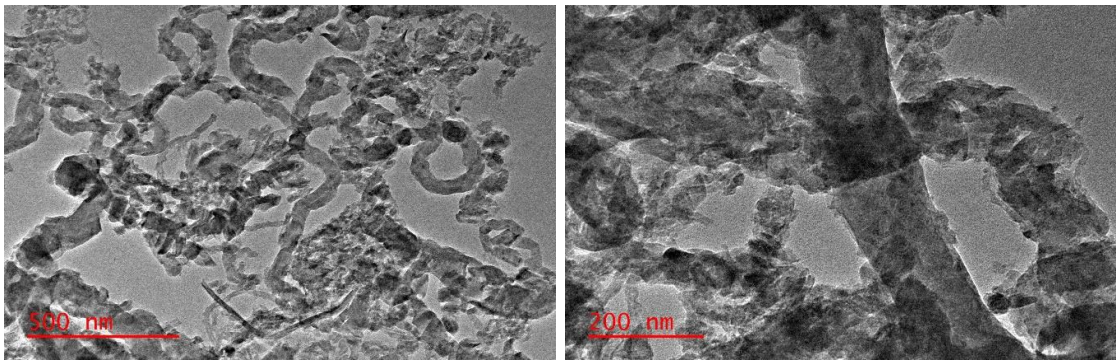

Figure 74. TEM images of carbon nanotubes and carbides (dark area) for the coke product from samples exposed for 168 h at 525°C, left – low magnification and right – high magnification.

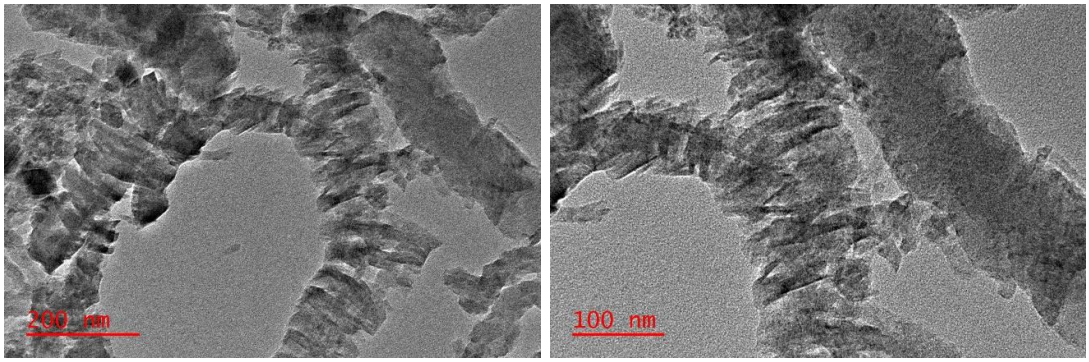

Figure 75. TEM images of carbon nanotubes and carbides (dark area) for the coke product from samples exposed for 168 h at 525°C, left – low magnification and right – high magnification.

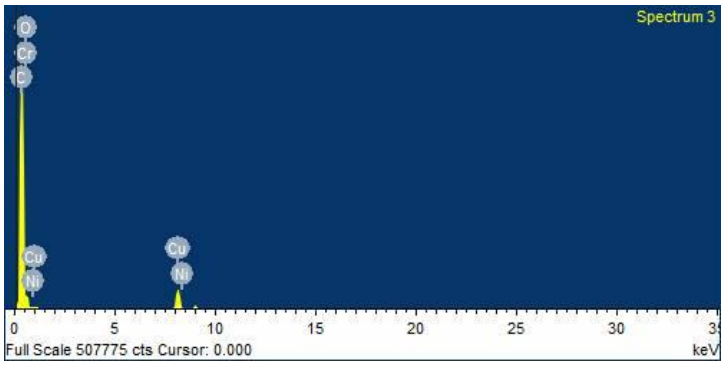

Figure 76. TEM spectrum of the coke product from the samples exposed for 168 h at 525°C, which consisted of carbon, nickel and chromium with oxygen. The copper is from the thin film used to put the coke particles for TEM analysis.

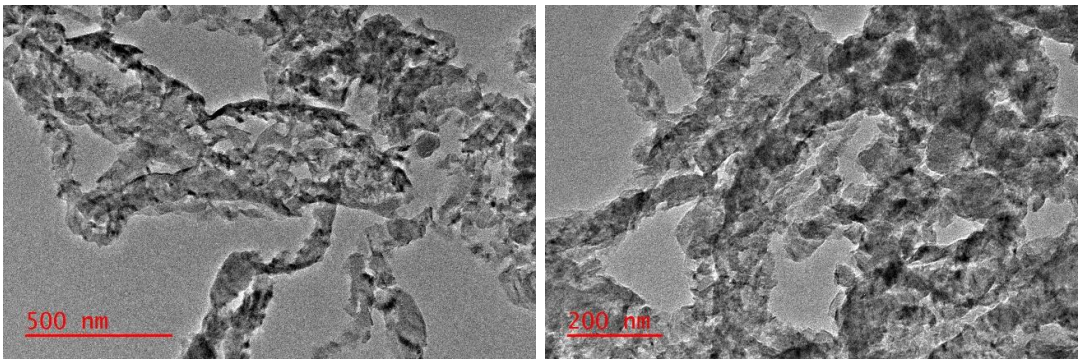

Figure 77. TEM images of carbon nanotubes and carbides (dark area) for the coke product from samples exposed for 168 h at 650°C, left – low magnification and right – high magnification.

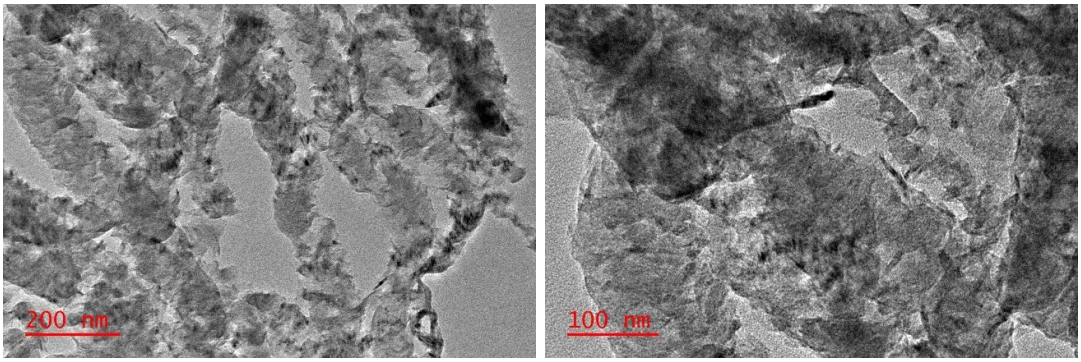

Figure 78. TEM images of carbon nanotubes and carbides (dark area) for the coke product from samples exposed for 168 h at 650°C, left – low magnification and right – high magnification.

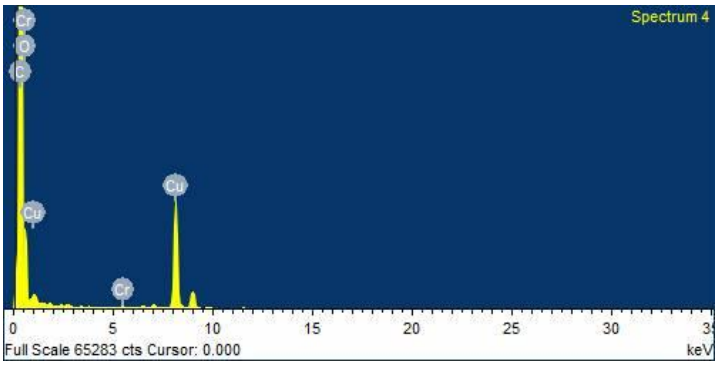

Figure 79. TEM spectrum of the coke product from samples exposed for 168 h at 650°C, which consisted of carbon and chromium with oxygen. The copper is from the thin film used to put the coke particles for TEM analysis.

4.4 336 h exposure

This was the last set of test that was performed on the Alloy 800 for 168 h at both temperatures of 525°C and 650°. The samples were labelled as 1, 2, 5 and 6. **Please note that the number 1 & 2 is duplicated here (labelled the same as 24 h exposure at a temperature of 650°C samples) but it is a new set of samples.**

4.4.1 Visual examination

There was significantly more attack and coking on these samples as expected, as seen in Figure 80 to 82. These photographs also illustrate how the samples were suspended in a ceramic boat with ceramic rods during exposure in the test rig. More coking and pitting was observed on these samples as compared to the three exposure periods of 24, 72 and 168 h. The samples exposed at 650°C had more coking as compared to the ones tested at 525°C and this might be to the higher temperature of 650°C. Figure 82 is the photographs of the samples tested at 650°C after cleaning showing the pits at a closer view. Please note that because of the shape of the

test rig (tube furnace), the samples were unintentional tilted during removal from the furnace after exposure. Therefore, some of the coke shifted to one side of the boat as shown in Figure 80.

Figure 80. Photographs of the samples after 336 h exposure at 525°C, showing coking (a) and discolouration (b).

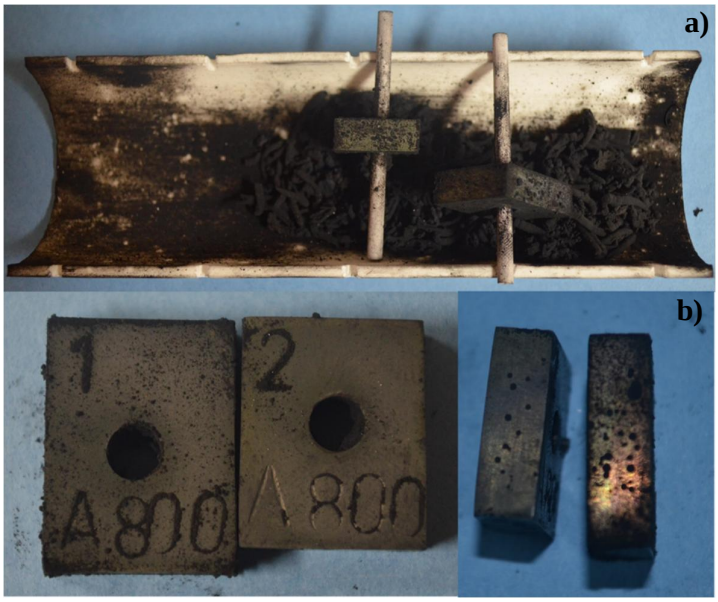

Figure 81. Photographs of the samples after 336 h exposure at 650°C, showing coking (a) and discolouration and pitting (b).

Figure 82. Photographs of the samples after 336 h exposure at a temperature of 650°C, after cleaning, showing discolouration and pitting.

Figure 83 and 84 show relatively big and deep pits on Alloy 800 exposed at 650°C. The alloy experienced pitting when exposed for 336 h at 650ºC, with pits of various sizes and orientations. The maximum depth penetration was approximately 205 µm with a total width of around 1283 µm.

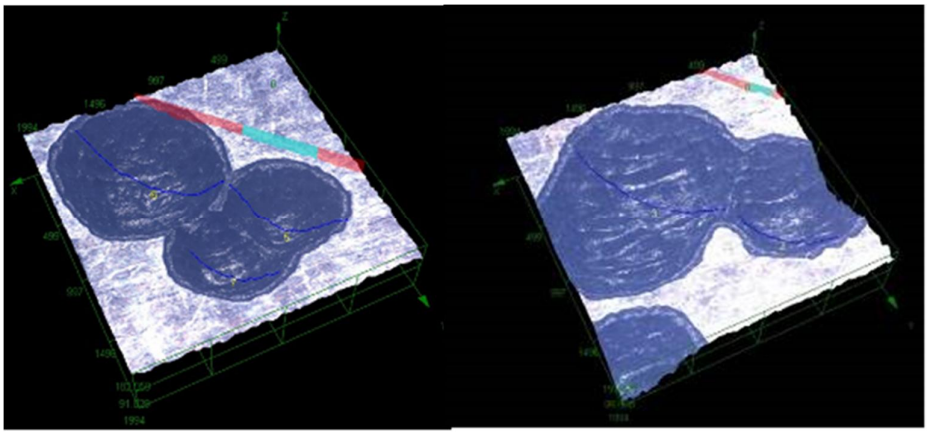

Figure 83. 3D images of the topical view of pits observed on the sample after 336 h exposure at 650°C.

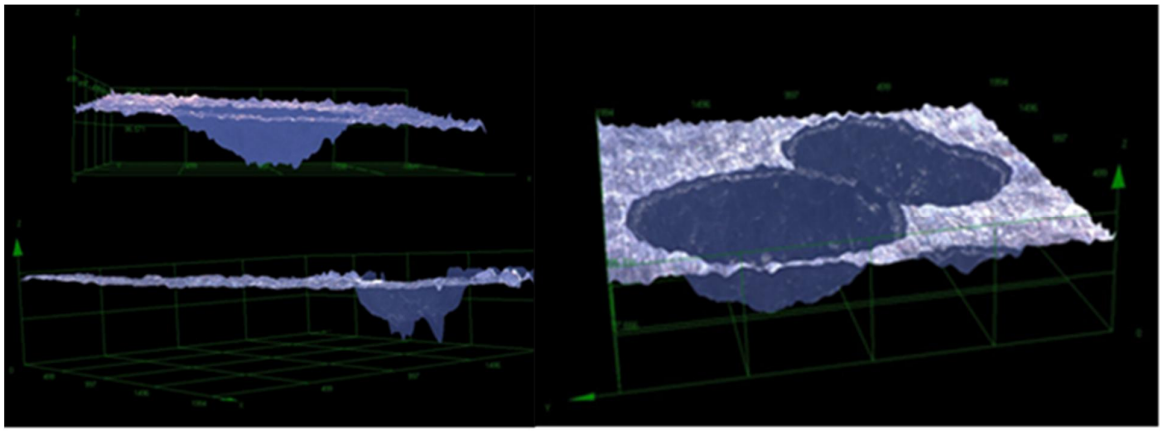

Figure 84. 3D images of the side view of pits observed on the sample after 336 h exposure at 650°C.

4.4.2 Weight change

These samples showed significant weight loss, see Table 1. This is due the fact that significant amount of coking and pitting occurred on the samples after exposure.

4.4.3 Metallography

These samples were also sectioned and analysed in the as-polished as well as etched condition. Figure 85 and 88 show micrographs of the samples exposed for 168 h at 525°C and 650°C in the as-polished condition showing pits on the surface. There were also some attack in the form of nitride precipitation on the microstructure, see Figure 86. This attack is more pronounced on the etched images of the micrograph, on and along the grain boundaries, as seen in Figure 87 and 89.

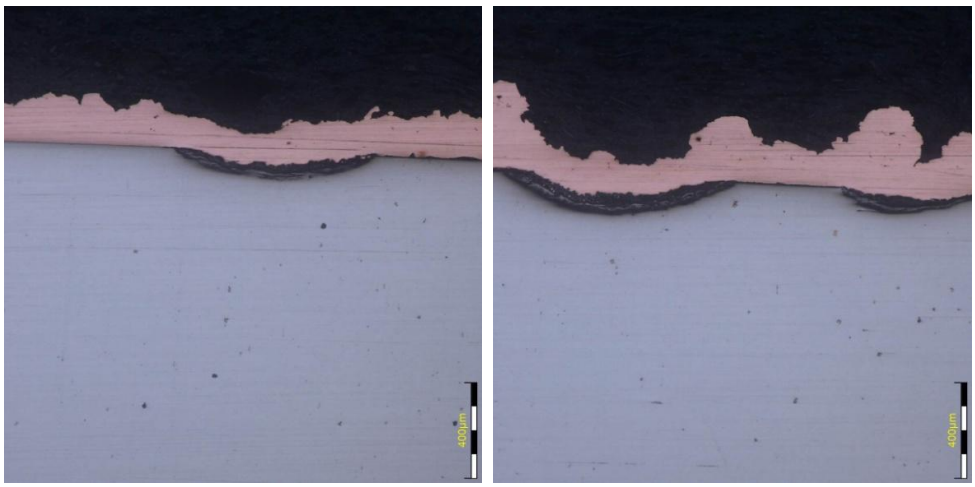

Figure 85. Micrographs of the samples after 336 h exposure at 525°C showing pits on the surface edges.

Figure 86. Micrographs of the samples after 336 h exposure at 525°C in the as-polished condition (left) and etched (b) showing a pit on the surface and some grain boundary attack.

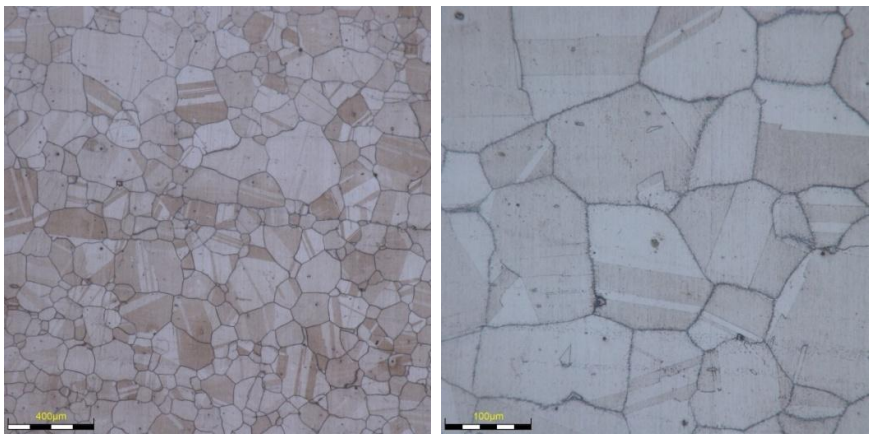

Figure 87. Micrographs of the samples after 336 h exposure at 525°C in the etched condition showing the general microstructure of the alloy and some attack on and along the grain boundaries.

Figure 88. Micrographs of the samples after 336 h exposure at 650°C in the as-polished condition showing pits on the surface.

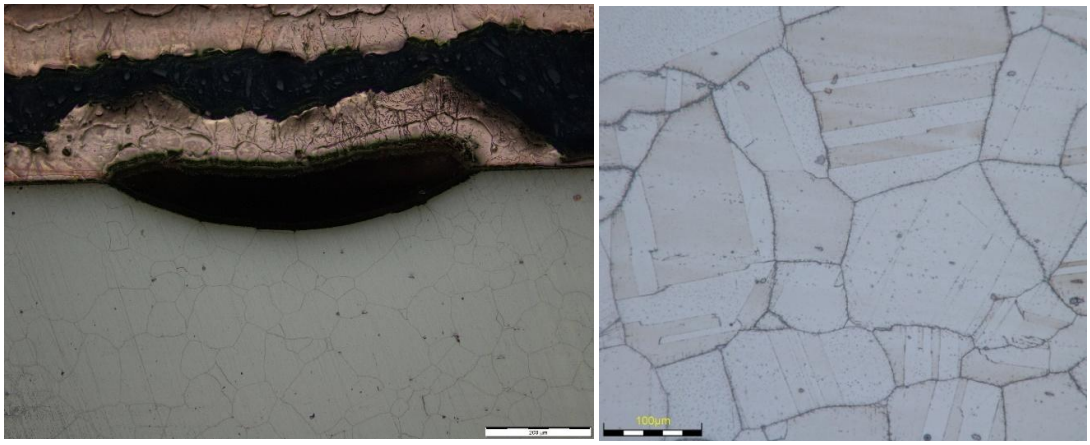

Figure 89. Micrograph of the samples after 336 h exposure at 650°C showing some attack in the form of nitride precipitation on the microstructure, on and along the grain boundaries.

4.4.4 Scanning Electron Microscopy (SEM)

4.4.4.1 SEM of metal samples

After the 336 h exposure at 525°C, more platelets and black deposits were evident on the surface of the samples under the SEM, as shown in Figure 90 to 92. Figure 93 and 94 show the SEM images of the sample surface after 336 h exposure at 650°C, showing more black deposits and coke inside the pits and on the surface. SEM images of the sample surface after 336 h exposure at 650°C, showing more attack on and along the grain boundaries (black spots), are shown in Figure 95.

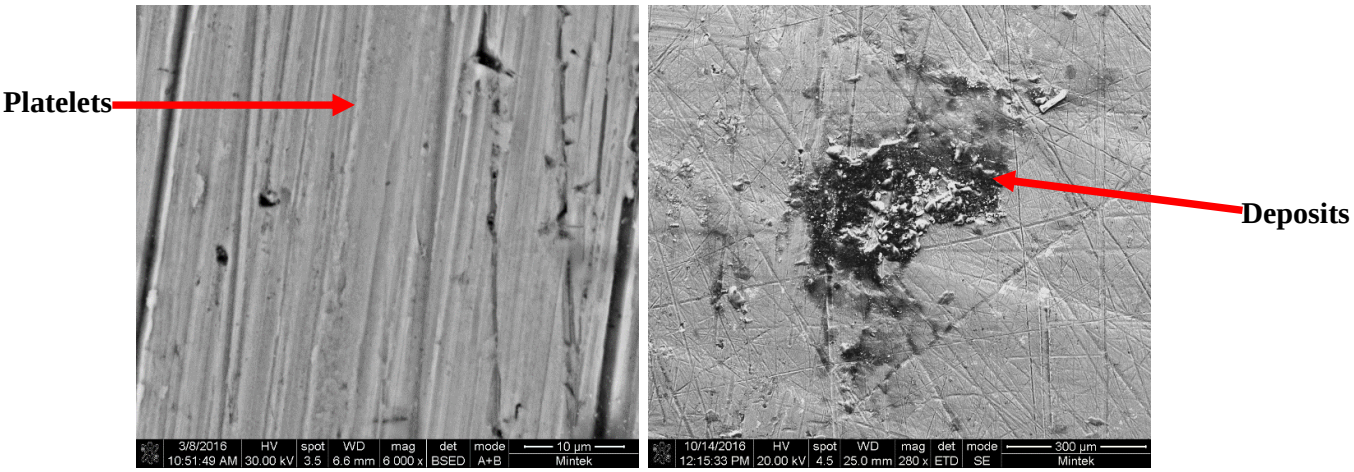

Figure 90. SEM images of the sample surface after 336 h exposure at 525°C, showing more platelets (left) and black deposits (right).

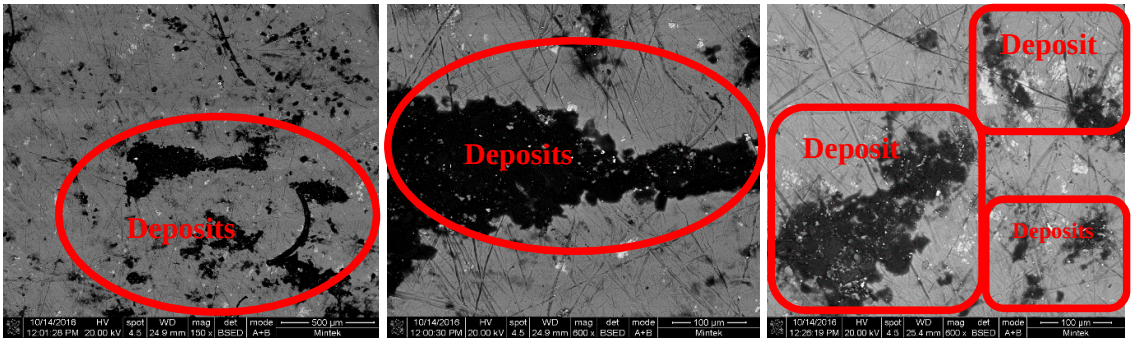

Figure 91. SEM images of the sample surface after 336 h exposure at 525°C, showing more black deposits (circled).

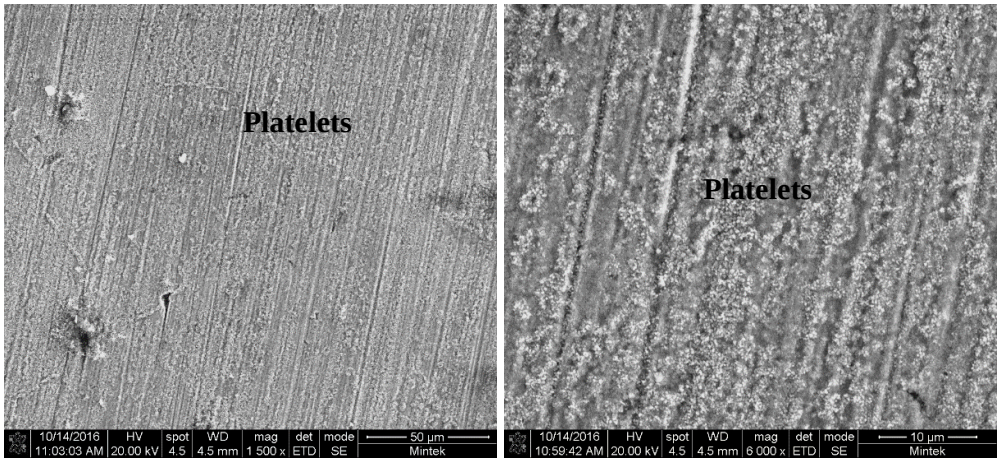

Figure 92. SEM images of the sample surface after 336 h exposure at 650°C, showing more platelets – low and high magnification.

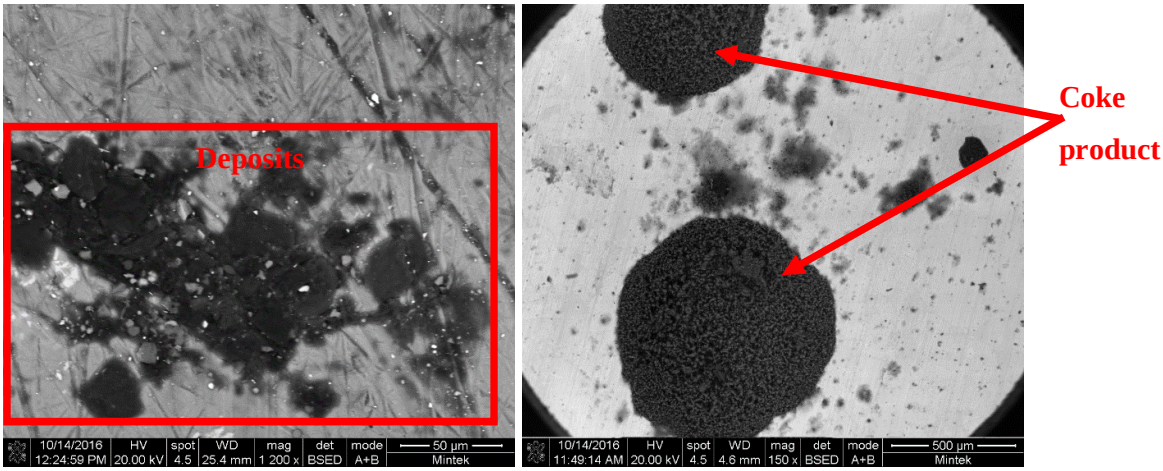

Figure 93. SEM images of the sample surface after 336 h exposure at 650°C, showing more black deposits and coke on the surface.

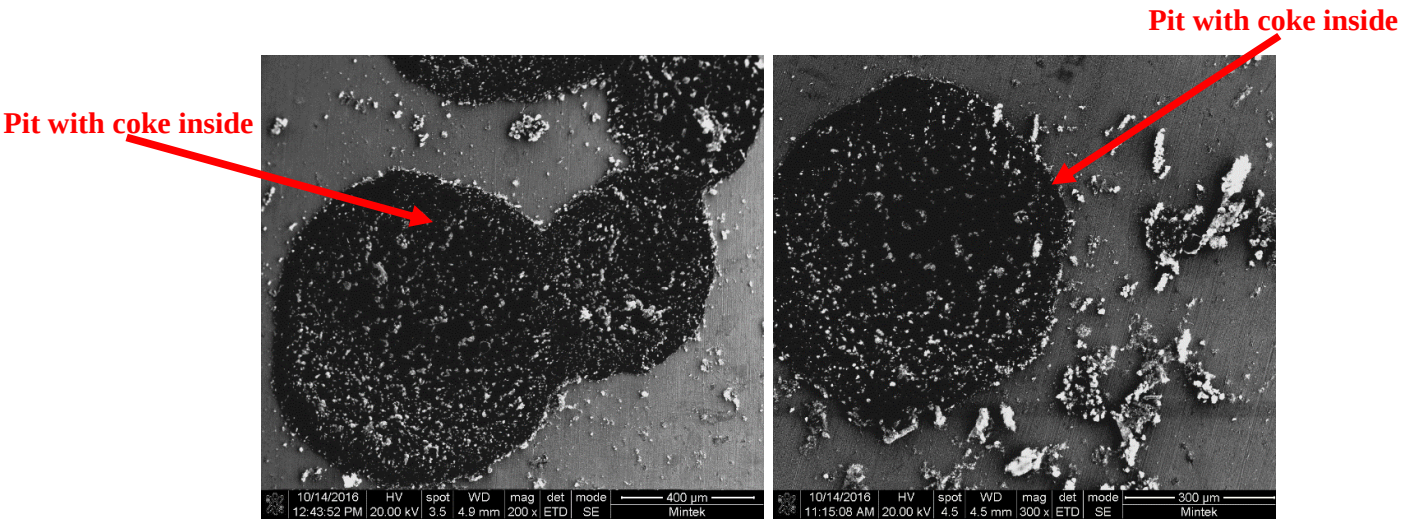

Figure 94. SEM images of the sample surface after 336 h exposure at 650°C, showing more black deposits (coke product) inside the pits.

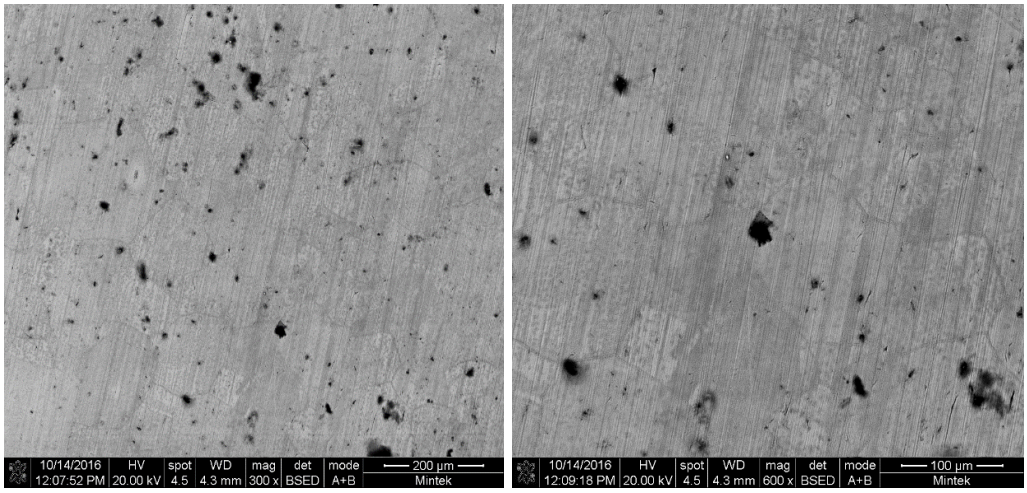

Figure 95. SEM images of the sample surface after 336 h exposure at 650°C, showing more attack on and along the grain boundaries (black spots) – low and high magnification.

4.4.4.2 SEM of coke samples

The coke product from these samples after exposure for 336 h at 525°C were analysed under the SEM, see Figure 96 and 97. Metal dust (carbides) were observed on the tips of the coke product, as seen in Figure 96 and Figure 97 is an EDX spectrum of the coke product from the samples that were exposed for 336 h at 525°C which consisted of carbon, iron, nickel, and chromium with oxygen.

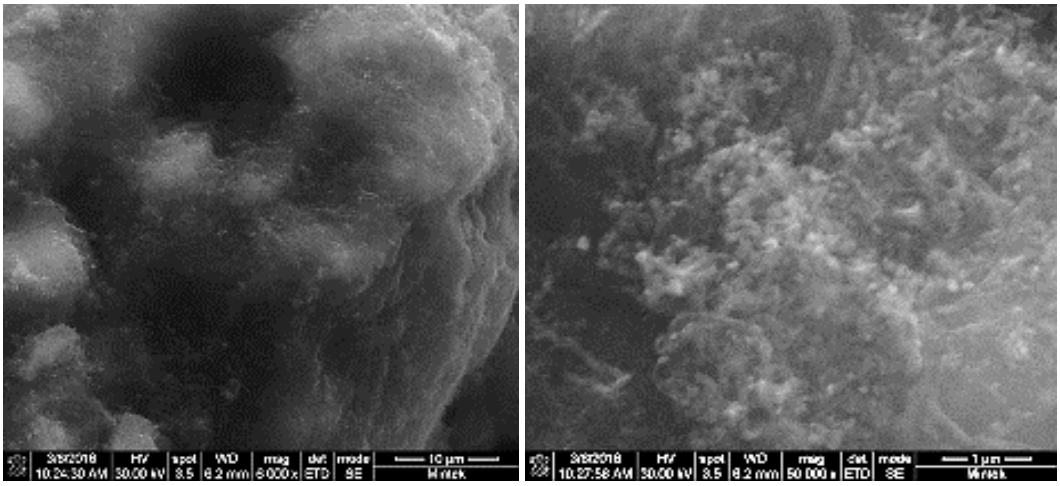

Figure 96. SEM images of carbon filaments of the coke and carbides (metal dust) at the tips after 336 h exposure at 525°C, low and high magnification.

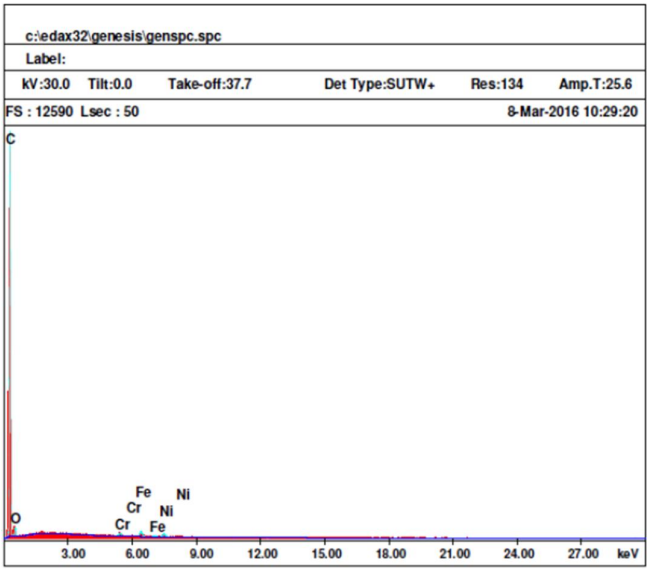

Figure 97. EDX spectrum of the coke product from the samples that were exposed for 336 h at 525°C which consisted of carbon, iron, nickel, and chromium with oxygen.

Longer exposure time results in more carbon deposition and the nanotubes of the coke become finer as compared to the coarser ones for shorter exposure time. Cr contributes to the formation of pits as it reacts with carbon on the surface to form carbides which can result in pits formation, as in the case of the 336 hour exposure at 650°C, seen in Figure 98 and Figure 99 is an EDX spectrum of the coke product from the samples that were exposed for 336 h at 650°C which consisted of carbon, iron, nickel, and chromium with oxygen.

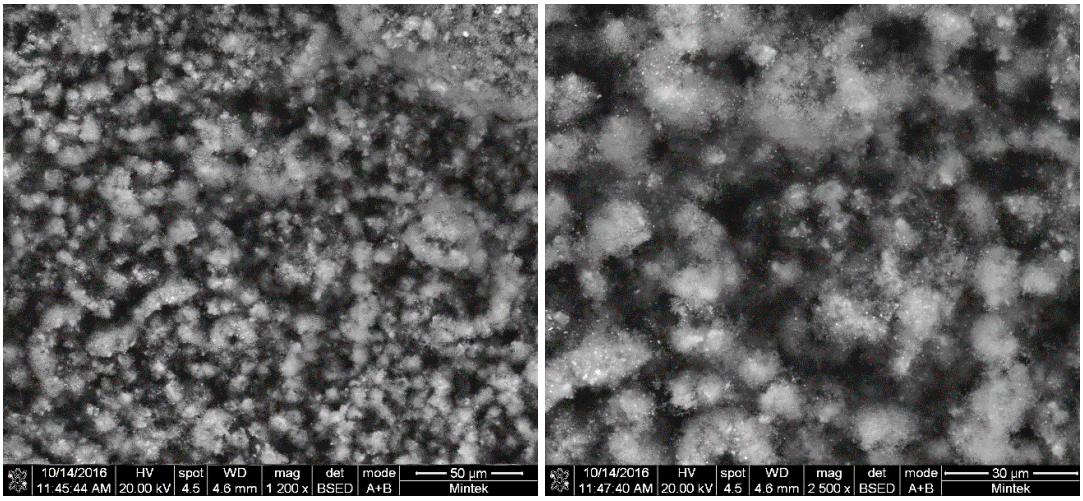

Figure 98. SEM images of carbon filaments of the coke and carbides (metal dust) at the tips after 336 h exposure at 650°C, low and high magnification.

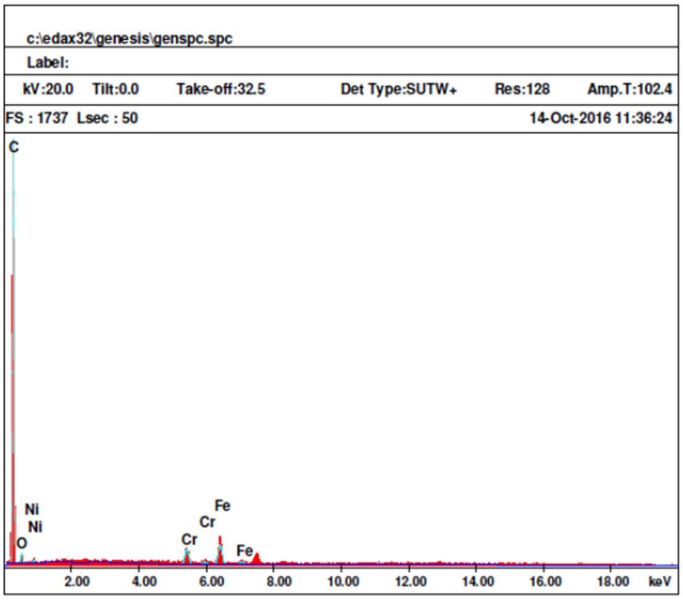

Figure 99. EDX spectrum of the coke product from the samples that were exposed for 336 h at 650°C which consisted of carbon, iron, nickel, and chromium with oxygen.

4.4.5 X-ray diffraction (XRD) – 336 h exposure at 525°C and 650°C

These samples were also analysed under the XRD and the metal seemed to be Ferrite (Fe) and with no Cr-carbide (C_6Cr_{23}), as compared to the other exposure periods of 24, 72 and 168 h. The coke was a mix of carbon nanotubes and graphite, as expected. The XRD spectrums of all the samples exposed at for 336 hours are shown in Figure 100 to 103. Note the shift on the peaks on these spectrums; it was not clear as to why they appeared this way. It must have been vibrations with the XRD machine at that specific time that the analyses were performed on these samples.

4.4.5.1 XRD of metal samples

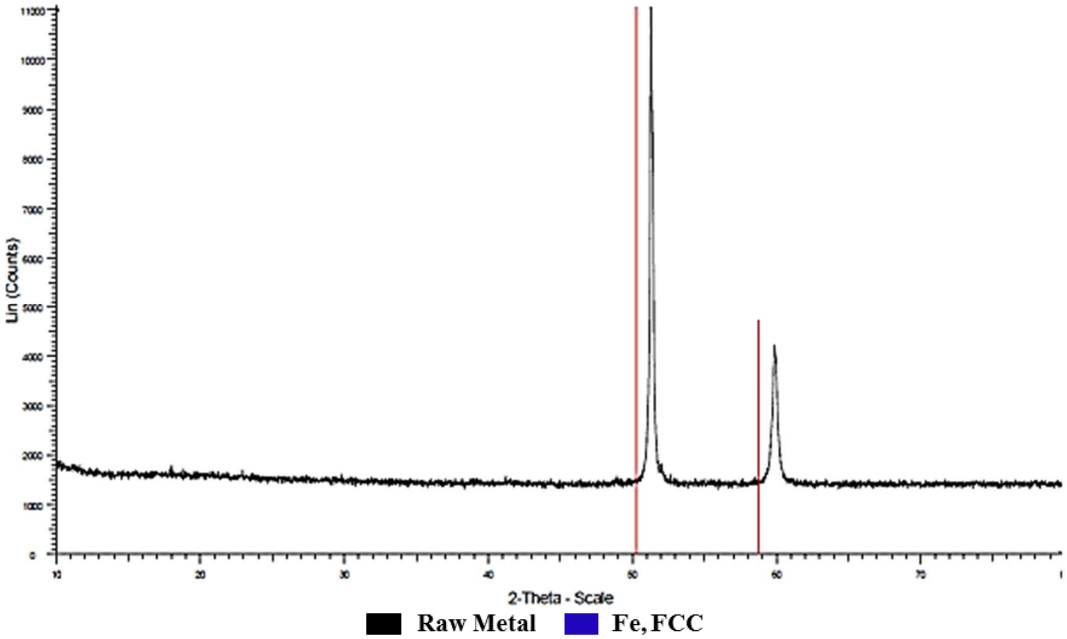

Figure 100. X-ray spectrum of the samples exposed for 336 h at 525°C showing the Fe peaks.

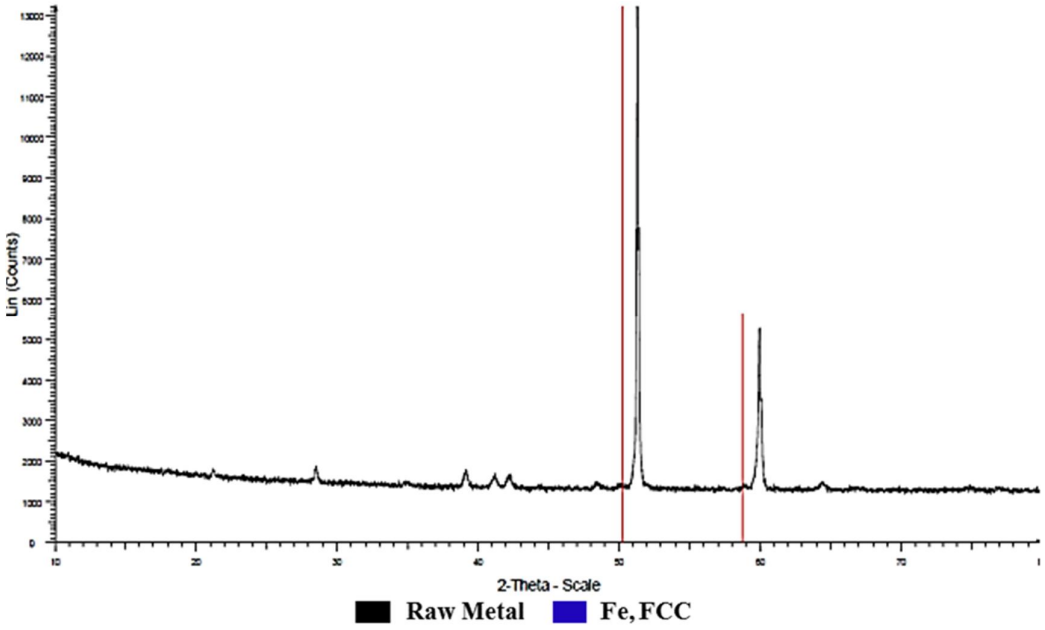

Figure 101. X-ray spectrum of the sample exposed for 336 h at 650°C, showing the Fe peaks.

4.4.5.2 XRD of coke samples

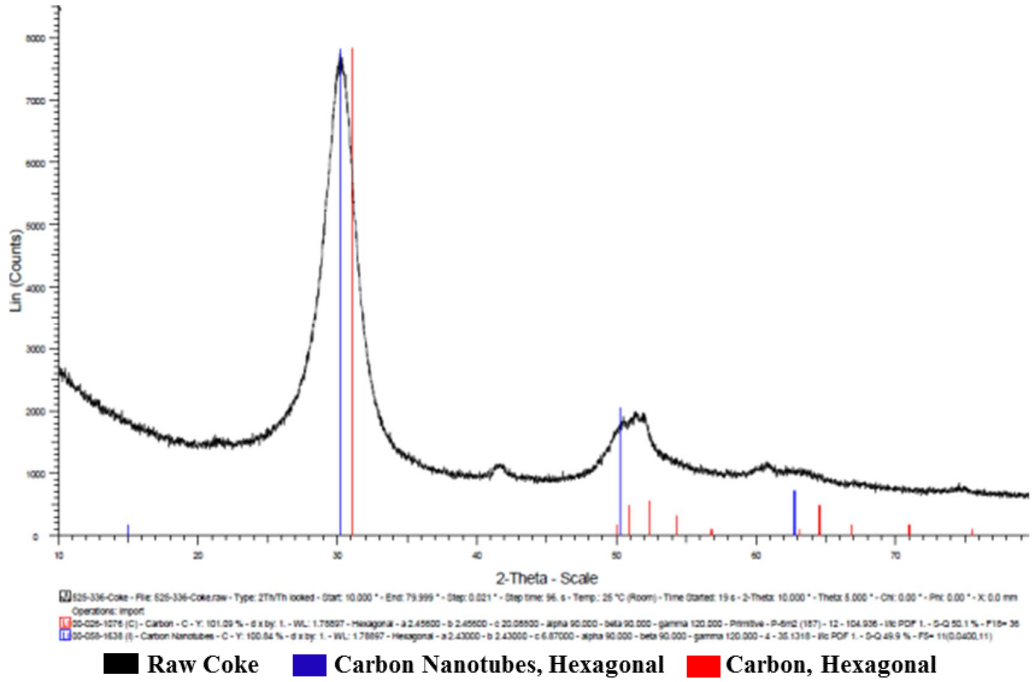

Figure 102. X-ray spectrum of the coke product from samples exposed for 336 h at 525°C, which consisted of carbon and carbon nanotubes

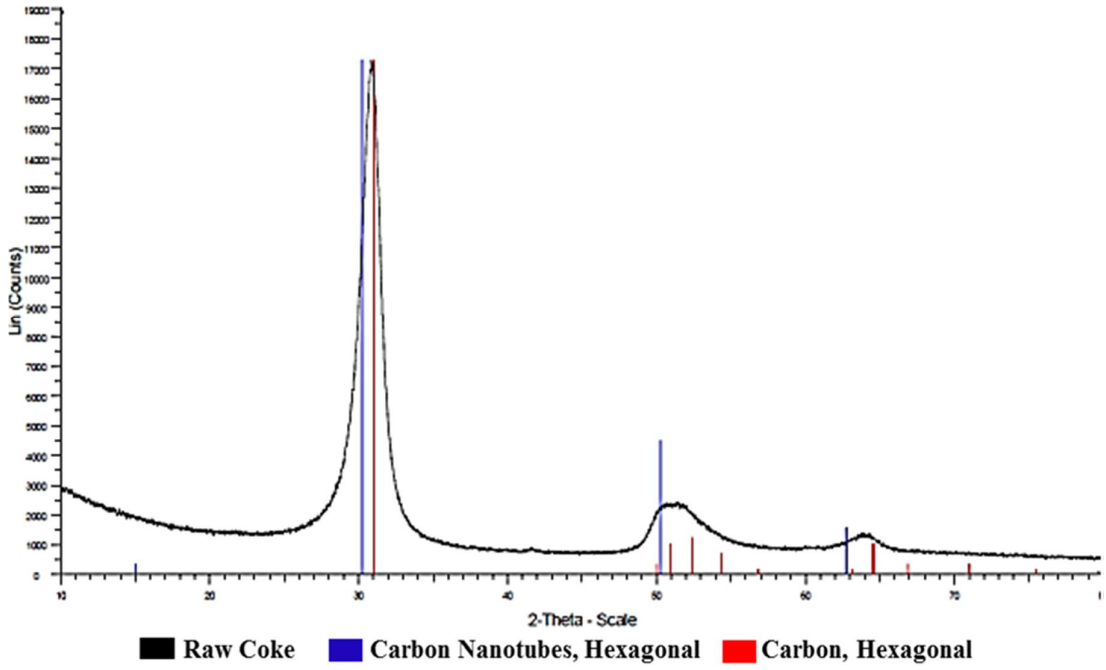

Figure 103. X-ray spectrum of the coke product from samples exposed for 336 h at 650°C, which consisted of carbon and carbon nanotubes.

4.4.6 Transmission Electron Microscopy (TEM) of coke product

The coke product of these samples were also analysed under the TEM, see Figure 104 to 109, illustrating that the coke product consisted of carbon nanotubes and carbide (dark area). Figure

91 and 94 are higher magnification TEM images of Figure 90 and 93, which show that the nanotubes are hollow.

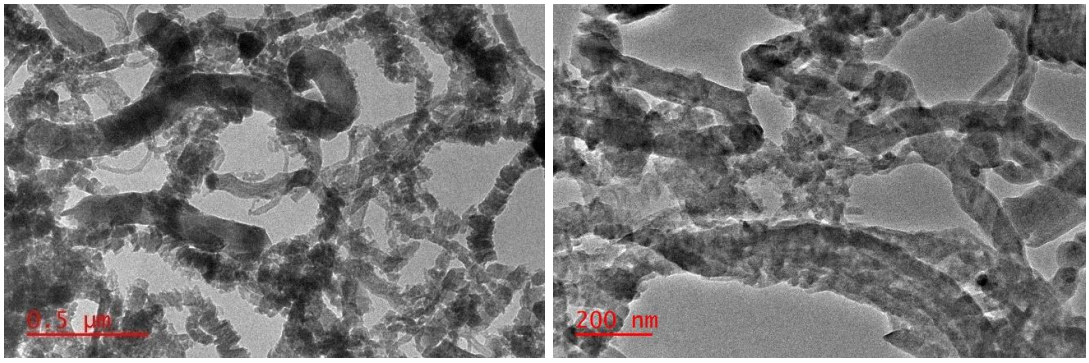

Figure 104. TEM images of carbon nanotubes and carbides (dark areas) of the coke product from the samples exposed for 336 h at 525°C, left – low magnification and right – high magnification.

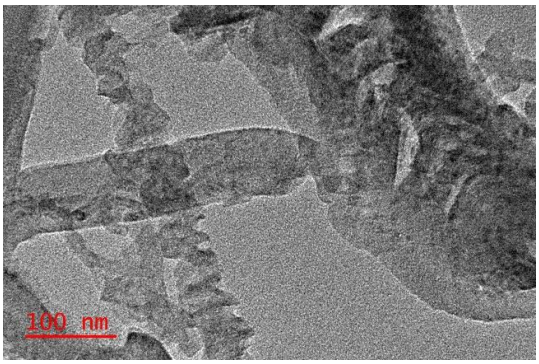

Figure 105. TEM image of carbon nanotubes and carbides (dark area) of the coke product from the samples exposed for 336 h at 525°C, at a higher magnification than Figure 104 showing that the nanotubes are hollow.

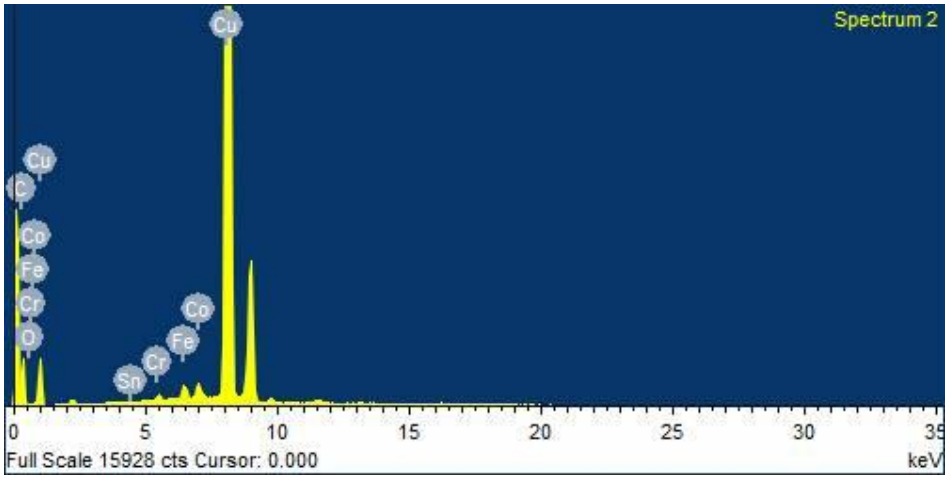

Figure 106. TEM spectrum of the coke product from the samples exposed for 336 h at 525°C, which consisted of carbon, iron, and chromium with oxygen, cobalt and tin. The copper is from the thin film used to put the coke particles for TEM analysis.

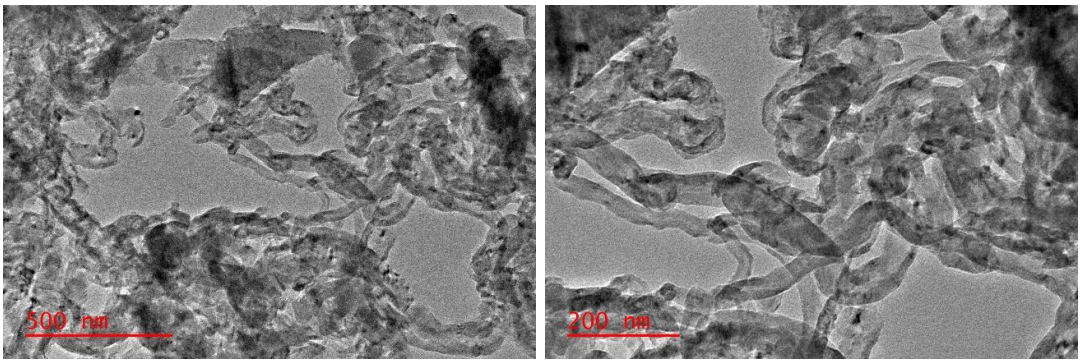

Figure 107. TEM images of carbon nanotubes and carbides (dark areas) of the coke product from the samples exposed for 336 h at 650°C, left – low magnification and right – high magnification.

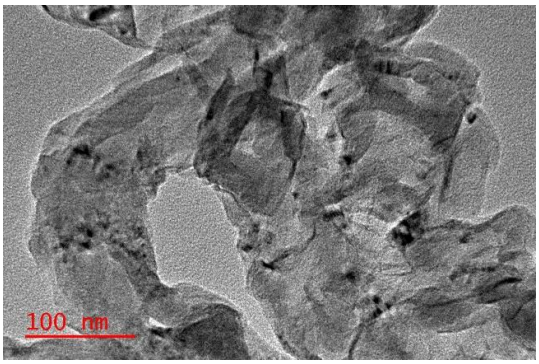

Figure 108. TEM image of carbon nanotubes and carbides (dark area) of the coke product from the samples exposed for 336 h at 650°C, at a higher magnification than Figure 107 showing that the nanotubes are hollow.

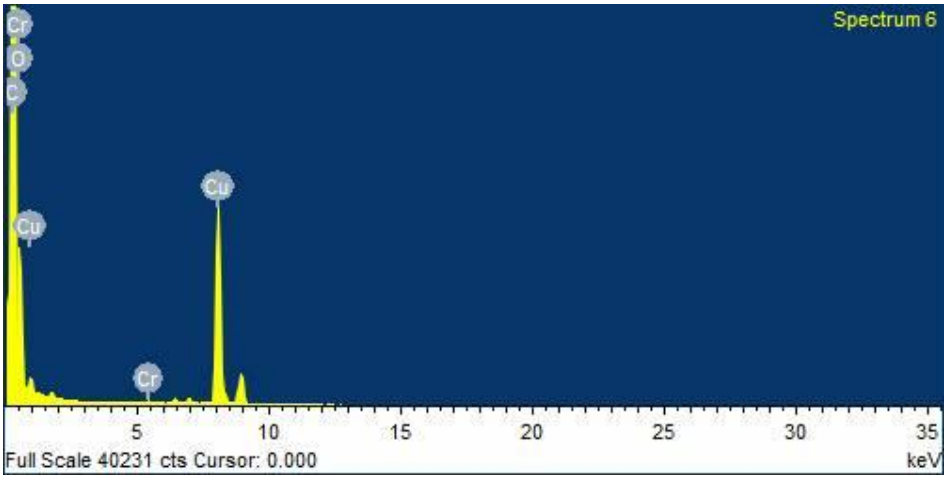

Figure 109. TEM spectrum of the coke product from samples exposed for 336 h at 650°C, which consisted of carbon and chromium with oxygen. The copper is from the thin film used to put the coke particles for TEM analysis.

CHAPTER 5: DISCUSSION

Metal dusting (MD) is a catastrophic form of corrosion in which metals and alloys disintegrate when exposed to carbon-supersaturated gas, forming metal-rich particles (the dust) dispersed in a voluminous carbon deposit.

This phenomenon was simulated successfully in the test rig. The main aim was to compare the effect or influence of temperature on the MD of Alloy 800 when exposed at 525°C and 650°C, over four different exposure periods of 24, 72, 168 and 336 h in a gas mixture of 25CO-70H_2-5H_2O.

Exposure for 24 h at both 525°C and 650°C, failed to produce any metal dusting attack on the samples 1 & 2, as seen on the results. The samples had a brownish/purplish colour on the surface after exposure of 24 h. As the exposure time was increased to 72 h very slight attack was observed on samples 20 and 21 at both 525°C and 650°C, little coking was also observed on these samples. The weight change data showed that the alloy started losing some weight or mass after 72 h exposure, i.e. longer than 24 h. Therefore, Alloy 800 suffered MD after a relatively short period of exposure time (i.e. 72 h). Increasing exposure periods showed different results for the alloy. It appears that Alloy 800 suffered metal dusting attack when exposed for longer than 24 h periods. The results also show a low mass loss. The alloy did not show significant surface features under the SEM after the 24 and 72 h exposures.

In all the cases (all exposure periods where MD attack was observed, i.e. 72, 168 and 336 h) carbon nanofilaments/tubes were observed to have formed. Under XRD, Fe and C_6Cr_{23} were the major phase observed after the MD attack, which is what was expected. Many of the other constituents such as Fe, Ni, Cr with Mn, Ti, O, Cl & Mo were also observed under the SEM. Carbon nanofilaments/tubes formed after longer exposure periods.

Table 4 gives a summary of most of the results obtained and it can be seen that the metal dusting attack and coking are more pronounced at 650 °C as compared to 525°C, for 72, 168 and 336 h, i.e. for all the exposure periods where metal dusting attack took place.

Table 4. Summary of some of the results obtained after the exposure of the samples of Alloy 800.

Exposure Periods (hours)	**24**		**72**		**168**		**336**	
Temp. (°C)	**525**	**650**	**525**	**650**	**525**	**650**	**525**	**650**
Visual Exam.					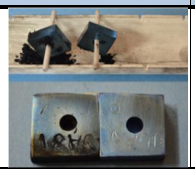			
650°C – 336 Hours exposure – Deep pits	 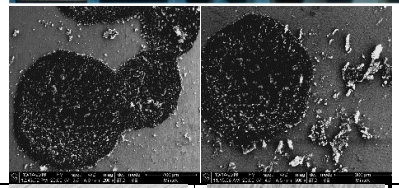		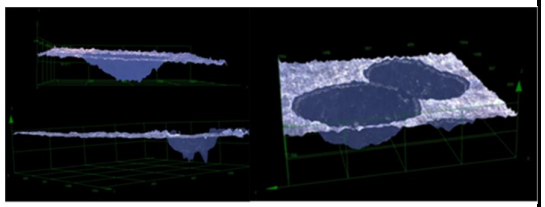				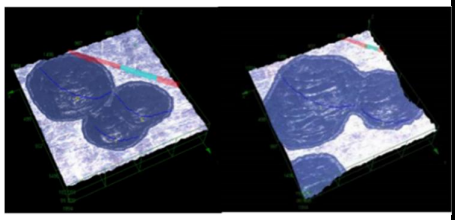	
SEM: Surface	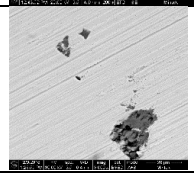	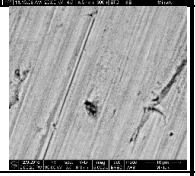	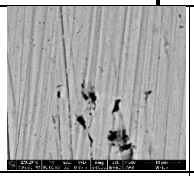	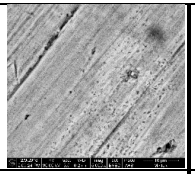	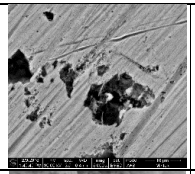	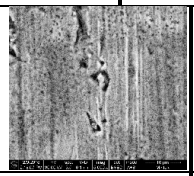	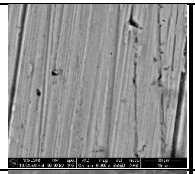	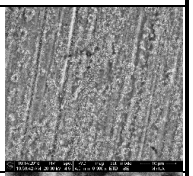
SEM: Coke	No coking observed		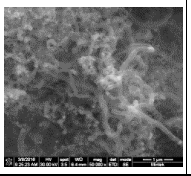	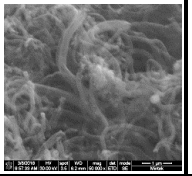	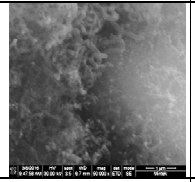	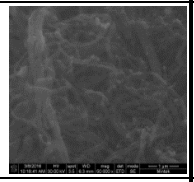	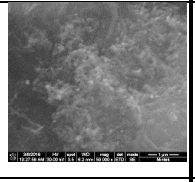	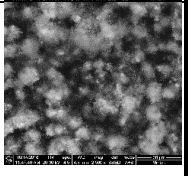
SEM: Metal	Fe, Ni, Cr with Mn, Ti, O, Cl & Mo	Fe, Cr, O, Cl & S	Fe, Ni, Cr, V &Ti	Fe, Ni, Cr, V &Ti	Fe, Ni, Cr, V &Ti	Fe, Ni, Cr, V &Ti	C, Fe, Ni, Cr, Mn& O	C, Fe, Ni, Cr, Mn& O

SEM: Coke	No coking observed		C, Fe, Ni, Cr & O	C, Fe, Ni, Cr & O	C, Fe, Ni, Cr & O	C, Fe, Ni, Cr & O	C, Fe, Ni, Cr & O	C, Fe, Ni, Cr & O
XRD: Metal	Fe & C_6Cr_{23}	Fe & C_6Cr_{23}	Fe & C_6Cr_{23}	Fe & C_6Cr_{23}	Fe & C_6Cr_{23}	Fe & C_6Cr_{23}	Fe	Fe
XRD: Coke	No coking observed		Carbon nanotubes & graphite	Carbon nanotubes & graphite	Carbon nanotubes & graphite	Carbon nanotubes & graphite	Carbon nanotubes & graphite	Carbon nanotubes & graphite
Raman spectrometry	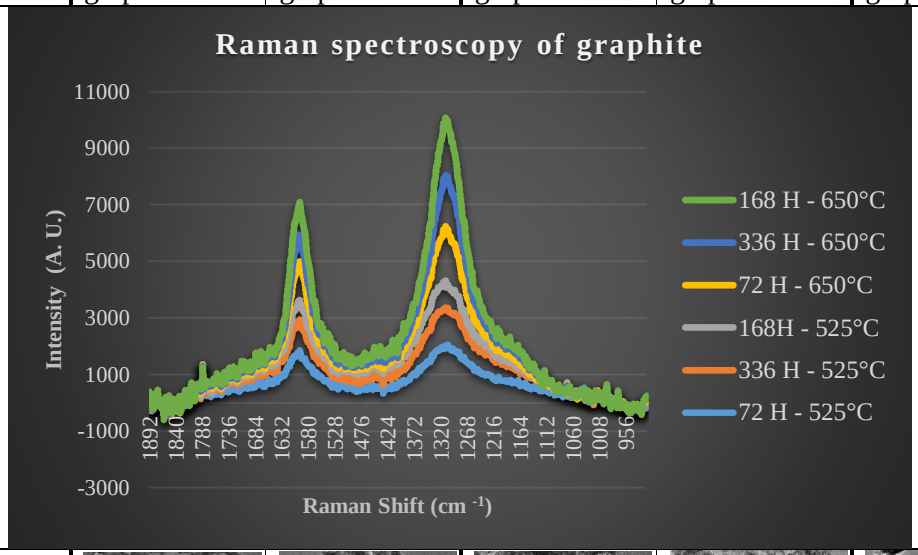						
TEM: Coke	No coking observed		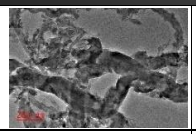	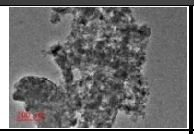	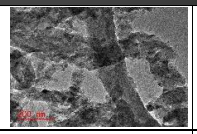	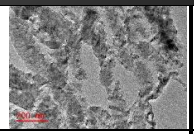	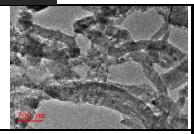	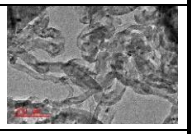
TEM: Contituents	No coking observed		Fe, Ni, Cr & O	C, Cr & O	Ni, Cr & O	C, Cr & O	C, Fe, Cr, O, Co & Sn	C, Cr & O

Low chromium steels of CrNiFe steels are capable of forming protective oxide films, and in this case the corrosion is local and leads to formation of hemispherical pits and holes, from which the coke grows in various forms such as cones, worms and leeches etc. The following sequence of steps has been proposed by Grakbe and Schütze, 2007.

(i) Carbon is transferred from the carbon-supersaturated environment to the steel surface and dissolves in the steel through local defects in the oxide film. (ii) The dissolved carbon diffuses inward and causes internal precipitation of stable carbides ($M_{23}C_6$ and M_7C_3). (iii) Upon further carbon transfer, metastable M_3C carbide forms on the internal carbide. (iv) Metastable M_3C carbide subsequently decomposes into carbon and metal upon carbon deposition. (v) Metal particles generated by the disintegration of the steel act as catalyst for the formation of coke arising from the growing pit alloys (Grakbe and Schütze, 2007). This is shown in Figure 110.

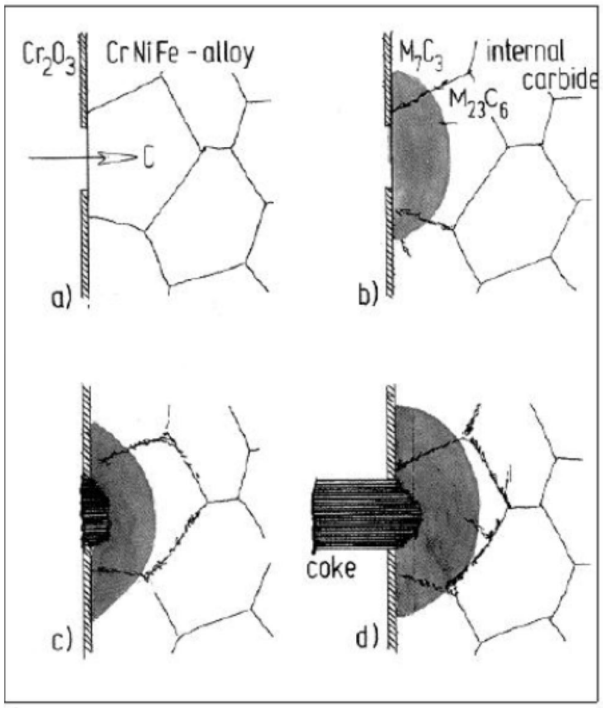

Figure 110. Schematic illustration of the metal dusting mechanism on CrFeNi-alloys (Grakbe and Schütze, 2007).

The process whereby a protective oxide scale can be depleted, leading to a growth of the MD pit as shown in Figure 111 and it involves four stages as follows:

An intact oxide scale on the surface of the alloy, (ii) The scale undergoes intrinsic oxide growth stresses (i.e. internal corrosion or damage) which leads to the formation of cracks, (iii) Graphite precipitates in these cracks, widening them, causing further cracking, and (iv) Pits form as a

consequence of the local cracking processes by graphite formation (Young, Zhang , Geers and Schütze, 2011).

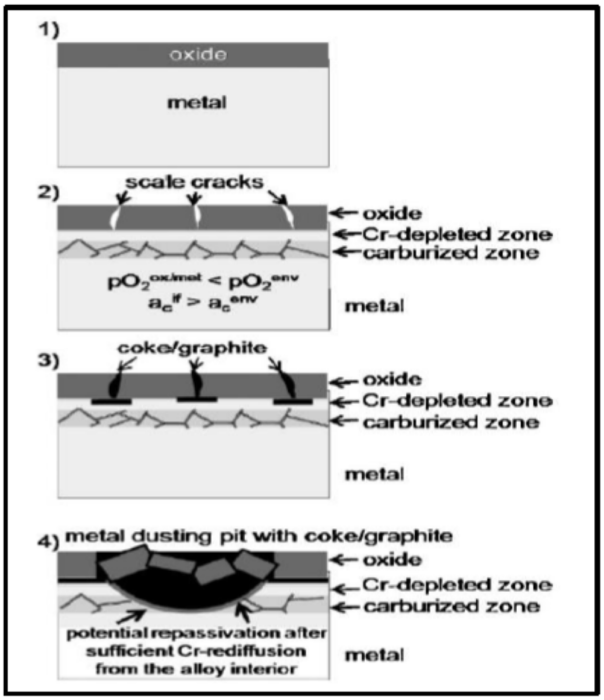

Figure 111. Processes occurring on high alloy materials during local oxide scale failure leading to a growing metal dusting pit (Young et al., 2011).

This process is in agreement with the findings in this study. Longer exposure time resulted in more carbon deposition and the nanotubes of the coke became finer as compared to the coarser ones for shorter exposure time. Cr contributes to the formation of pits as it reacts with carbon on the surface to form carbides which can result in pits formation. The alloy experienced pitting when exposed for 336 hours at a temperature of 650ºC, with pits of various sizes and orientations.

A mechanism for the formation of carbon filament was proposed. Decomposition of gas molecules at the surface of a metal particle produces adsorbed carbon, which diffuses through the bulk of the metal particle to the metal-carbon filament interface. At this stage precipitation of carbon occurs to form the filament body. It was also suggested by the same authors that surface migration of carbon species around the metal particle is the one that forms the skin component of the filament. These filaments are now recognized as nanotubes. A concentration or a temperature gradient has been proposed as the driving force for the diffusion process. The limited temperature gradients that are possible across small particles under conditions where filament is observed (<0.1K) is the reason why activity gradients represent a more likely

driving force than temperature gradients (Toh, Munroe and Young, 2002). Most practical alloys, such as iron, nickel or Fe-Ni, form protective oxide scales, such as chromia, which can act as a barrier to carbon ingress. When relatively low temperatures are involved, the diffusion of the alloy is rather slow, and the ability of these alloys to repair or reheal damaged scales is limited. Carbon will eventually attack the chromium depleted substrate once the capacity to repair/reheal has been exhausted. The mechanism and morphology of this reaction is in most respects characteristics of the dusting of alloy basis metals such as Alloy 800.

CHAPTER 6: CONCLUSIONS

Alloy 800 showed small amounts of coke deposits after 72 hr exposure period at both temperatures of 525°C and 650°C. Increasing amounts of coke deposits were formed with increased exposure time and temperature. Pitting started occurring at 650°C rather than 525°C even at pro-longed exposure periods. Therefore at higher temperature attack is increased, i.e. increasing the exposure time and temperature increases the attack. Significant amounts of platelets on the surface of the samples were seen after 168 and 336 h exposure. Carbon filaments and nanotubes with metal particles at the tips were also observed under SEM and TEM. XRD showed that Alloy 800 has a complex phase mix consisting of Fe & C_6Cr_{23} and carbon nanotubes & graphite, after metal dusting attack. The D and G peaks were clearly depicted on the Raman spectrum, which is evident of a typical graphite structure found as a result of metal dusting attack.

All the results are in agreement with the metal dusting mechanism of FeNiCr alloys, in this case Alloy 800. All the results obtained are in agreement with literature. There is some indication in terms of the influence of temperature on the metal dusting of Alloy 800, although it is not significant. The effect or influence of increasing exposure period is clearer.

REFERENCES

1. Agüero A., Gutiérrez M., Korcakova L., Nguyen T.T.M., Hinnemann B., and Saadi S. (2011), Metal Dusting Protective Coatings. A literature Review, Oxidation of Metals, Vol. 76, pp 23-42.
2. Albertsen, J.Z. (2007), Experimental and theoretical investigations of metal dusting corrosion in plant exposed nickel-based alloys. Doctoral thesis, Norwegian University of Science and Technology, Trondheim.
3. Alvarez, J., Melob, D., Salas, O.J. Oseguerac, J. and López, V. (2008). Protective coatings against metal dusting. *Surface & Coatings Technology*, 203, 422-426.
4. Agüero A., Gutiérrez M., Korcakova L., Nguyen T.T.M., Hinnemann B., and Saadi S. (2011), Metal Dusting Protective Coatings. A literature Review, Oxidation of Metals, Vol. 76, pp 23-42.
5. Atkinson A. and Smart D.W. (1987), Report AERE R 2762, United Kingdom Atomic Energy Authority, Harwell.
6. Baker, B.A. and Smith, G.D. (2016), Alloy solutions to metal dusting problems in the petrochemical industry. Special Metals Corporation, Huntington, WV, USA.
7. Grakbe H.J. and Schütze M. (2007), Corrosion by Carbon and Nitrogen (Metal Dusting, Carburization and Nitridation), Woodhead Publishing Limited, Cambridge, England.
8. Grabke H.J., Muller-Lorenz E.M. and Zinke M. (2003), Metal dusting behaviour of welded Ni-base alloys with different surface finishes, Materials and Corrosion, Vol. 34, pp. 758-792.
9. Grabke H.J. and Spiegel M. (2003), Occurrence of metal dusting – referring to failure cases, Materials and Corrosion, 54, No. 10, Weinheim.
10. Hochman R.F. and Burson J.H. (1996), The fundamentals of Metal Dusting , Am. Petroleum Inst. Division of Refining, Proceedings, Vol. 46, pp. 331-344.
11. Holland M.L. and de Bruyn H.J. (1996), Metal dusting failures in methane reforming plant, International Journal of Pressure Vessel & Piping, Vol. 66 pp. 125-133.
12. Hultgren A. and Hillert M. (1953), Betingelsser för Bildningav Cementit vid UppkolningavNickelstål, Jernkont. Ann, 137:7.
13. Khanna A.S. and Jha B.B. (1987), Oxidation of Metals, Vol 27 (1-2), pp. 95-102.
14. Lai G.Y. (2007), High-Temperature Corrosion and Materials Applications, ASM International, United States of America.

15. Mulaudzi F.M.L., Cornish L.A., Slabbert G.A., and Papo M.J. (2012), Metal dusting on Alloys 602A and 800, The Journal of The Southern African Institute of Mining and Metallurgy, Vol. 7A, pp 589.
16. Nishiyama Y., Moriguchi K., Otsuka N, and Kudo T. (2005), Materials Corrosion, Vol. 56, pp. 806.
17. Rohnert D., Phillip F., Reuther H., Weber T., Wessel E. and Shutze M. (2007), Oxidation of Metals, Vol. 68, 271, pp. 271-293.
18. Shutze M. (1987), Protective Oxide Scales and Their Breakdown, John Wiley & Sons Ltd, Chichester, England.
19. Szakálos P. (2002), "Mechanisms of metal dusting on stainless steels", Licentiate Thesis, ISBN 91-7283-260-6, Stockholm.
20. Szakálos P. (2004), Mechanisms of Metal Dusting, PhD Thesis, Royal Institute of Technology and Swedish Institute for Metals Research, Stockholm, Sweden.
21. Szakálos P., Pettersson R., and Hertzman S. (2002), An Active Corrosion Mechanism for Metal Dusting on 304L Stainless Steel, Corrosion Science, Vol. 44, No. 10, pp. 2253 – 2270.
22. Toh C.H., Munroe P.R. and Young D.J. (2002), Metal Dusting of Fe-Cr and Fe-Ni-Cr Alloys under Cyclic Conditions, Oxidation of Metals, Vol. 58, Nos. 1/2, pp 2.
23. Wolf I. and Grabke H.J. (1985), Solid State Communication, Vol. 54, pp. 5-10.
24. www.hightempmetals.com (08-06-2017), High Temp Metals Alloy 800/800AT/800H Technical Data, Incoloy 800 Tech Data.
25. www.specialmetals.com (2004), Special Metals Corporation, 2004 (Sept 04)
26. Young D.J., Zhang J., Geers C and Schütze M. (2011), Recent advances in understanding metal dusting: A review, Materials and Corrosion, 62, No. 1, Weinheim.
27. Zeng Z. and Natesan K. (2006), Initiation of Metal-Dusting Pits and a method to Mitigate Metal-Dusting Corrosion, Oxidation of Metals, Vol. 66, Issue 1, pp. 1-20.
28. Zhang J., Schneider A. and Inden G. (2003), Characterisation of the coke formed during metal dusting of iron in CO-H_2-H_2O gas mixtures, Corrosion Science, vol. 45, 2003. pp. 1329–1341.
29. Franks A. R., Bagnall S. L., Brear J. M., Williamson J., Conlin^{+} P. and Reid$^{\#}$ G., (2017), Carburization and Metal Dusting in Fired Heaters and Steam Methane Reformers: Plant Integrity Issues, www.researchgate.net, conference paper: September 2017